NATIONAL ADVISORY COMMITTEE
FOR AERONAUTICS

TECHNICAL NOTE

No. 1337

JUN 19 1947

EFFECT OF HORIZONTAL-TAIL POSITION ON THE HINGE MOMENTS

OF AN UNBALANCED RUDDER IN ATTITUDES

SIMULATING SPIN CONDITIONS

By Ralph W. Stone, Jr. and Sanger M. Burk, Jr.

Langley Memorial Aeronautical Laboratory
Langley Field, Va.

Washington

June 1947

NATIONAL ADVISORY COMMITTEE FOR AERONAUTICS

TECHNICAL NOTE NO. 1337

EFFECT OF HORIZONTAL-TAIL POSITION ON THE HINGE MOMENTS

OF AN UNBALANCED RUDDER IN ATTITUDES

SIMULATING SPIN CONDITIONS

By Ralph W. Stone, Jr. and Sanger M. Burk, Jr.

SUMMARY

An investigation was made in the Langley 15-foot free-spinning
tunnel to determine the effect of horizontal-tail position on rudder
hinge moments in attitudes simulating spinning conditions. Hinge-
moment measurements were made on an unbalanced rudder on a rectangular
vertical tail for six positions of the horizontal tail. The hinge-
moment measurements were supplemented by tuft tests to determine the
air flow about the vertical tail.

The results of this investigation are based on the rudder-pedal
forces of the airplane without regard to the effectiveness of the
rudder in producing recovery from a spin. In general, the results
indicated that a low rearward position of the horizontal tail gave
the smallest rudder hinge-moment coefficients, which, in turn,
indicated that the rudder shielding was greater for this position of
the horizontal tail than for other positions. Conversely, a high
forward position gave the largest rudder hinge-moment coefficients,
which indicated the least rudder shielding for this horizontal-tail
position. The results of tuft observations of air flow about the
vertical tail substantiated these results. The rudder hinge-moment
coefficients generally decreased in magnitude with increased angle
of attack for all horizontal-tail positions. The effect of rudder
deflection on rudder hinge-moment coefficient was not appreciably
affected by the horizontal-tail positions except in very flat spins.
Computations of rudder-pedal forces based on the results of the
tests and upon empirical drag-coefficient data of spinning models
indicate that for all tail positions the highest forces are obtained
at the lowest angle of attack in the spin. The pedal forces for
airplanes in the light-airplane category are well within the capabili-
ties of the pilot for all angles of attack. For heavier airplanes,
the rudder may require some form of balance, particularly if the spins
are steep.

INTRODUCTION

The problem of spin recovery is considered to be one of great importance for all airplane designs. Methods of obtaining effective tail designs for spin recovery of airplanes have been presented in reference 1. Such tail designs, however effective, do not produce recovery if the controls cannot be moved as such movement is generally necessary for recovery. The control forces of either the elevator or the rudder may be excessive and thus recovery may be prevented. Estimations of elevator hinge moments and the corresponding stick forces in spins have been presented in reference 2. The present investigation was undertaken to provide general information on the pedal forces in spins without regard to the effectiveness of the rudder in producing recovery.

At the high angles of attack encountered with a spinning airplane the vertical tail may be shielded by the horizontal tail, fuselage, or wing. The present investigation provides information on pedal forces in spins with particular reference to the effect of the position of the horizontal tail. The wake of the horizontal tail may shield the vertical tail and influence the rudder control force — the extent, in general, depending on the relative positions of the horizontal and vertical tails.

The tests were performed in the Langley 15-foot free-spinning tunnel with an unbalanced rudder and elevator on rectangular vertical and horizontal tails. The hinge-moment measurements were supplemented by tuft tests to determine the general nature of the air flow about the vertical tail at high angles of attack. Six different positions of the horizontal tail were investigated as well as the vertical tail alone.

COEFFICIENTS AND SYMBOLS

C_h rudder hinge-moment coefficient $\left(H/qb_r\bar{c}_r^2\right)$

C_D drag coefficient of airplane (D/qS)

F rudder-pedal force (positive when push force is on right rudder pedal), pounds

H rudder hinge moment (positive when it tends to deflect rudder to left), foot-pounds

q dynamic pressure, pounds per square foot $\left(\dfrac{\rho V^2}{2}\right)$

ρ mass density of air, slugs per cubic foot

V true rate of descent, feet per second

b_r rudder height, feet

$\bar{c}_r$ root-mean-square chord of rudder (rearward of hinge axis), feet

D drag of airplane, pounds

S wing area, square feet

W normal gross weight of airplane, pounds

l_r total rudder-pedal travel (assumed as 0.54 ft), feet

δ_r rudder deflection with respect to fin (positive when trailing edge is to left), degrees

α angle of attack referred to chord of horizontal tail, degrees

ψ angle of yaw (positive when nose of airplane is to right of flight path), degrees

β angle of sideslip (positive when relative wind comes from right of plane of symmetry), degrees

$C_{h_{\delta_r}}$ rate of change of rudder hinge-moment coefficient with rudder deflection

C_{h_ψ} rate of change of rudder hinge-moment coefficient with angle of yaw

APPARATUS

A plan view and side view of the rectangular vertical and horizontal tails used for the tests are presented in figure 1. A sketch of the model mounted in the Langley 15-foot free-spinning tunnel with a dashed outline of a fuselage sketched in for reference is shown in figure 2. Figure 3 is a photograph of the vertical tail alone mounted in the tunnel. A photograph of the tail assembly with the horizontal tail in a typical position (low center position) in the tunnel is presented in figure 4. The tails were made of laminated mahogany and had NACA 0009 airfoil sections; and the elevator and rudder chords were 33.3 percent of the airfoil chord. The gaps between the movable and fixed surfaces were unsealed. The elevator and rudder had no aerodynamic balance. The rudder, however, was mass

balanced so that no moment would be exerted on the strain gage because of the weight of the rudder.

The six combinations of the horizontal tail mounted on the vertical tail are sketched in figure 5 and are as follows:

Position I: The low forward position for which the chord line of the horizontal tail was 1 inch above the bottom of the vertical tail and the elevator hinge line was forward of the rudder hinge line by approximately 1 rudder chord.

Position II: The low center position for which the chord line of the horizontal tail was 1 inch above the bottom of the vertical tail and the elevator hinge line coincided with the rudder hinge line.

Position III: The low rearward position for which the chord line of the horizontal tail was 1 inch above the bottom of the vertical tail and elevator hinge line was rearward of the rudder hinge line by 1 rudder chord.

Position IV: The high forward position for which the chord line of the horizontal tail was at a height midway of the vertical tail and the elevator hinge line was forward of the rudder hinge line by approximately 1 rudder chord.

Position V: The high center position for which the chord line of the horizontal tail was at a height midway of the vertical tail and the elevator hinge line coincided with the rudder hinge line.

Position VI: The high rearward position for which the chord line of the horizontal tail was at a height midway of the vertical tail and the elevator hinge line was rearward of the rudder hinge line by 1 rudder chord.

The dimensional characteristics of the horizontal and vertical tails are as follows:

Vertical tail surfaces:
    Total area, square inches 216
    Span, inches 18
    Chord, inches 12
    Rudder root-mean-square chord, inches 4
    Aspect ratio 1.5
    Rudder area for positions I, II, IV,
        and V, square inches 72
    Rudder area for position III, square inches 65.25
    Rudder area for position VI, square inches 67.00
    Airfoil section . . . . NACA 0009

Horizontal tail surfaces:
    Total area, square inches 414.26
    Span, inches 36
    Chord, inches 12
    Aspect ratio 3.13
    Elevator area, square inches 126.26
    Airfoil section . . . . .NACA 0009

Because of construction difficulties, the horizontal tail was
actually moved 4.38 inches forward of the rudder hinge line for the
forward position, whereas in the rearward position it was 4.00 inches
(1 rudder chord) rearward of the rudder hinge line. For the two
rearward positions of the horizontal tail (positions III and VI)
cut-outs were necessary in the lower and center parts (respectively)
of the rudder to allow it to swing over the stabilizer. (See fig. 1.)
A second rudder was constructed with cut-outs for these rearward
horizontal-tail positions. A cut-out, made in the elevator (fig. 1)
to allow the rudder to swing through its desired range for horizontal-
tail positions II and V, was retained for all other tail positions.

The elevator and rudder were held by a friction clamp at the
desired deflection on the hinge rod, and all deflections were set
by templets. The rudder hinge moments were measured electrically
by a strain gage. This gage was calibrated by applying a series of
known moments to the rudder.

The tufts used to determine the general nature of the air flow
about the vertical tail were fine silk threads approximately $1\frac{1}{4}$ inches
in length. Two rows of tufts at approximately 1-inch intervals were
attached to each side of the vertical tail by Scotch cellulose tape;
one row was placed along the fin and the other was placed along the
rudder.

TESTS

The tests were conducted in the Langley 15-foot free-spinning
tunnel which has a turbulence factor of 1.78. All tests were made
at a dynamic pressure of 2.66 pounds per square foot, which corres-
ponds to an airspeed of 32.3 miles per hour under standard sea level
conditions.

The attitude of the tail assembly was varied to give the desired
angles of attack and sideslip. The angle of sideslip was simulated by
the angle of yaw as shown in figure 2. The desired values of sideslip
were obtained by yawing the model about the stability Z-axis, which is
perpendicular to the vertically rising airstream. The stability axes
are defined as an orthogonal system of axis in which the Z-axis is in
the plane of symmetry and perpendicular to the relative wind, the X-axis

is in the plane of symmetry and perpendicular to the Z-axis, and the
Y-axis is perpendicular to the plane of symmetry.

Hinge-Moment Tests

In order to simulate spinning conditions for the hinge-moment tests,
the model was tested throughout an angle-of-attack range from 0° to 90°
in 10° increments and through a yaw range of 30° to -30° in 10° incre-
ments. The angles of yaw as set on the model may be interpreted as
angles of sideslip that would be encountered at the tail of an airplane
in a spin. The actual angle of sideslip is equal in magnitude to the
angle of yaw but has the opposite sign. The angles of attack as set
represent the angles of attack of the stabilizer and not angles of attack
of the vertical tail as an airfoil. The rudder at each angle of attack
and yaw angle was deflected from 0° to 30° in 10° increments. For the
foregoing conditions, the vertical tail was tested with the horizontal
tail in each of the six positions and also with the horizontal tail
removed. The elevator deflection was zero for all tests.

As there was no fin offset, results obtained with a positive rudder
deflection may also be considered as representative of negative rudder
deflection provided the hinge-moment coefficient signs are reversed.
Each configuration, therefore, represents a spin with the rudder set
either with or against the spin. For example, a negative angle of yaw
with left rudder may be considered as representative of outward sideslip
in a left spin with rudder with the spin or of inward sideslip in a right
spin with rudder against the spin. Similarly, a positive angle of yaw
with left rudder may be considered as representative of outward sideslip
in a right spin with rudder against the spin or of inward sideslip in a
left spin with rudder with the spin. Table I shows in detail how the
various figures may be interpreted for a right or left spin and how the
angles of yaw may be interpreted to represent sideslip.

Tuft Tests

Tuft tests were made on the vertical tail for various positions of
the horizontal tail and for the condition with the horizontal tail
removed. These tests were arbitrarily made at angles of attack of 0°,
10°, 20°, 50°, and 80° and for angles of yaw of 0° and -15° when the
horizontal tail was installed and for 0° and $\pm20^\circ$ when the horizontal
tail was removed.

CORRECTIONS

No corrections were made for the effect of the tunnel walls on the
tail surfaces as the size of the surfaces was small compared to the

diameter of the tunnel and the corrections would therefore be negligible.
Strut interference effects have also been neglected. At first the
rectangular wooden arm which supported the vertical tail (fig. 3)
was expected to cause an increase in the effective aspect ratio of the
vertical tail. The hinge-moment tests with the horizontal tail removed,
however, gave coefficients of the order expected for a rudder on a tail
of aspect ratio 1.5 as computed exclusive of the supporting member which
indicates negligible interference effects.

RESULTS AND DISCUSSION

Rudder Hinge Moments

Rudder hinge-moment coefficients obtained from tests of the
vertical tail in various combinations with the horizontal tail are
presented in figures 6 to 14. In order to show the shielding effect
of the horizontal tail on the vertical tail, the hinge-moment coef-
ficients obtained from tests of the vertical tail alone have been
plotted on these same figures. The analysis of these data is based
on aerodynamic forces on the rudder without regard to any frictional
or centrifugal forces that may exist on the airplane control surfaces
in a spin.

<u>Effect of angle of attack on rudder hinge-moment coefficients.</u>—
The variation of rudder hinge-moment coefficient with angle of attack
for various positions of the horizontal tail and with the horizontal
tail removed are presented in figures 6 to 9. The rudder hinge-moment
coefficients for all positions of the horizontal tail decreased in
magnitude from those for the vertical tail alone; this amount of
decrease increased, in general, with angle of attack. The coefficients
changed with angle of attack so that they generally approached the line
of zero hinge-moment coefficient at very high angles of attack.

In a very few cases the hinge-moment coefficients of the rudder
in the presence of the horizontal tail changes sign from those of the
rudder alone. This tendency is analogous to overbalancing in that the
rudder tends to float in the direction opposite to that expected.

In general, the high forward position of the horizontal tail
(position IV) led to the highest values of rudder hinge-moment coefficient,
whereas the low rearward position (position III) led to the lowest values.
These results indicate that position IV produced the least rudder shielding
or blanketing effect, whereas position III produced the most shielding.
The shielding effect of the horizontal tail on the vertical tail was small
at low angles of attack (0° to 10°) but increased as the angle of attack
increased. The relative difference in the shielding effect caused by
tail position was small at low angles of attack (0° to 20°) but generally
increased as the angle of attack increased up to angles of attack of
about 80°, beyond which the relative difference tended to decrease again.

Effect of rudder deflection on rudder hinge-moment coefficients.—
The variation of rudder hinge-moment coefficient with rudder defloction
for various angles of yaw is presented in figures 10 to 12. These
figures are cross plots of figures 6 to 9 for a range of angles of yaw
most commonly encountered in spins. The slope $C_{h_{\delta_r}}$ was not greatly

affected by the installation of the horizontal tail on the vertical tail
or by the various positions of the horizontal tail at low and moderate
angles of attack but decreased negatively an appreciable amount at high
angles of attack ($60°$ and $80°$) which simulate the conditions for very
flat spins.

Effect of yaw on rudder hinge-moment coefficients.— The variation
of rudder hinge-moment coefficient with anglo of yaw for rudder deflec-
tions of $0°$ and $30°$ is presented in figures 13 and 14. The specific
rudder deflections of $0°$ and $30°$ were chosen to represent neutral and
full rudder deflection in a spin. These figures were obtained by cross-
plotting from figures 6 to 9.

The slope C_{h_ψ} was not appreciably affected by the installation
of horizontal tail at low angles of attack. In the normal spinning
range of angle of attack ($30°$ to $50°$) and for high anglos of attack,
however, there was a marked change in the slopes. As previously indicated,
the slope $C_{h_{\delta_r}}$ was not affected in the normal range of angle of attack.

Therefore, the direct effect of shielding of the rudder by the horizontal
tail in the normal spinning range of angle of attack is to change the
values of C_{h_ψ}.

Tuft Tests

Some indication of the shielding effect of the horizontal tail on
the vertical tail was obtained from tuft observations. The results of
the tuft tests are presented in figures 15 to 21. The photographs give
some indication of the shielding effect of the horizontal tail on the
vertical tail and in general substantiate the results of the hinge-
moment tests.

Application of Hinge-Moment Data

The hinge-moment coefficients presented herein may be used to
estimate the rudder-pedal forces required to reverse the rudder on an
airplane in a spin, provided that the angle of attack and sideslip at
the tail are known. The rudder-pedal force is

$$F = C_h q \bar{c}_r^2 b_r \frac{\delta_r \pi}{180 l_r}$$

In a steady spin the weight of an airplane equals its drag; therefore,

$$W = D = C_D q S$$

or

$$q = \frac{W/S}{C_D}$$

By substitution, then,

$$F = C_h \frac{W/S}{C_D} \bar{c}_r{}^2 b_r \frac{\delta_r \pi}{180 l_r} \tag{1}$$

The variation of drag coefficient with angle of attack for a spinning airplane is given in figure 22. This curve was determined from an average of experimental values obtained from spin-tunnel tests of numerous models.

In order to illustrate this method of computing the rudder-pedal forces for a specific design, the following example is given. Consider an airplane that has a tail configuration similar to the high rearward position of the horizontal tail (position VI), a normal gross weight of 8000 pounds, a wing area of 270 square feet $\left(\frac{W}{S} = 29.6 \text{ lb/sq ft}\right)$, and a vertical tail area of 25 square feet. Assume that the airplane is spinning to the right at an altitude of 15,000 feet at an angle of attack of 30° with 20° outward sideslip at the tail and that the rudder is deflected 30° against the spin. From figure 22, the drag coefficient is found to be 0.74. The rudder-pedal force can now be determined. The total pedal travel is assumed to be 0.54 feet and the total rudder deflection, 60°. The rudder dimensions are assumed to be proportional to those of the model used in the current tests (b_r, 6.12 ft and $\bar{c}_r$, 1.36 ft). From table I, if the airplane is assumed to be in a right spin, the rudder 30° against the spin, and the sideslip 20° outward, the figure that applies to this condition can be determined. In this case, the figure is 9(b) and the value of the hinge-moment coefficient is -0.255. Thus, substituting this value in the force formula (equation (1)) gives a rudder-pedal force of -222 pounds. This push force is that which is required on the left pedal to move the rudder fully against the spin.

In order to determine the magnitude of the rudder-pedal forces likely to be encountered with airplanes in a spin, computations have been made for three representative sizes of airplanes for different horizontal-tail positions and for the vertical tail alone. The airplanes represented are light-airplane, fighter, and light-bomber types. Weights of 1500, 10,000, and 20,000 pounds were chosen, respectively, for these types. The wing areas used for the three types were 165, 305, and 475 square feet, respectively, and respective vertical tail areas of 12.0, 28.5, and 55.5 square feet were used. These areas were determined from an average of areas for numerous airplane designs tested in the spin

tunnel. The proportions of the vertical tail and rudder were assumed
to be proportional to those of the model used for the current hinge-
moment tests. For these computations, the angle of sideslip assumed
was zero, the rudder deflection used was 30°, and the value of ρ was
arbitrarily taken at an altitude of 15,000 feet. The results of the
computations are plotted on figure 23.

For airplanes in the light-airplane category (fig. 23(a)), it
appears that, for any position of the horizontal tail or for the
vertical tail alone, the rudder-pedal force required to set the rudder
against the spin in no case exceeds 140 pounds. This force is much
smaller than the maximum of approximately 400 pounds that a pilot can
exert on a rudder pedal. (See reference 3.) Figure 23(a) also indicates
that the horizontal-tail position affects the rudder-pedal forces of
light airplanes only slightly, because the maximum force for any
horizontal-tail position or for the vertical tail alone is relatively
small. Only one curve was drawn through the numerous points for the
various positions of the horizontal tail in this particular figure.
Thus, for a light airplane it seems that the rudder-pedal forces
encountered in spins should be well within the capabilities of a pilot
regardless of horizontal-tail position.

For larger and heavier airplanes (fig. 23(b) and 23(c)) the pedal
force is shown to be larger at any given angle of attack because of the
larger control surface and because of the increase in rate of descent
in the spin.

If a fighter airplane spins at an angle of attack of 30° or greater
(fig. 23(b)), or if a light bomber airplane spins at an angle of attack
of 50° or greater (fig. 23(c)), the rudder-pedal force necessary to
reverse the rudder at these attitudes should be within the pilot's
capabilities. Below these respective angles of attack, however, some
type of rudder-balance or booster system may be used to overcome the
excessive forces. For example, in figure 23(c) a light bomber, spinning
at an angle of attack of 30° with the horizontal tail in the low rear-
ward position (position III), must have at least 30 percent of the
unbalanced rudder force balanced out in order to bring the pedal forces
within the limits of the forces that the pilot can exert.

In general, from an angle of attack of 10° to 40° (fig. 23(b) and
23(c)), the force gradient for all horizontal-tail positions was very
steep, which indicates that a small change in angle of attack led to a
large change in pedal force. This result may be taken as an indication
that, as the angle of attack decreases during the recovery, the pedal
force required to maintain the rudder full against the spin increases.
The low rearward position (position III) of the horizontal tail, in
general, required the smallest pedal force to reverse the rudder fully
or to maintain it full against the spin for any given angle of attack,

whereas the high forward position (position IV) required the largest force. Spin-tunnel results have indicated that, for the low rearward positions of the horizontal tail the rudder may be ineffective in producing a recovery and, for high forward positions of the horizontal tail, the rudder is generally effective in producing a recovery. Thus, for high forward positions of the horizontal tail maintaining the rudder full against the spin may not be necessary to obtain a satisfactory recovery, and such horizontal-tail positions may therefore not necessarily require large pedal forces for satisfactory recoveries.

CONCLUSIONS

The results of the investigation to determine the effect of horizontal-tail position on the rudder hinge-moment coefficients and pedal-force characteristics of an unbalanced rudder with rectangular plan form in attitudes simulating spin conditions indicate the following general conclusions without regard to the effectiveness of the rudder in producing a recovery:

1. The low rearward position of the horizontal tail gave the smallest rudder hinge-moment coefficients and pedal forces, which thus indicates that the shielding effect of this position was large relative to the other horizontal-tail positions. Conversely, the high forward position gave the largest hinge-moment coefficients and pedal forces which indicates that the relative shielding effect of this position was small. Tuft observations substantiated these relative shielding effects.

2. The rudder hinge-moment coefficients generally decreased with an increase in angle of attack for all horizontal-tail positions.

3. The rate of change of the rudder hinge-moment coefficient with rudder deflection was not appreciably affected by the horizontal-tail position except in very flat spins.

4. The rudder-pedal force for a light airplane for recovery from a spin should be well within the capabilities of the pilot. For heavier airplanes, the rudder may require some form of balance, particularly if the spins are steep.

5. The pedal force required for full rudder reversal for recovery from a spin increases rapidly as the airplane angle of attack in the spin decreases, especially at relatively low angles of attack.

Langley Memorial Aeronautical Laboratory
        National Advisory Committee for Aeronautics
                Langley Field, Va., March 26, 1947

REFERENCES

1. Neihouse, Anshal I., Lichtenstein, Jacob H., and Pepoon, Philip W.:
      Tail-Design Requirements for Satisfactory Spin Recovery. NACA
      TN No. 1045, 1946.

2. Seidman, Oscar, and Klinar, J. W.: Elevator Stick Forces in Spins
      as Computed from Wind-Tunnel Measurements. NACA ARR, Oct. 1942.

3. Gough, M. N., and Beard, A. P.: Limitations of the Pilot in
      Applying Forces to Airplane Controls. NACA TN No. 550, 1936.

TABLE I

INTERPRETATION OF RUDDER HINGE-MOMENT COEFFICIENT CURVES FOR RIGHT

OR LEFT SPIN

Rudder deflection, δ_r	Direction of sideslip (right spin)[b]					
With spin[a]	0	Inward	Outward	---	---	---
Neutral	---	---	---	0	Outward	Inward
Against spin	0	Outward	Inward	---	---	---
	Direction of sideslip (left spin)[b]					
With spin	0	Inward	Outward	---	---	---
Neutral	---	---	---	0	Inward	Outward
Against spin[a]	0	Outward	Inward	---	---	---
Read C_h from figs.—	7(d) 8(d) 9(d)	7(a), (b), (c) 8(a), (b), (c) 9(a), (b), (c)	7(e), (f), (g) 8(e), (f), (g) 9(e), (f), (g)	6(d)	6(a), (b), (c),	6(e), (f), (g)

[a]Sign of rudder hinge-moment coefficient, deflection, and angle of yaw must be reversed for this condition.

[b]Sideslip at the tail of the airplane is opposite in sign and equal in magnitude to values of ψ presented in figures.

NATIONAL ADVISORY
COMMITTEE FOR AERONAUTICS

0.54"R

45"

1.08"

18"
(test section)

₵ rudder hinge

B

4"

Mounting arm

Cut-out for
strain gage

A

12"

Section
A-A

6"

A

Cut-out for
mass balance

B

Vertical tail

Removable parts to
allow rudder to swing
across horizontal tail

1¼"

1¹¹⁄₁₆"

Tip

Root

₵ rudder hinge

9"

Rudder

Chord line

₵ hinge

Sections B-B and C-C

0.05"

₵

18"

C

₵ elevator
hinge

2⅛"

12"

60°

C

4"

36"
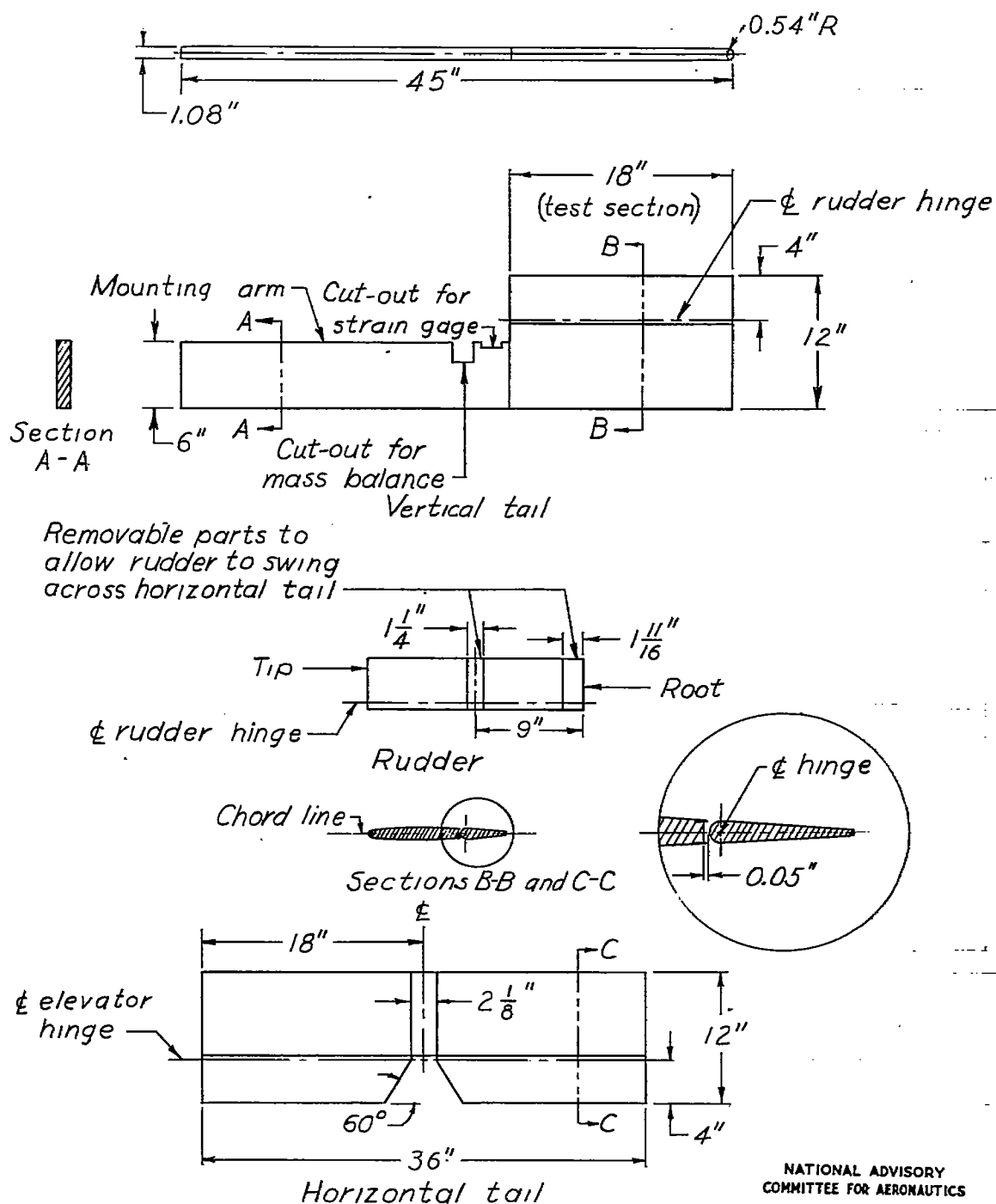
Horizontal tail

Figure 1.- Plan and side views of the rectangular vertical and
horizontal tails. Dimensions are full scale.

Fig. 2   NACA TN No. 1337
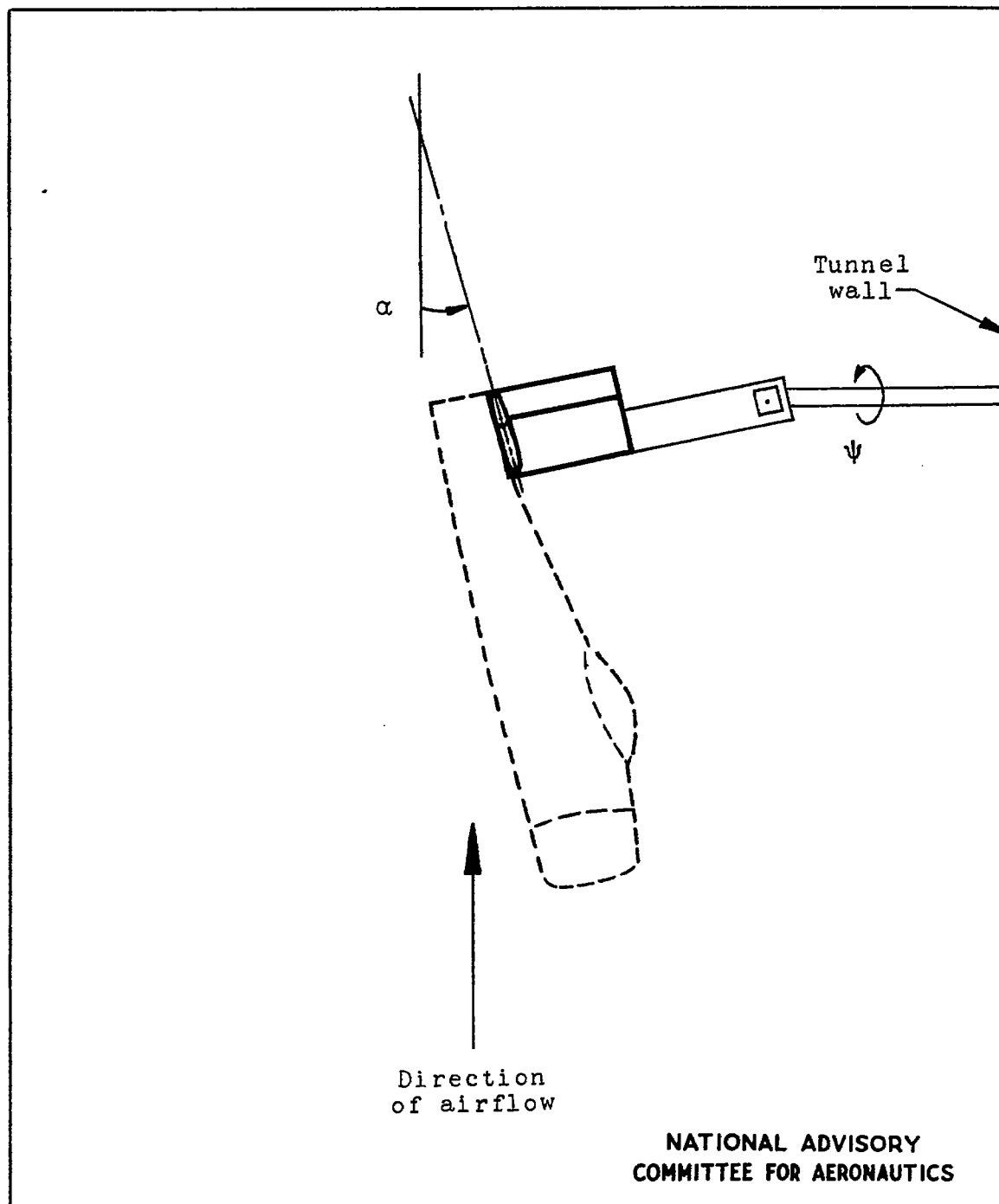
Figure 2.- Horizontal and vertical tail in attitude simulating spin with fuselage of airplane sketched in for reference. Arrows indicate direction of positive values of angles.
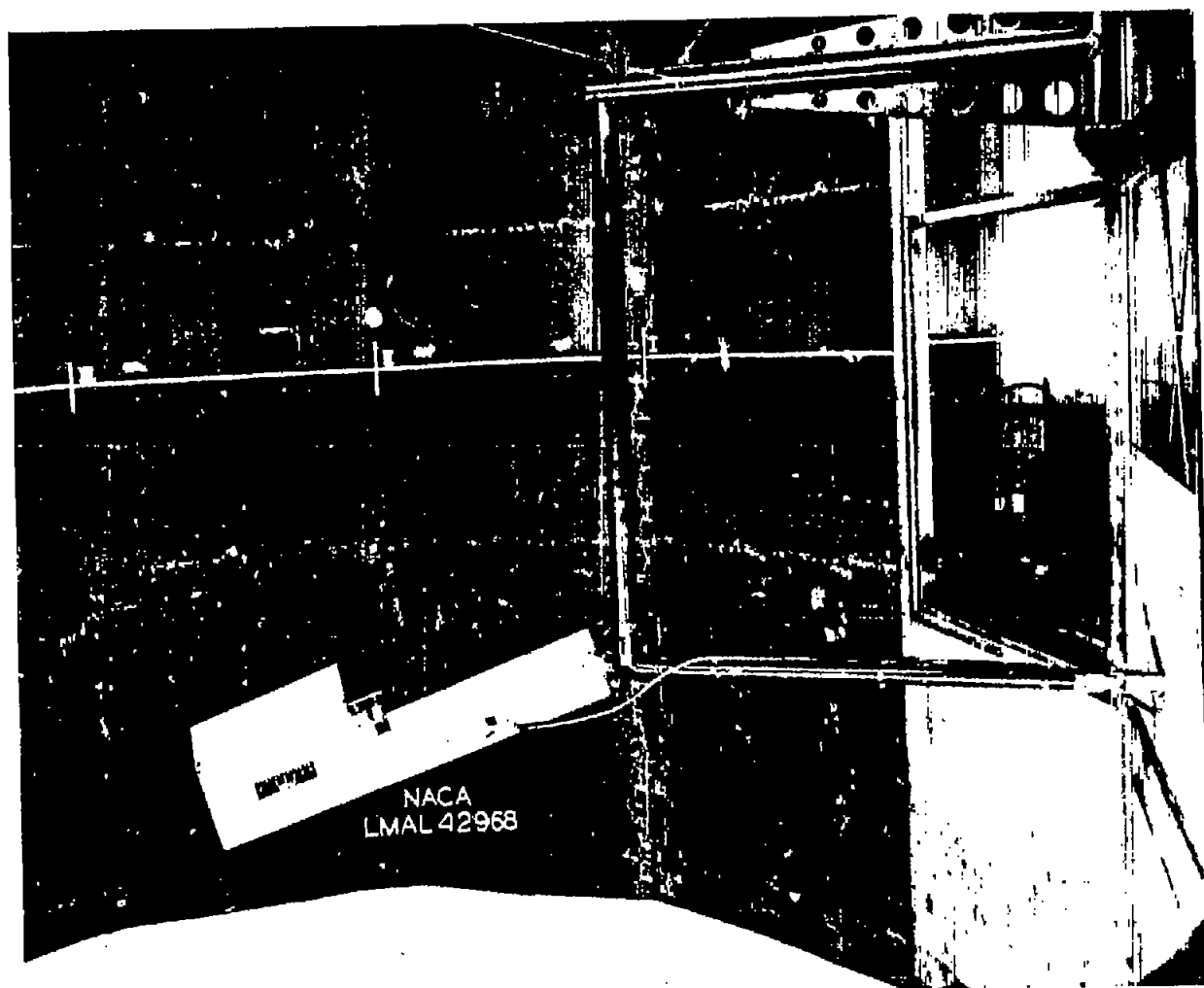
Figure 3.- Vertical tail mounted in Langley 15-foot free-spinning tunnel.

Fig. 3
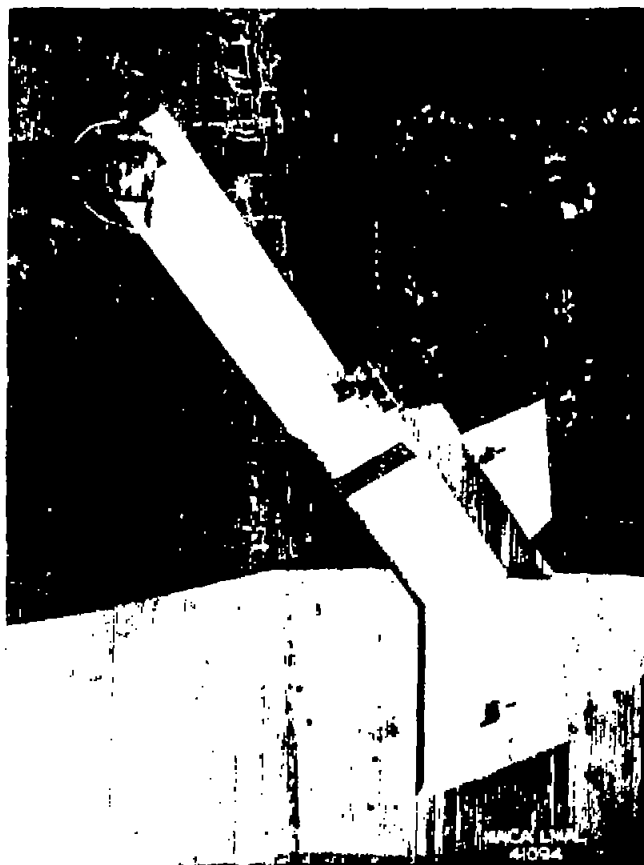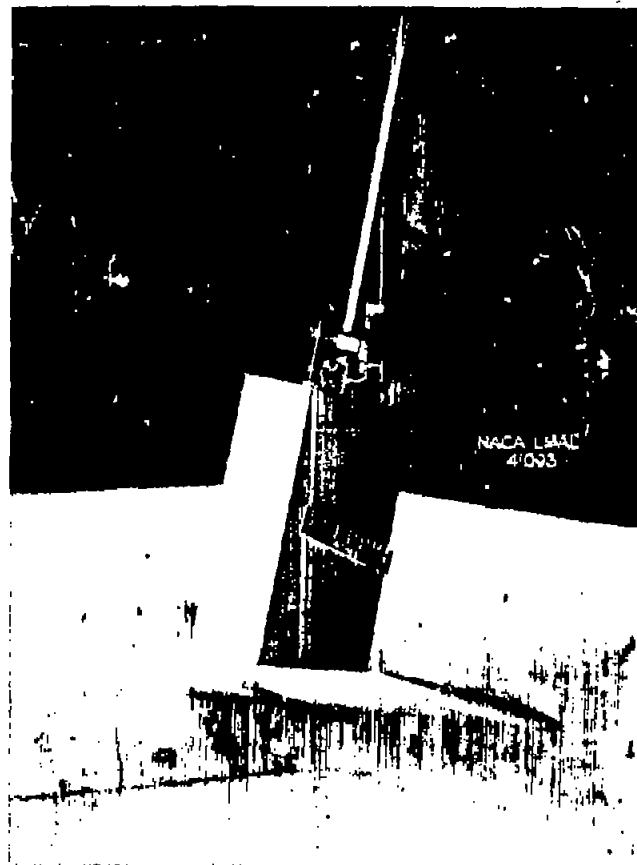
(a) Left-side view.

(b) Right-side view.

Figure 4.- Photographs of vertical tail with horizontal tail in position II.

Fig. 4

Vertical tail

Horizontal tail

Position I
(low forward)

Position II
(low center)

Position III
(low rearward)

Position IV
(high forward)

Position V
(high center)

Position VI
(high rearward)
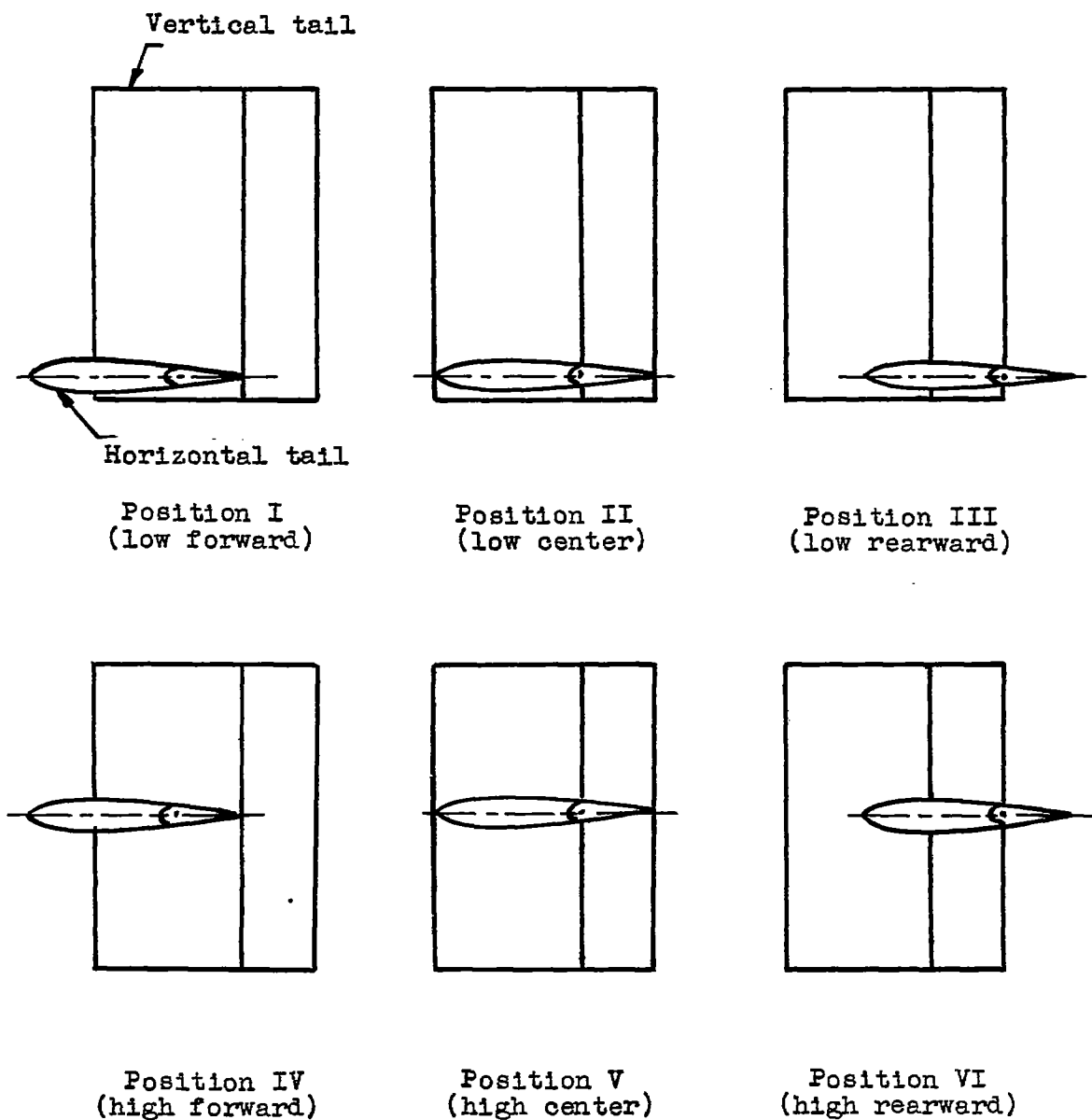
NATIONAL ADVISORY
COMMITTEE FOR AERONAUTICS

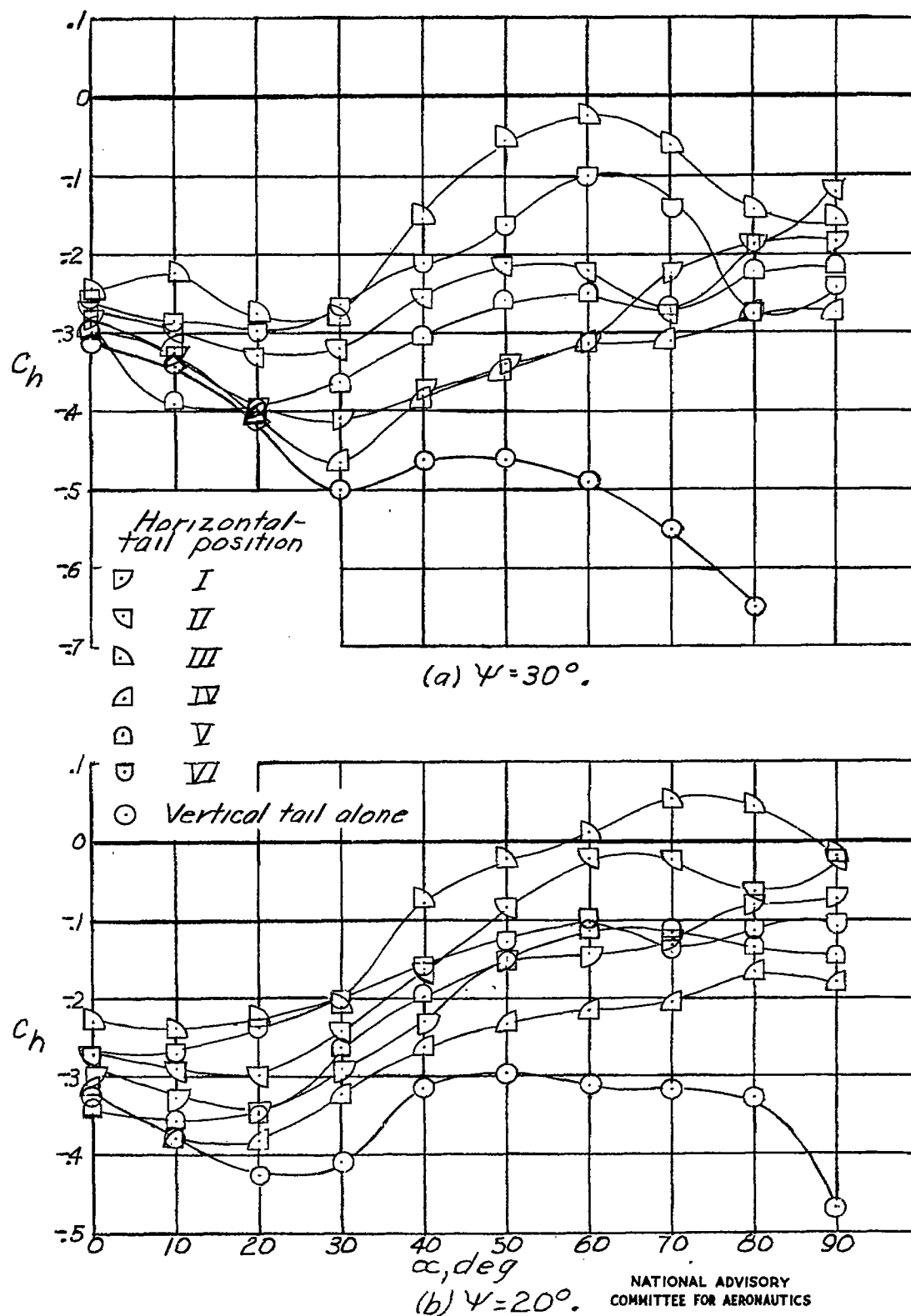Figure 5.- Sketches of vertical tail in six combinations with
horizontal tail.
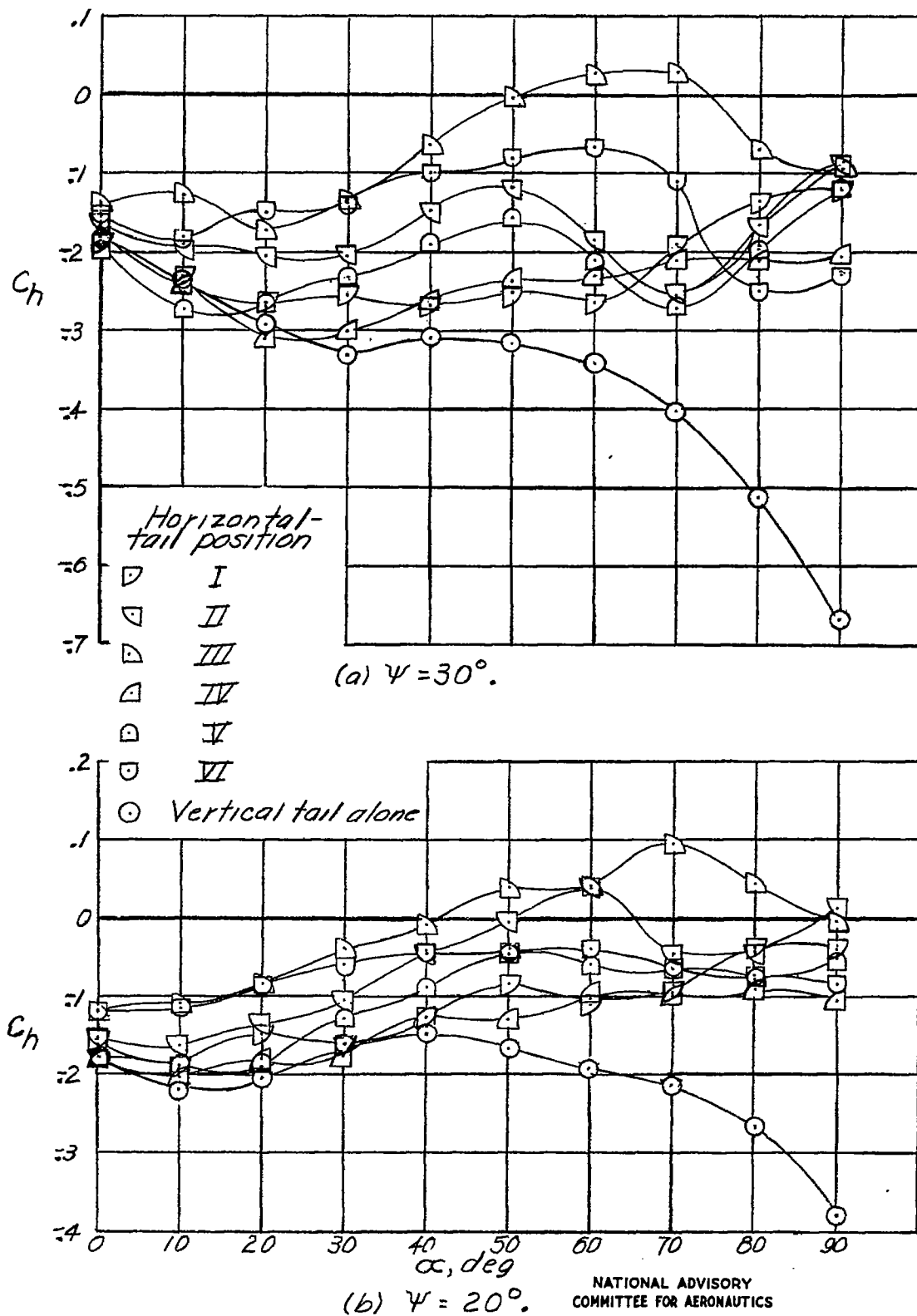
Figure 6.- Rudder hinge-moment coefficient as a function of angle of
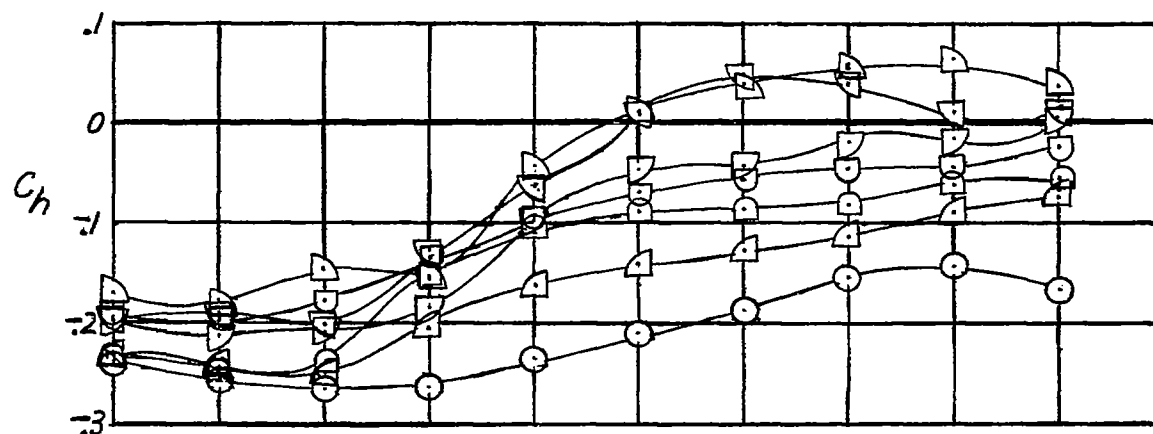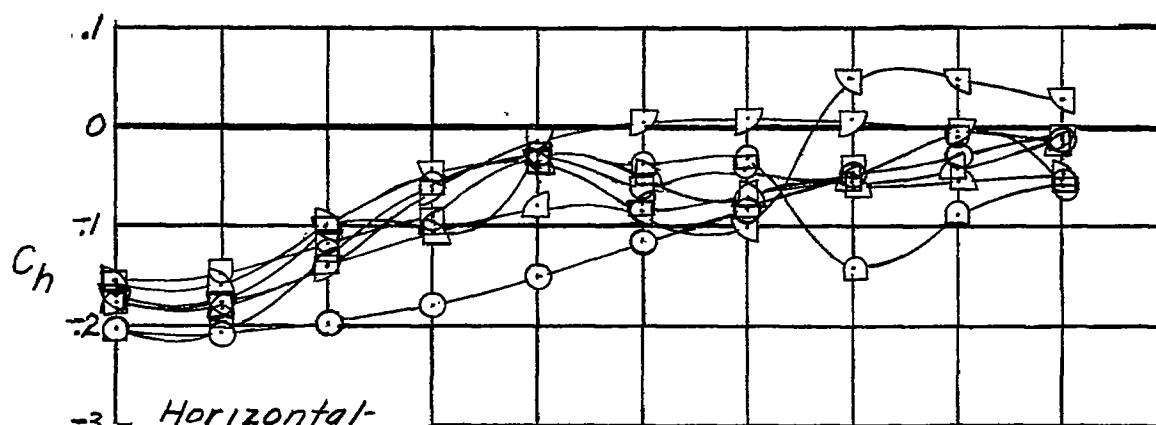   attack at $\delta_r = 0°$ for various angles of yaw and positions of
    horizontal tail.
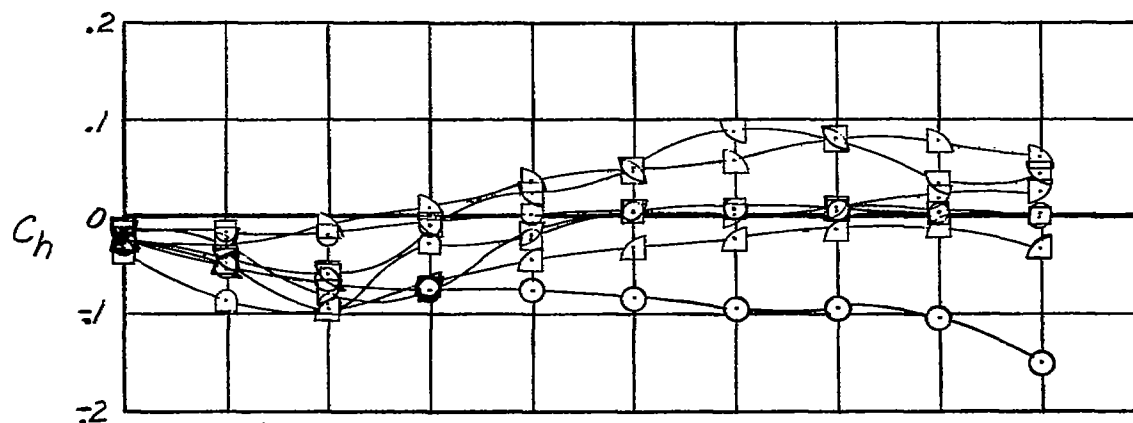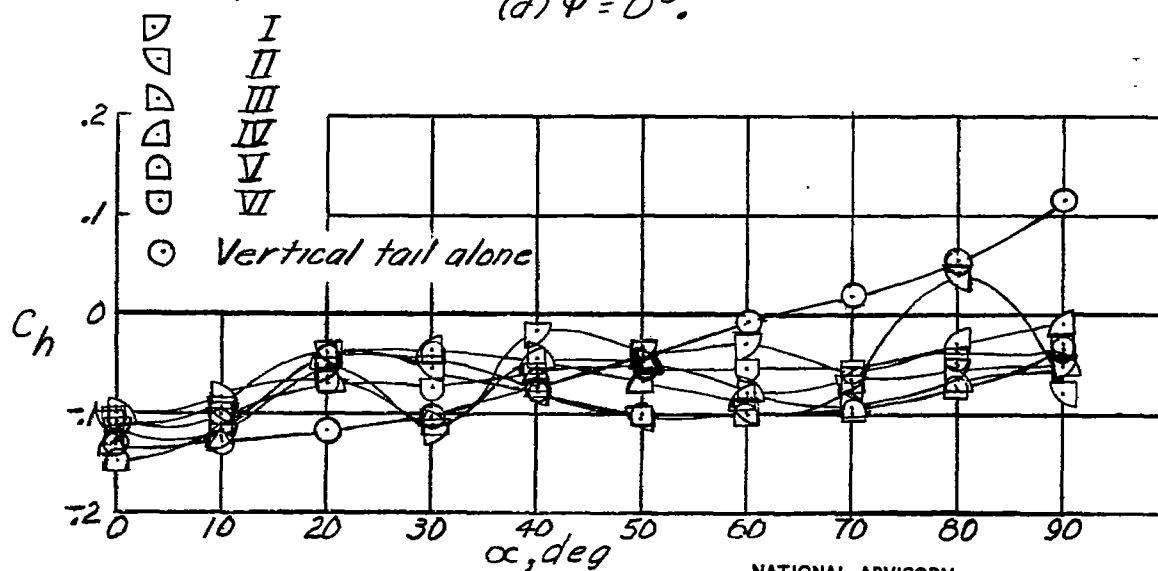
C_h

(c) $\psi = 10°$.

C_h

Horizontal-
tail position

▽   I
◁   II
◁   III
◁   IV
◲   V
◲   VI

(d) $\psi = 0°$.

⊙   Vertical tail alone

C_h

α, deg

(e) $\psi = -10°$.

Figure 6.- Continued.

C_h

Horizontal-
tail position

(f) $\psi = -20°$.

▽	I
◁	II
◁	III
◁	IV
◻	V
◻	VI
⊙	Vertical tail alone

C_h

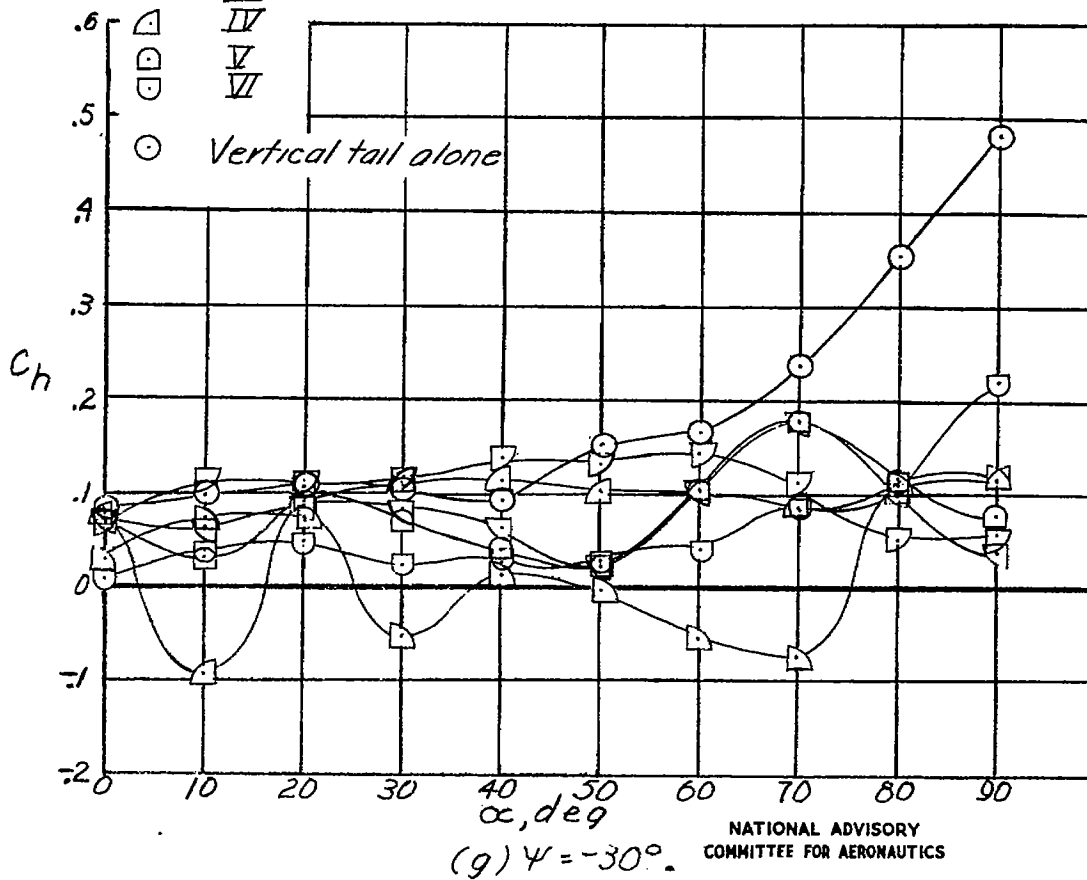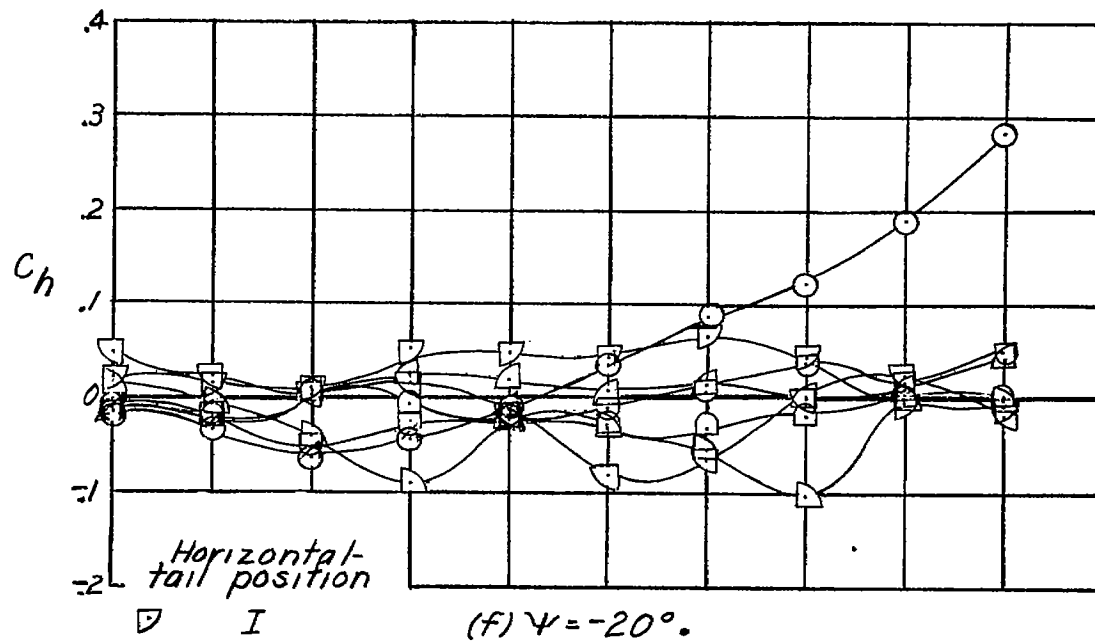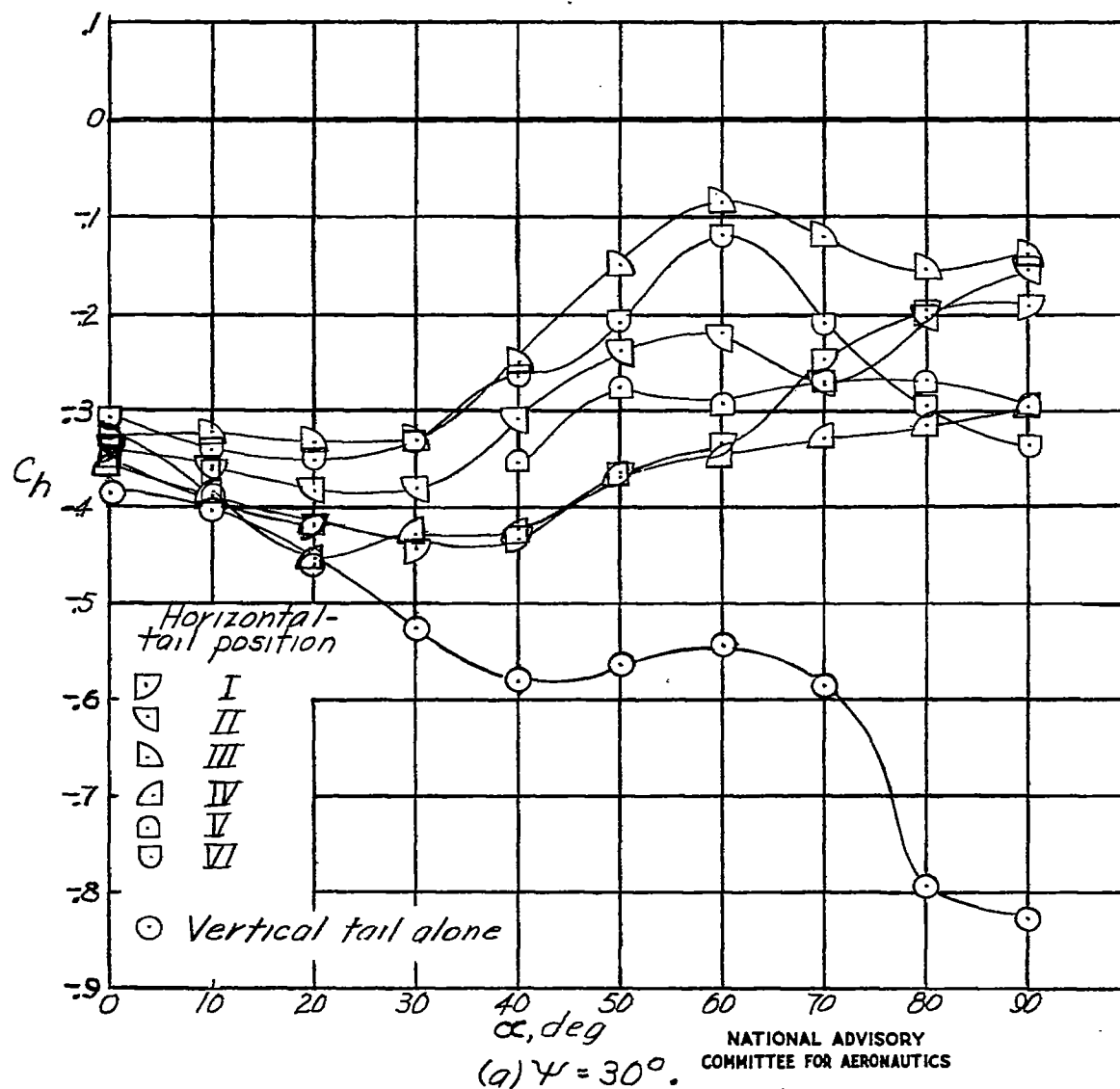α, deg

(g) $\psi = -30°$.
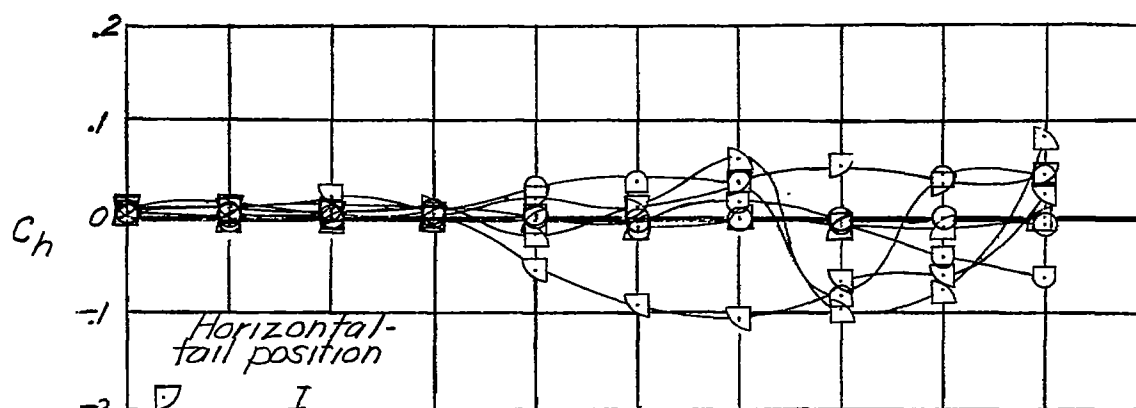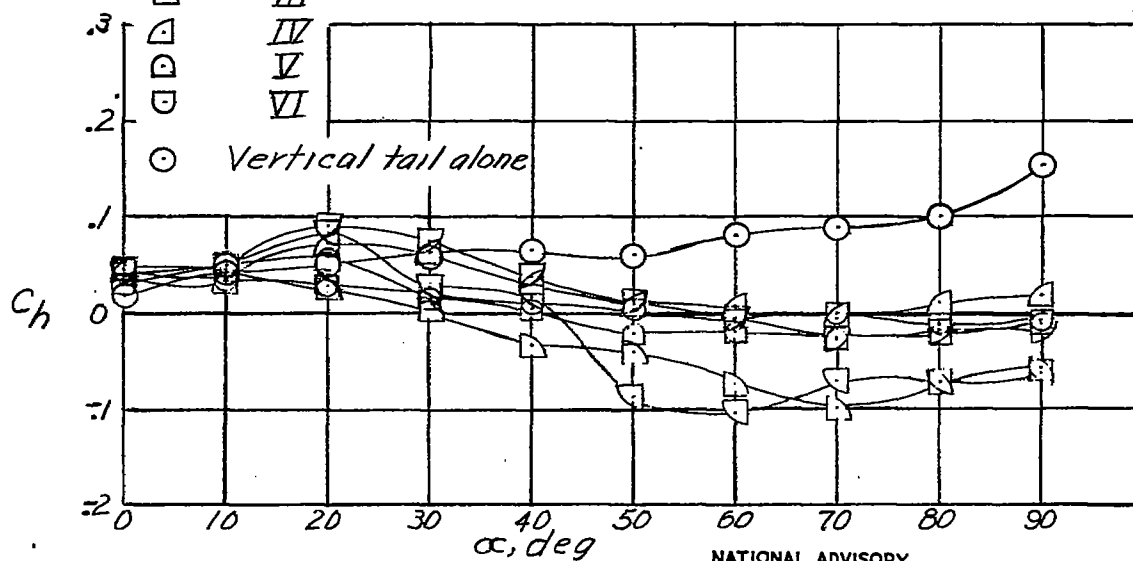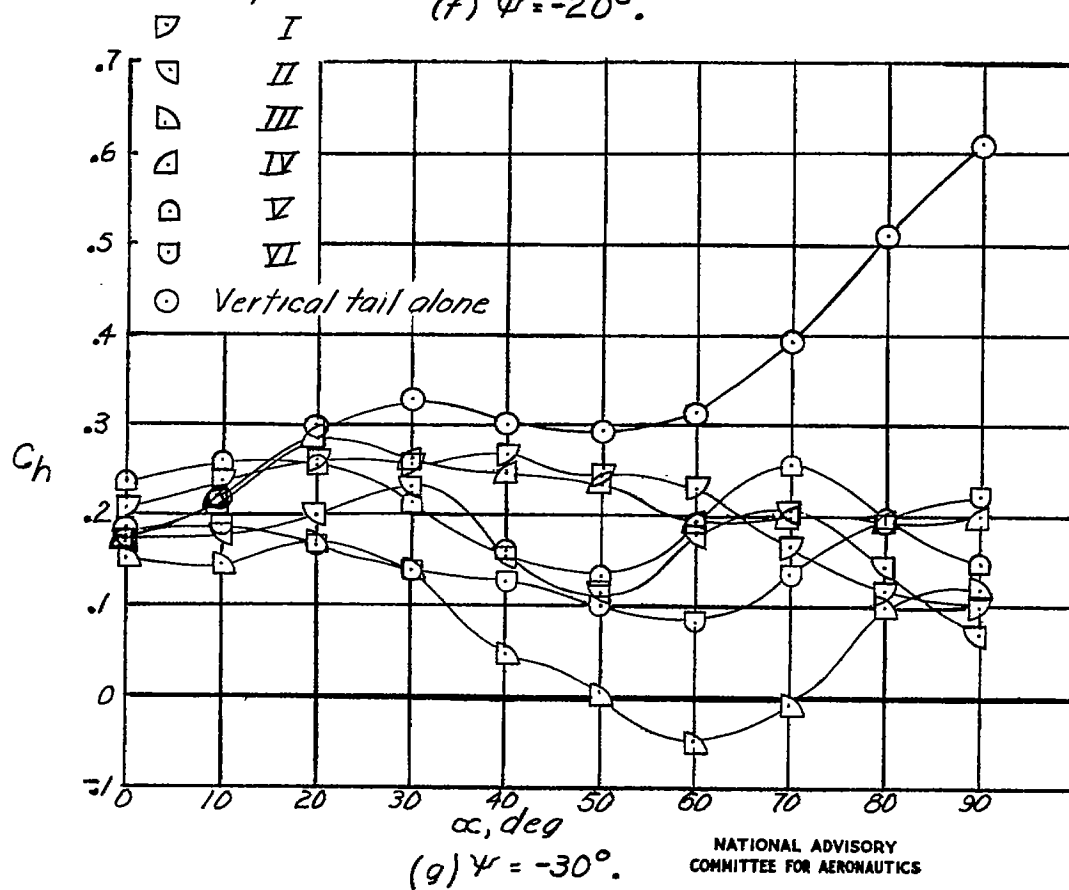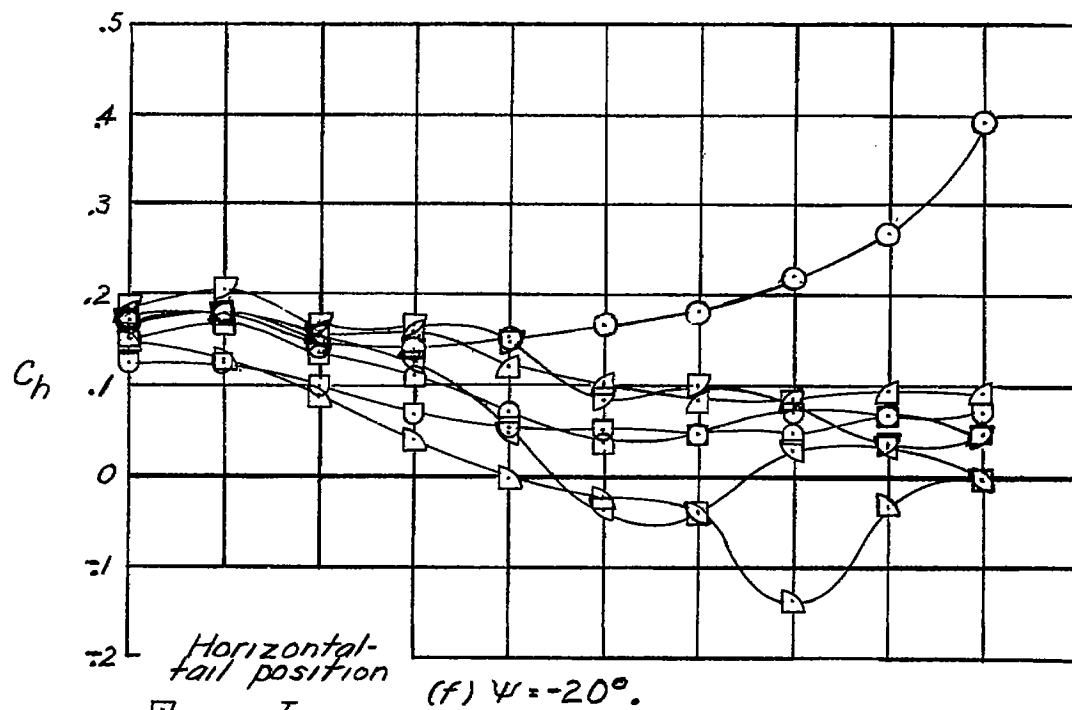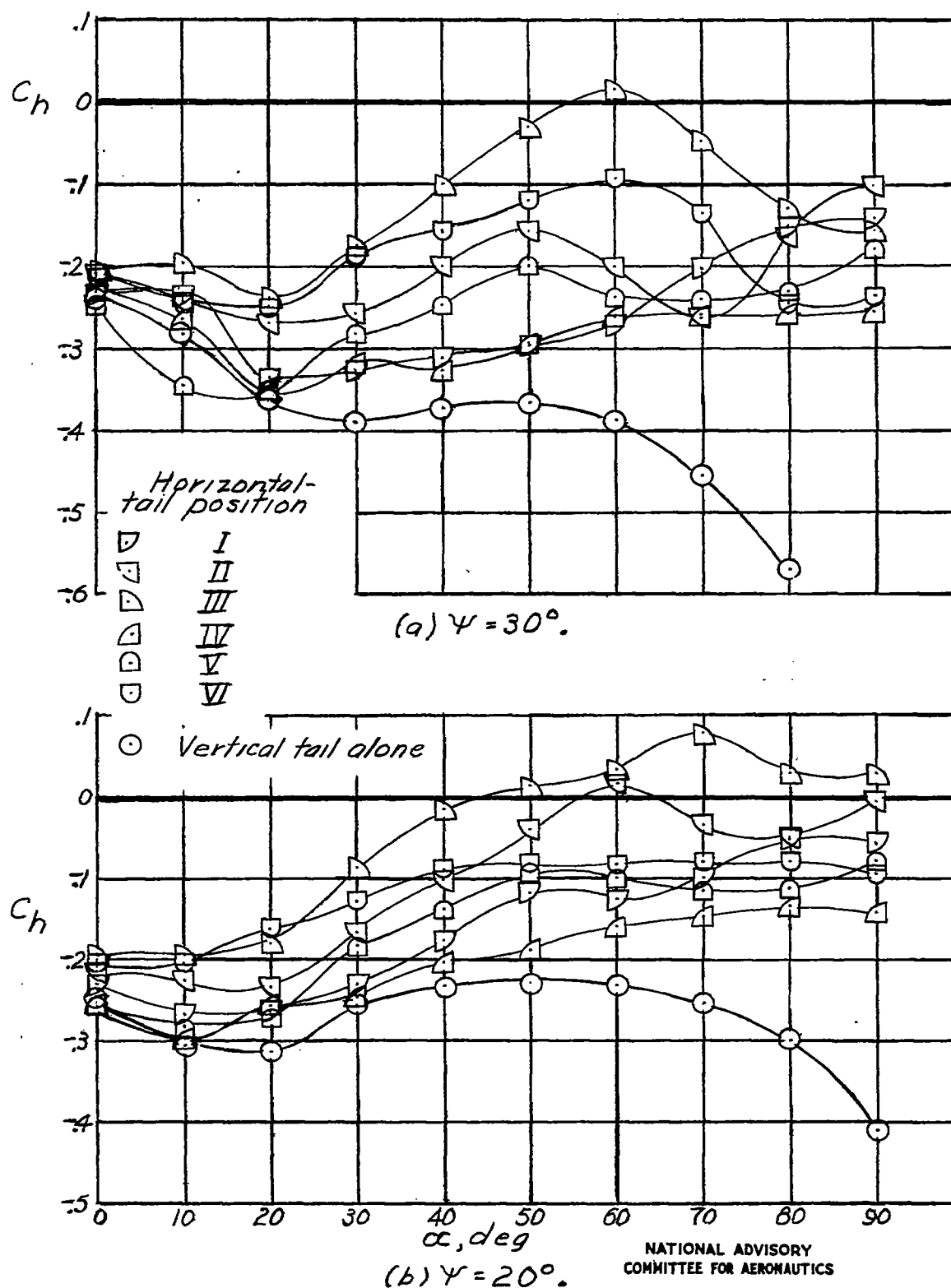
Figure 6.- Concluded.

Figure 7.- Rudder hinge-moment coefficient as a function of angle of attack at $\delta_r = 10^\circ$ for various angles of yaw and positions of horizontal tail.

(c) $\psi = 10°$.

(d) $\psi = 0°$.

Horizontal-tail position

I
II
III
IV
V
VI

Vertical tail alone

(e) $\psi = -10°$.

Figure 7.- Continued.

(f) $\Psi = -20°$.

Horizontal-tail position

I
II
III
IV
V
VI

⊙ Vertical tail alone

(g) $\Psi = -30°$.

α, deg

NATIONAL ADVISORY
COMMITTEE FOR AERONAUTICS

Figure 7.- Concluded.

(a) $\Psi = 30°$.

(b) $\Psi = 20°$.

Horizontal-tail position

▽	I
◁	II
▷	III
△	IV
◻	V
◻	VI
⊙	Vertical tail alone

α, deg
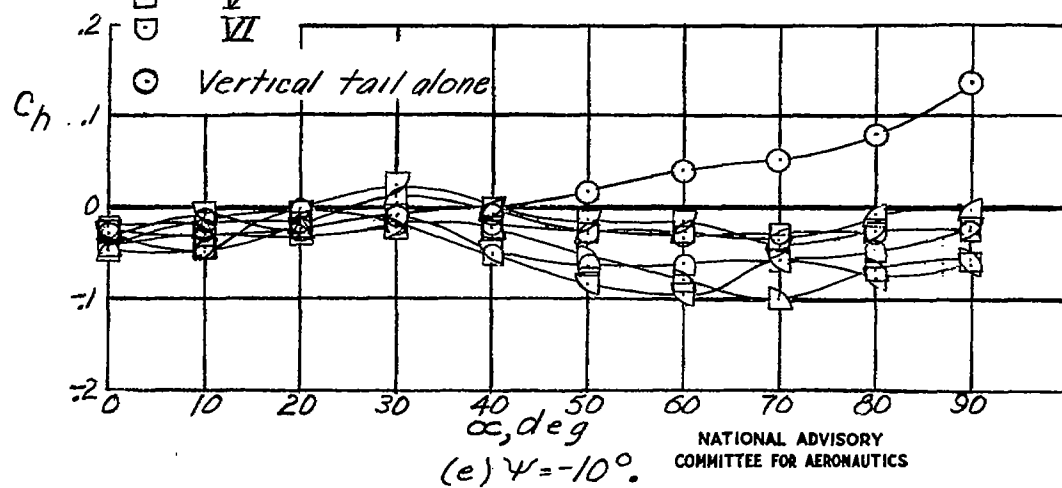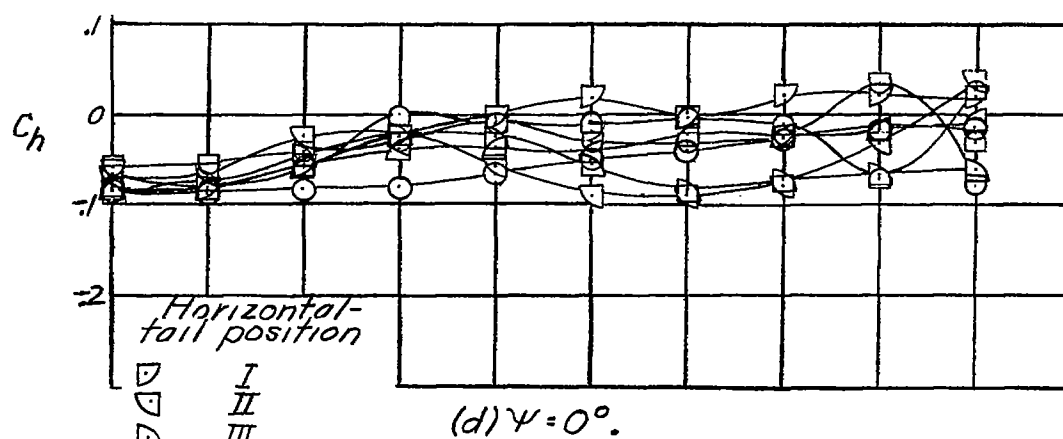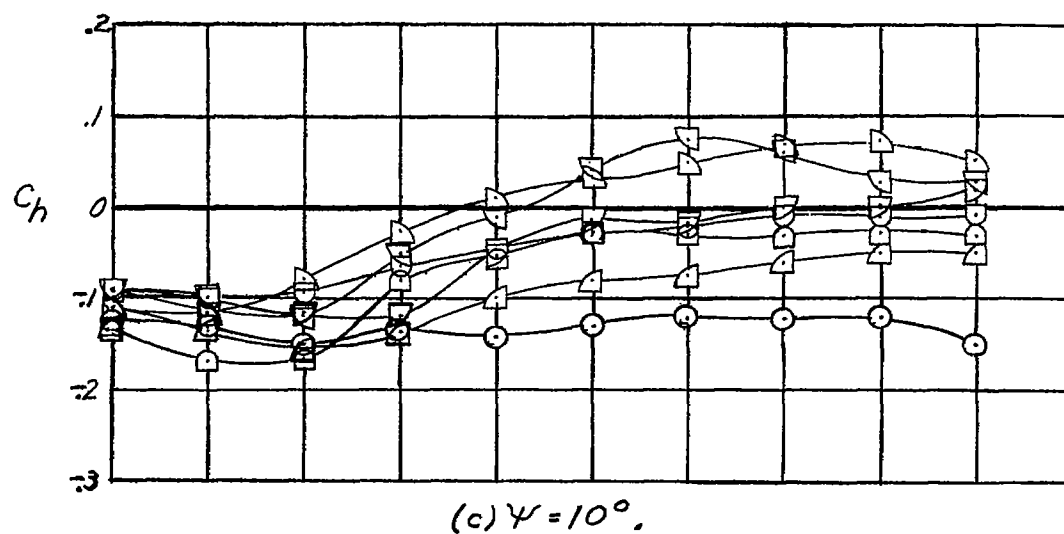
NATIONAL ADVISORY
COMMITTEE FOR AERONAUTICS
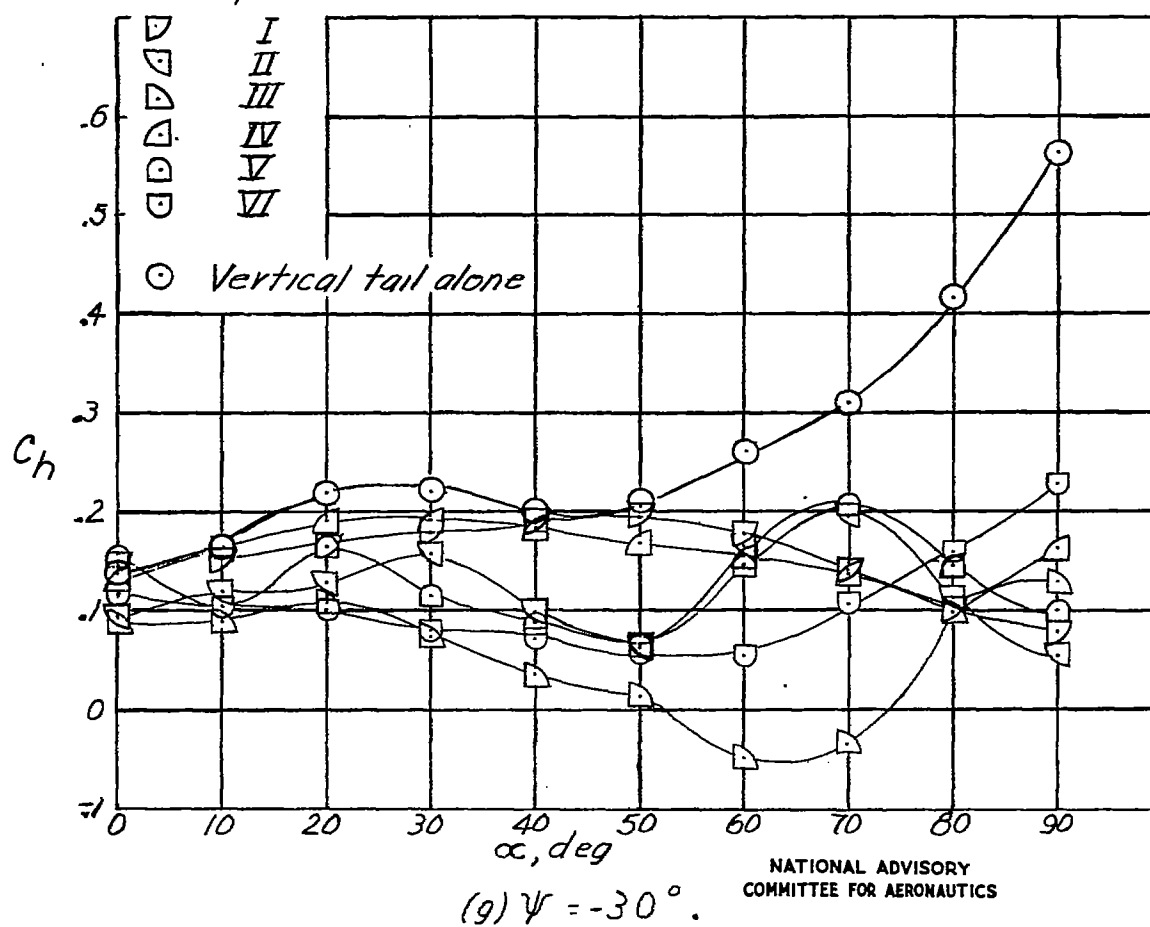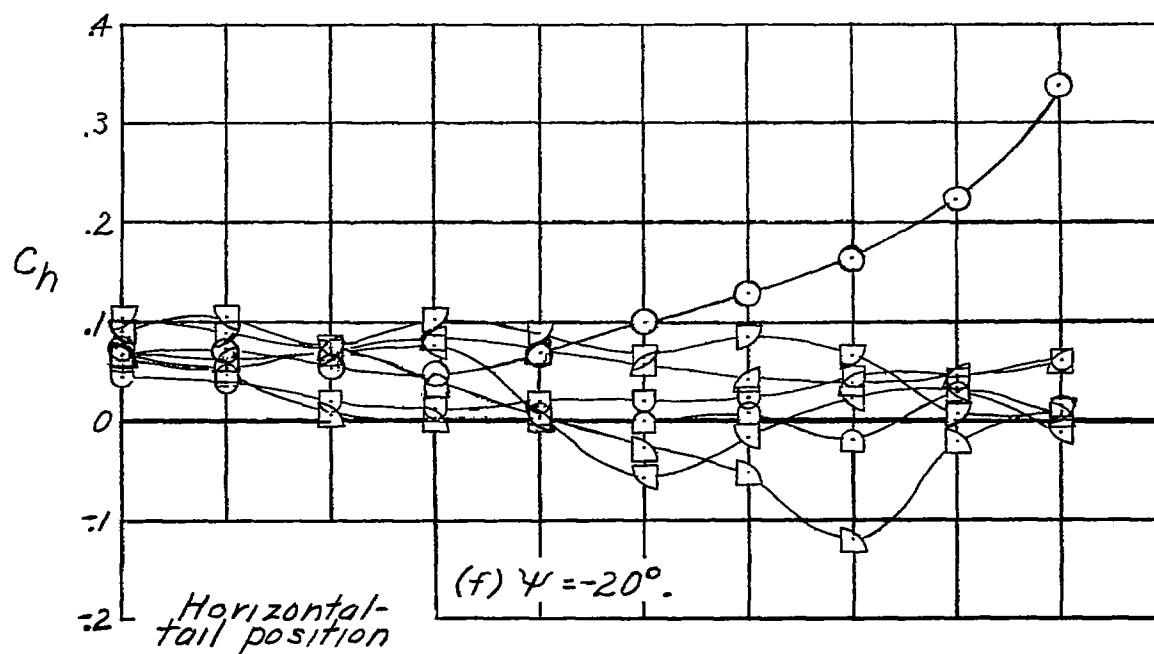
Figure 8.- Rudder hinge-moment coefficient as a function of angle of attack at $\delta_r = 20°$ for various angles of yaw and positions of horizontal tail.
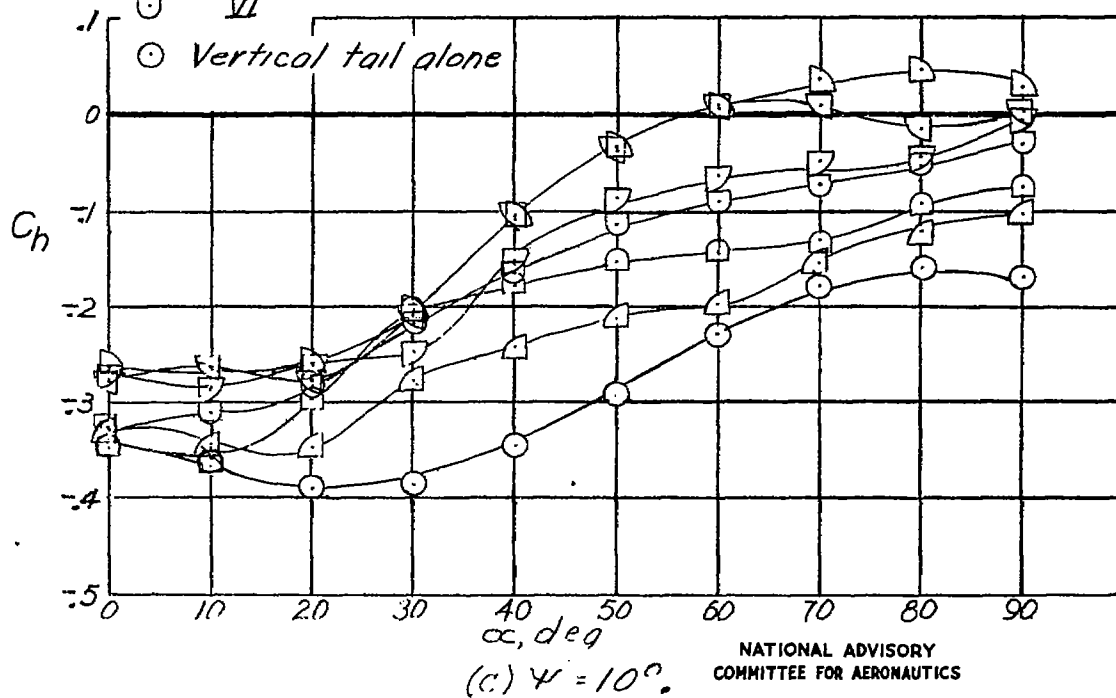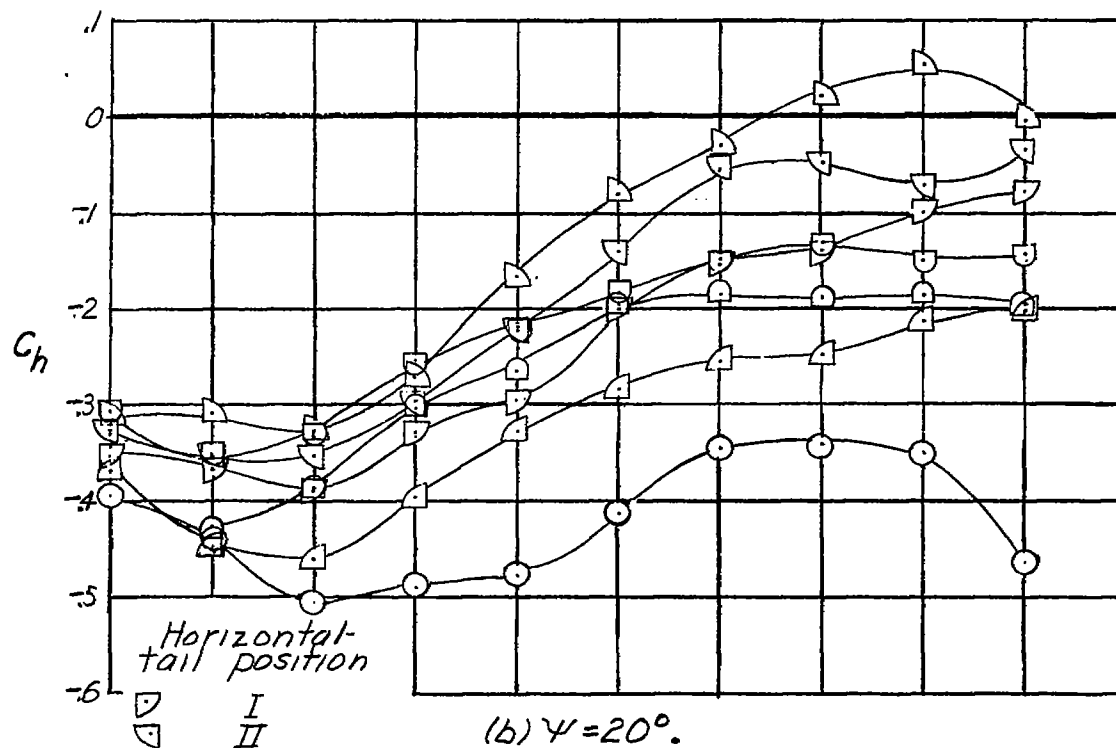
(c) $\psi = 10°$.

(d) $\psi = 0°$.

Horizontal-tail position

I
II
III
IV
V
VI

Vertical tail alone

(e) $\psi = -10°$.

Figure 8.- Continued.

(f) $\Psi = -20°$.

Horizontal-tail position

I
II
III
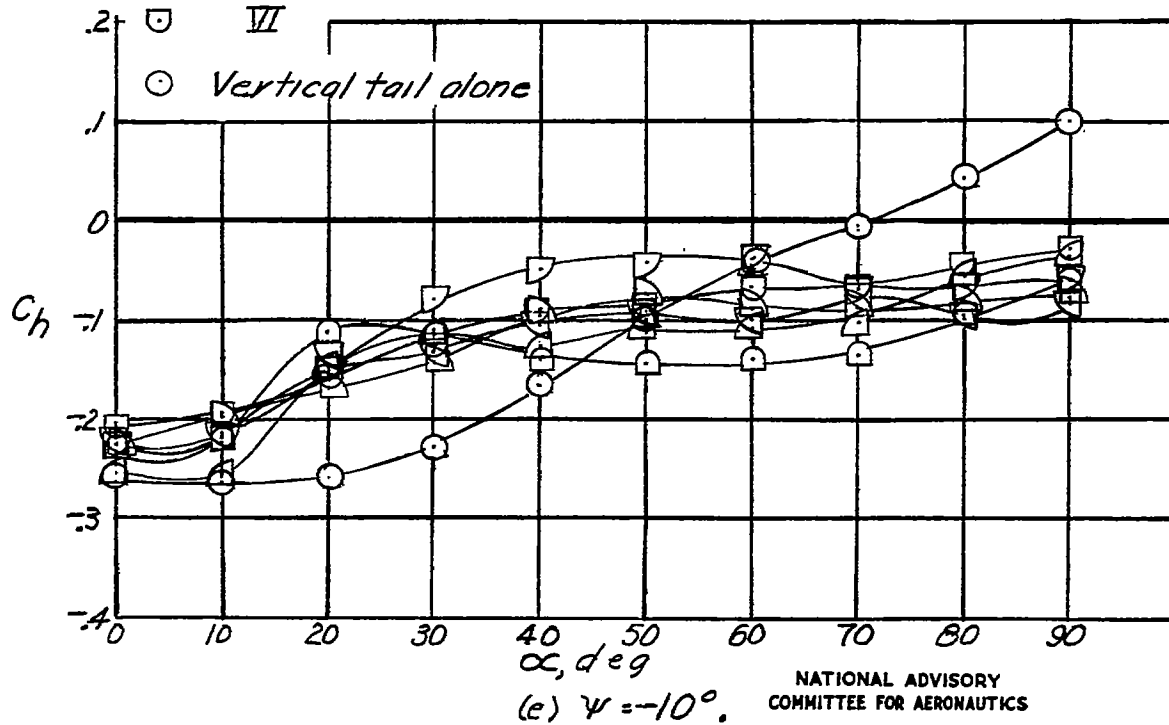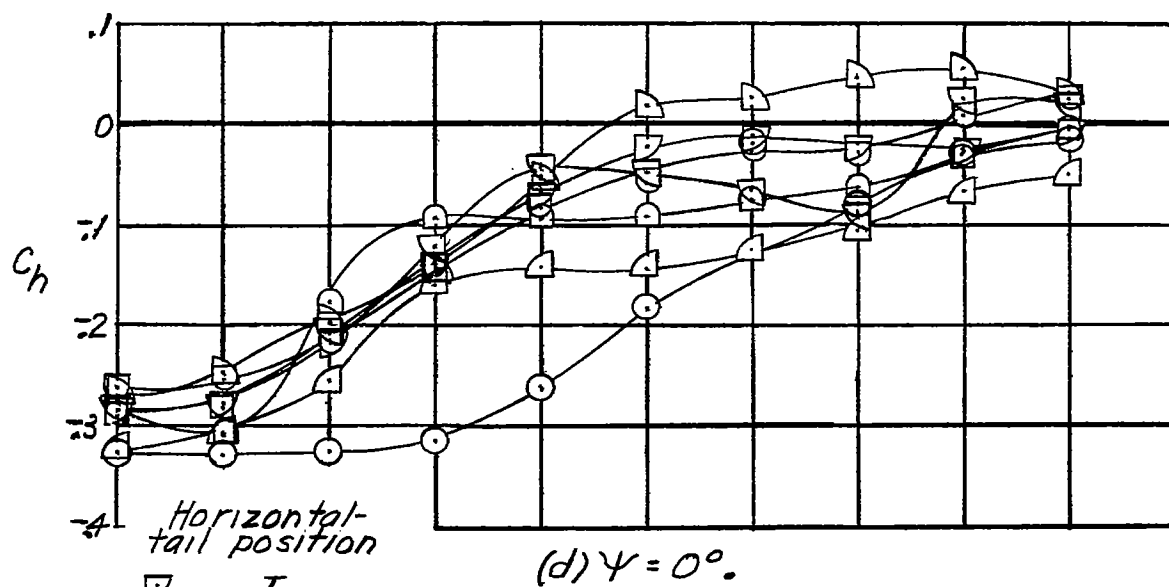IV
V
VI

⊙ Vertical tail alone

(g) $\Psi = -30°$.

α, deg

NATIONAL ADVISORY
COMMITTEE FOR AERONAUTICS

Figure 8.- Concluded.

(a) $\Psi = 30°$.

Figure 9.- Rudder hinge-moment coefficient as a function of angle of attack at $\delta_r = 30°$ for various angles of yaw and positions of horizontal tail.

C_h

Horizontal-
tail position

▽	I
◁	II
◸	III
◺	IV
⊡	V
⊡	VI

(b) $\Psi = 20°$.

⊙ Vertical tail alone

C_h

α, deg

(c) $\Psi = 10°$.

Figure 9.- Continued.

(d) $\psi = 0°$.

Horizontal-
tail position

▽ ◁	I
◁ ◁	II
▷ ◁	III
△ ◁	IV
⊕ ◁	V
⊖ ◁	VI

⊙   Vertical tail alone

(e) $\psi = -10°$.

α, deg

Figure 9.- Continued.

Horizontal-
tail position

C_h

(f) $\Psi = -20°$.

I
II
III
IV
V
VI
Vertical tail alone

C_h

α, deg

(g) $\Psi = -30°$.
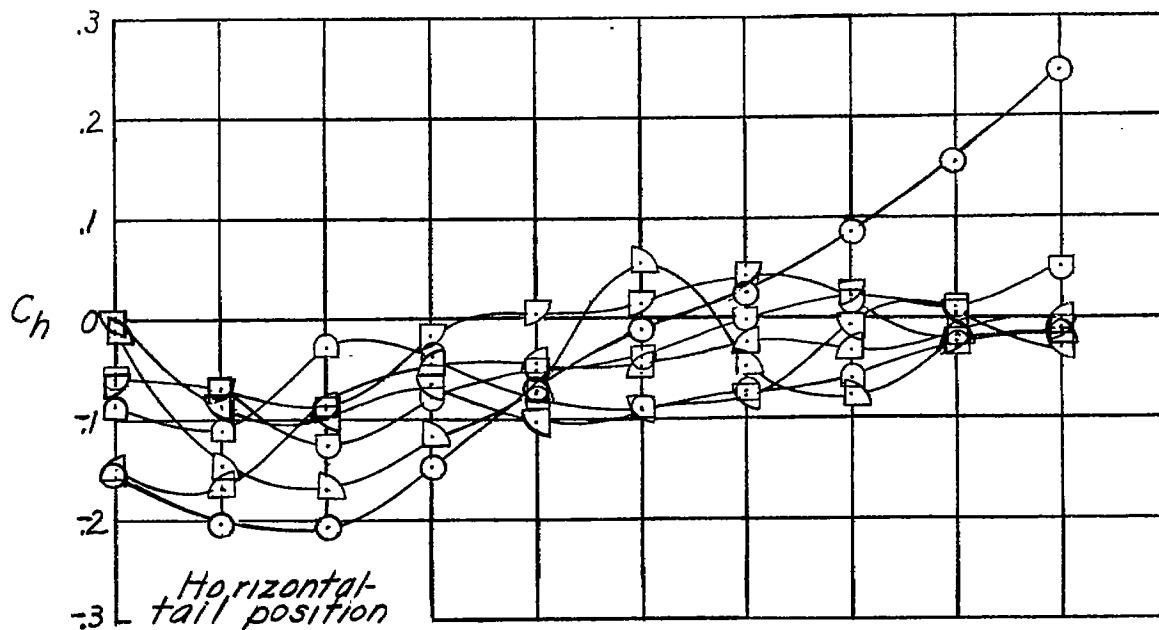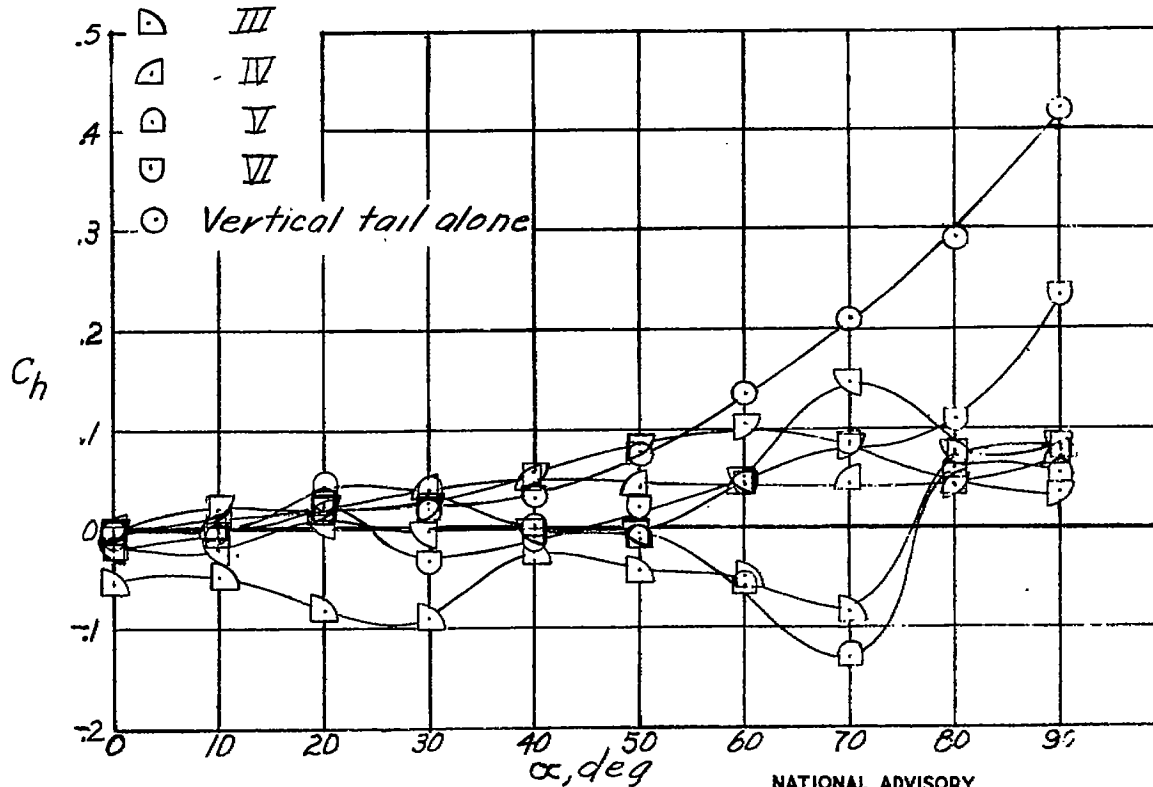
Figure 9.- Concluded.
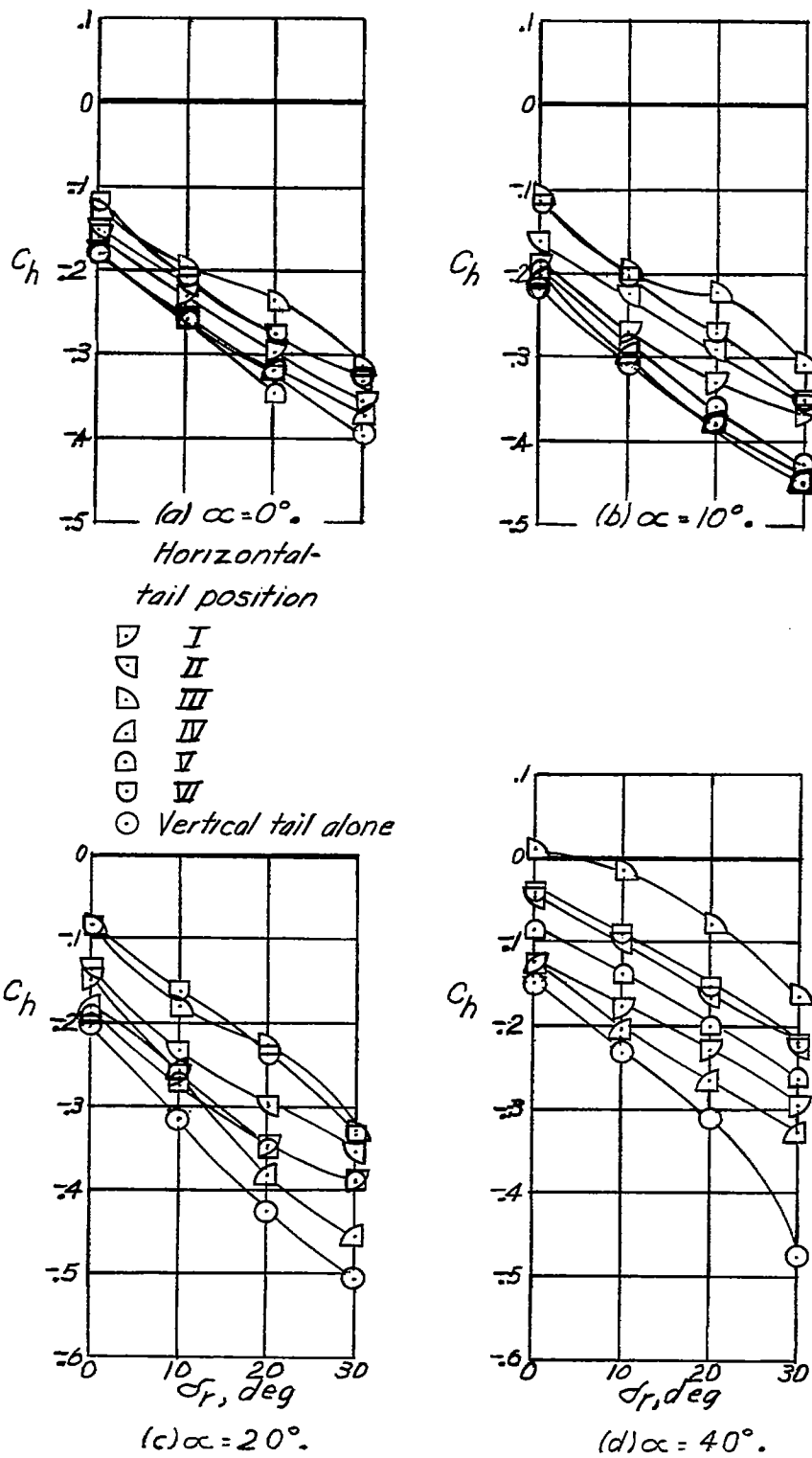
Figure 10.- Rudder hinge-moment coefficient as a function of rudder deflection at $\psi = 20°$ for various angles of attack and positions of horizontal tail.

(e) $\alpha = 60°$.

(f) $\alpha = 80°$.
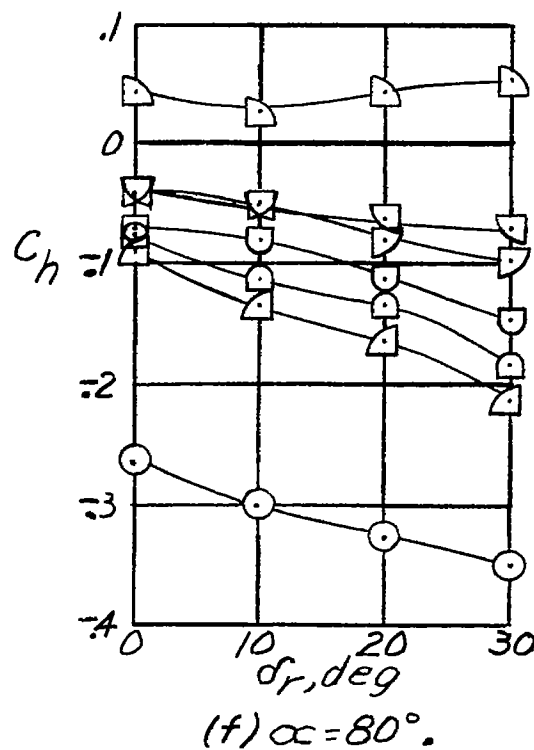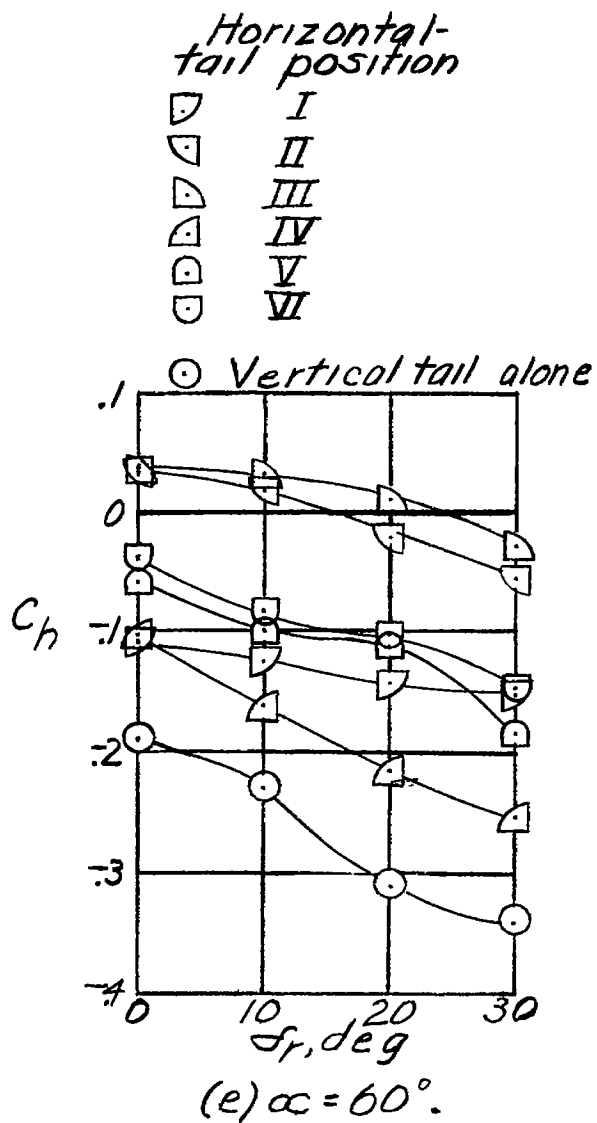
Figure 10.- Concluded.

(a) $\alpha = 0°$.

(b) $\alpha = 10°$.

Horizontal-
tail position

▽   I
◁   II
◁   III
◁   IV
◎   V
◎   VI
⊙   Vertical tail alone

(c) $\alpha = 20°$.

(d) $\alpha = 40°$.
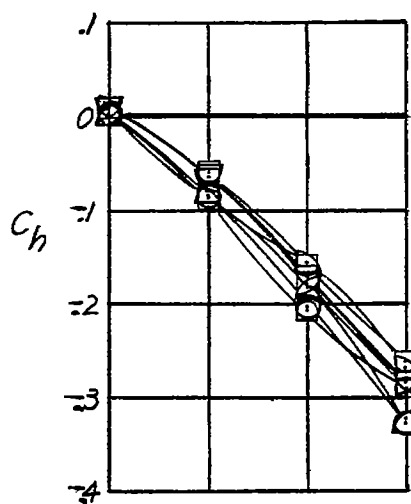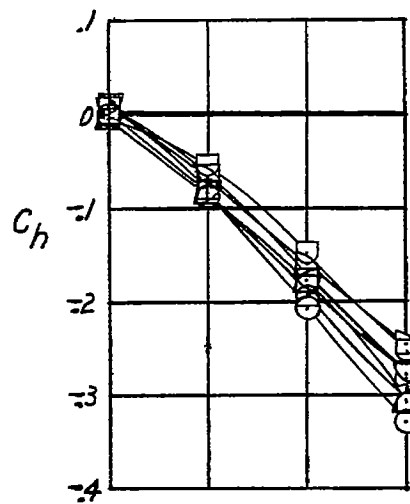
Figure 11.- Rudder hinge-moment coefficient as a function of rudder
    deflection at $\psi = 0°$ for various angles of attack and positions
    of horizontal tail.

(e) $\alpha = 60°$.

(f) $\alpha = 80°$.

NATIONAL ADVISORY
COMMITTEE FOR AERONAUTICS

Figure 11.- Concluded.

(a) $\alpha = 0°$.

(b) $\alpha = 10°$.

Horizontal-
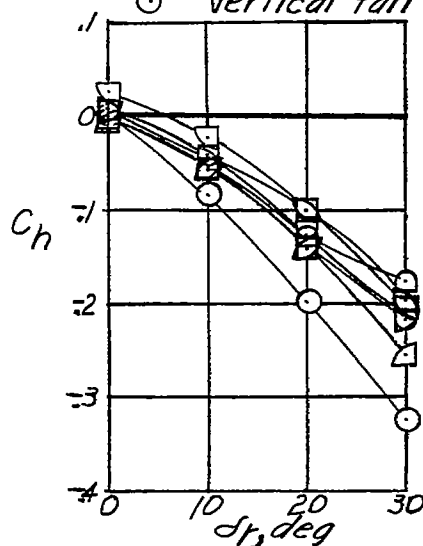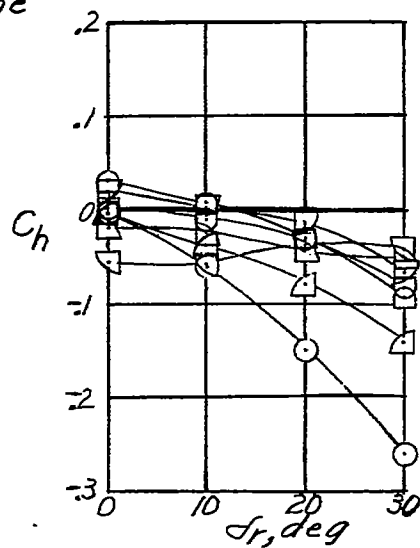tail position

I
II
III
IV
V
VI

⊙ Vertical tail alone

(c) $\alpha = 20°$.
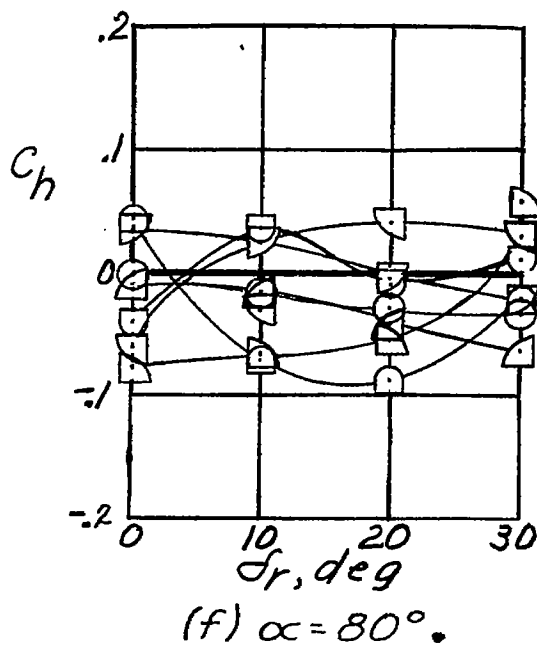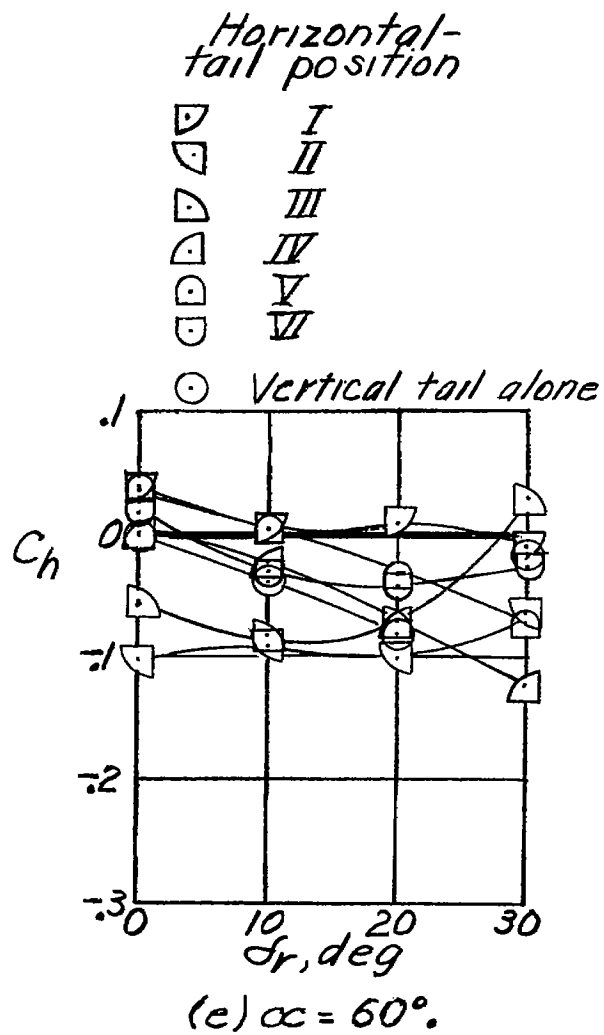
(d) $\alpha = 40°$.
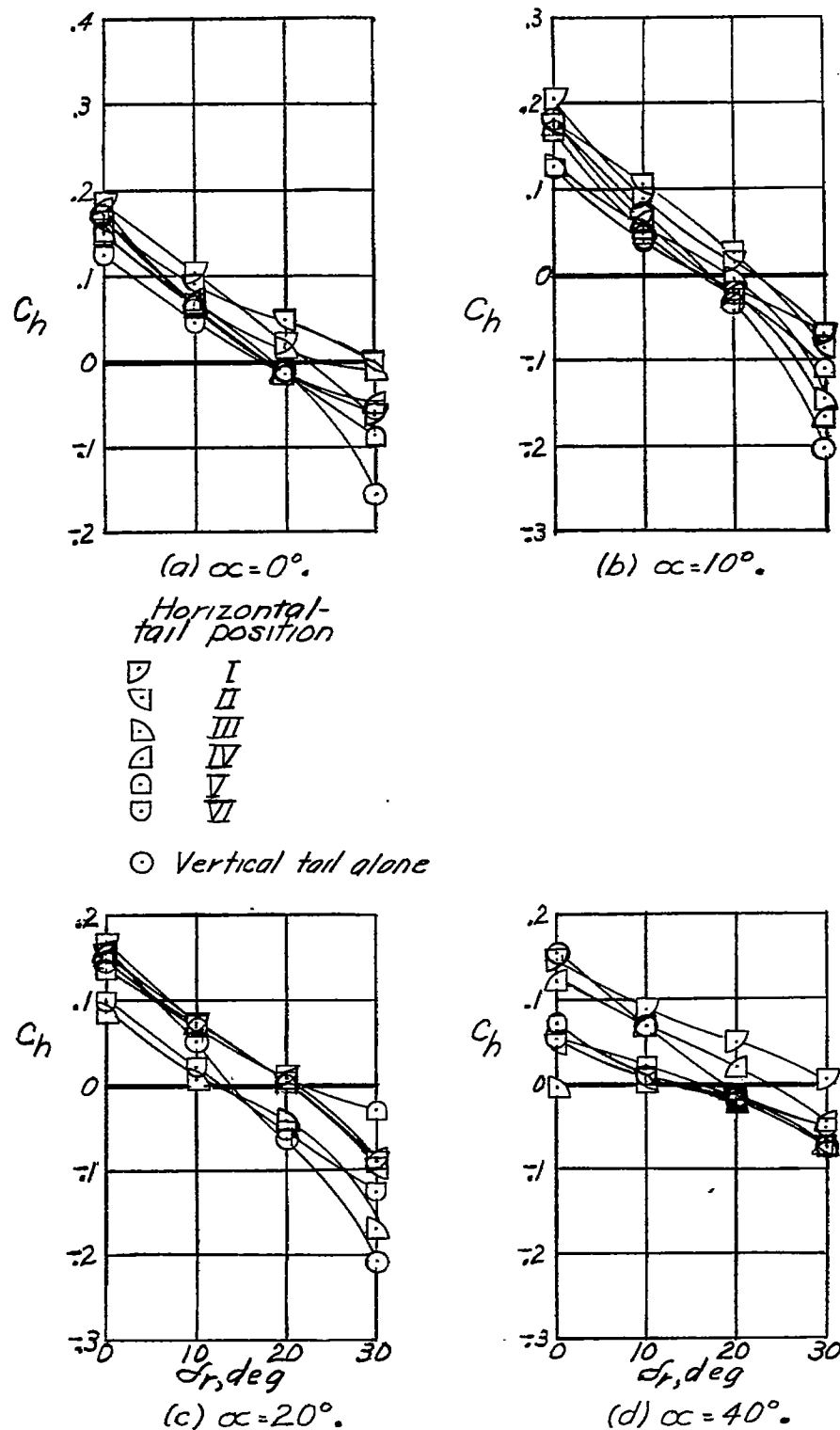
Figure 12.- Rudder hinge-moment coefficient as a function of rudder
deflection at $\psi = -20°$ for various angles of attack and positions
of horizontal tail.

Horizontal-
tail position

▽	I
◁	II
◁	III
◁	IV
◁	V
◁	VI

⊙   Vertical tail alone

(e) $\alpha = 60°$

(f) $\alpha = 80°$.

NATIONAL ADVISORY
COMMITTEE FOR AERONAUTICS

Figure 12.-   Concluded.

C_h

Horizontal-
tail position

I
II
III
IV
V
VI

⊙ Vertical tail alone

(a) $\alpha = 0°$.

(b) $\alpha = 10°$.

Ψ, deg

Figure 13.- Rudder hinge-moment coefficient as a function of angle of
yaw at $\delta_r = 0°$ for various angles of attack and positions of
horizontal tail.
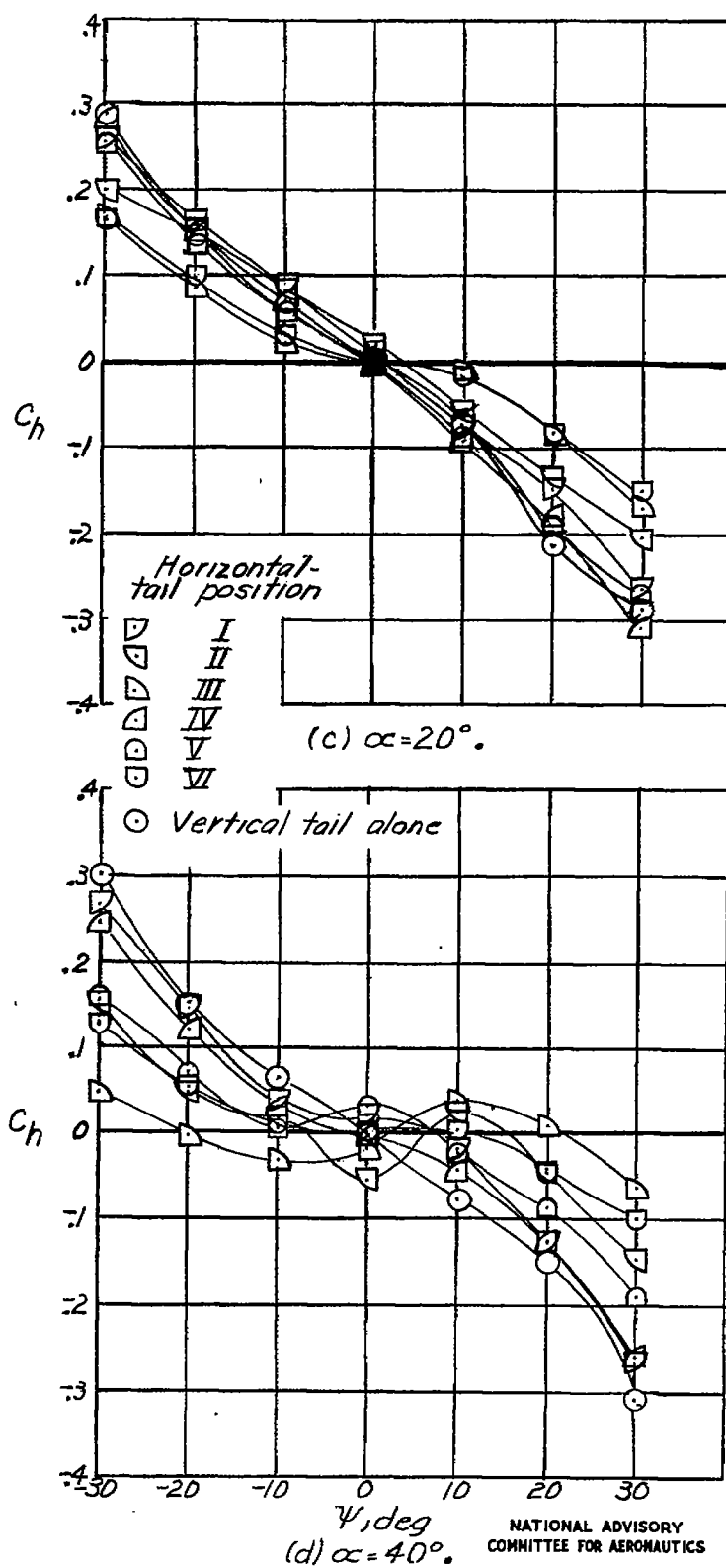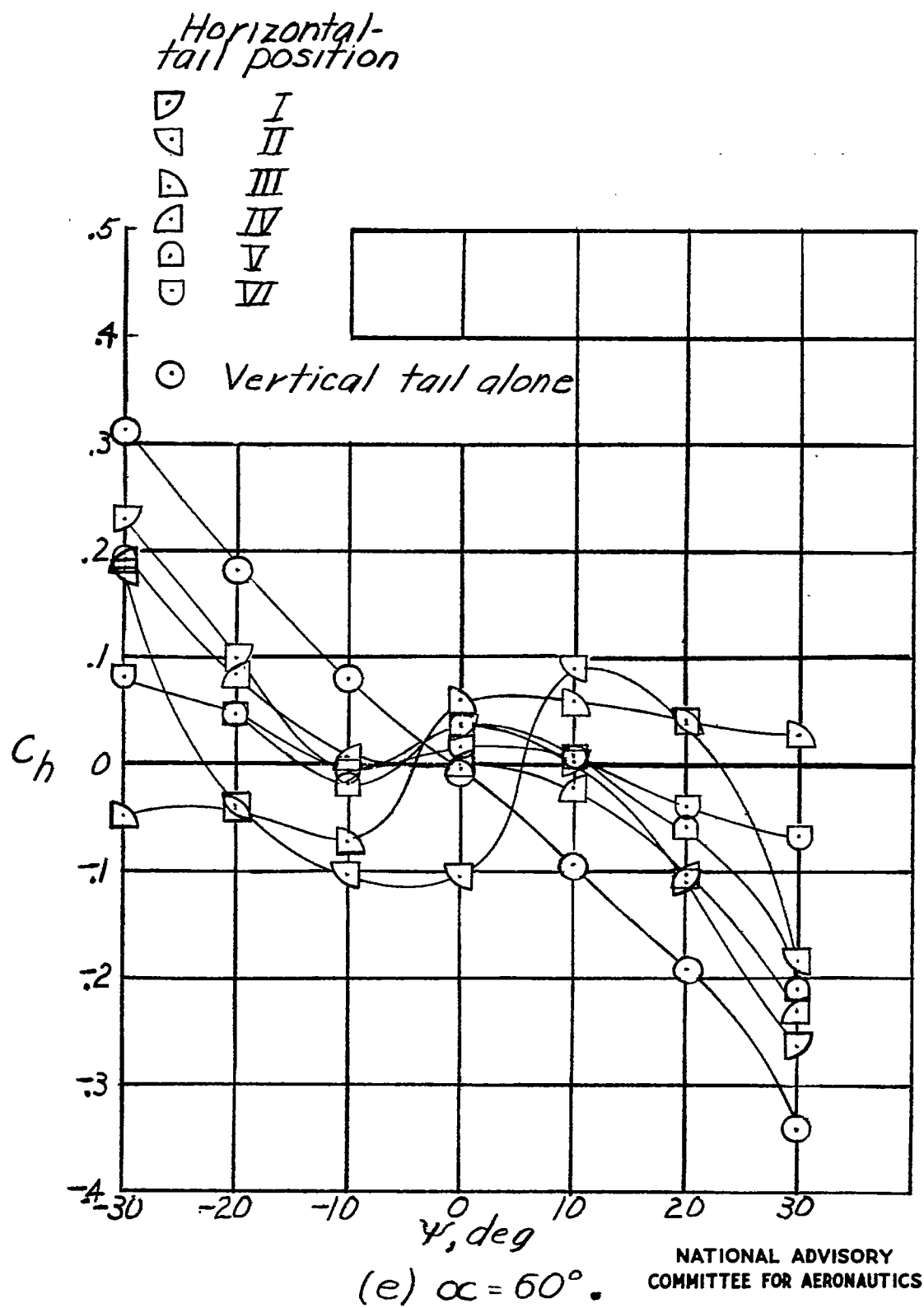
(c) $\alpha = 20°$.

(d) $\alpha = 40°$.

Figure 13.- Continued.

Horizontal-
tail position

I
II
III
IV
V
VI

⊙   Vertical tail alone

C_h

ψ, deg

(e) $\alpha = 60°$.

Figure 13.- Continued.

Horizontal-
tail position

I
II
III
IV
V
VI

Vertical tail alone

Ψ, deg

(f) $\alpha = 80°$.
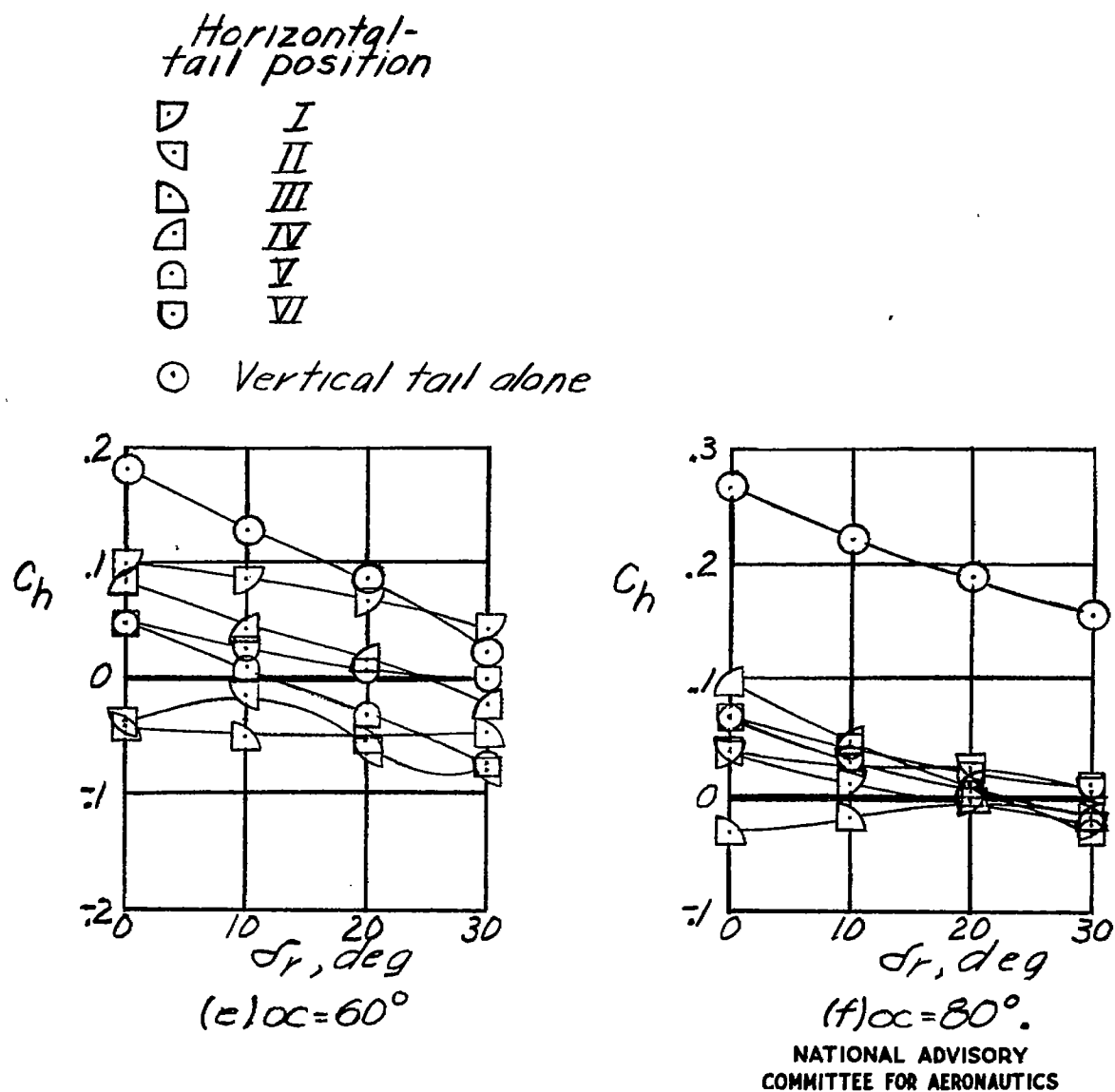
Figure 13.- Concluded.

(a) $\alpha = 0°$.

(b) $\alpha = 10°$.
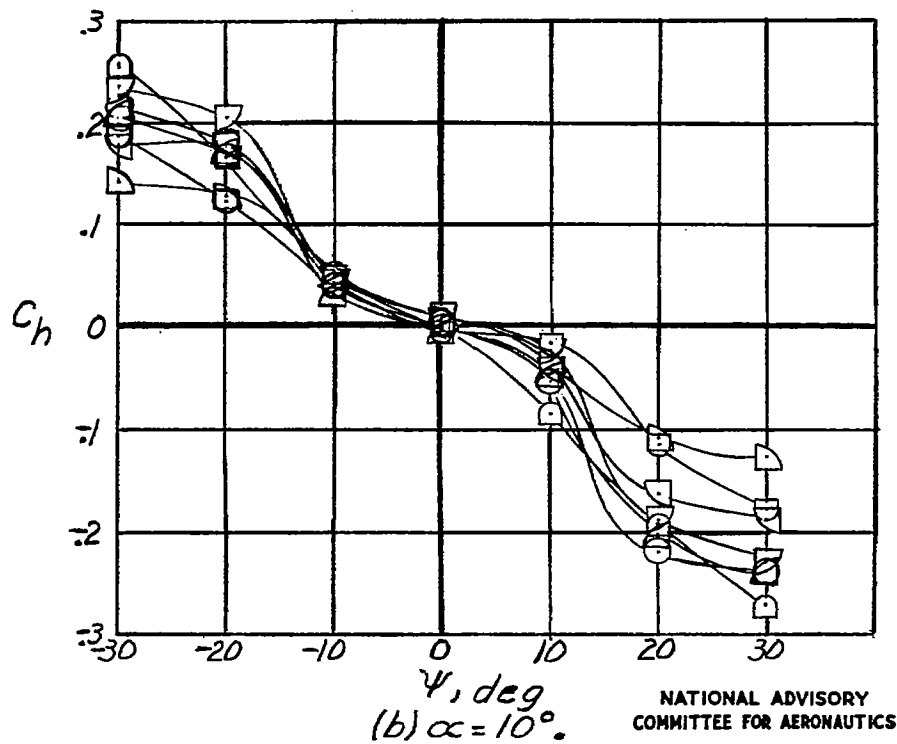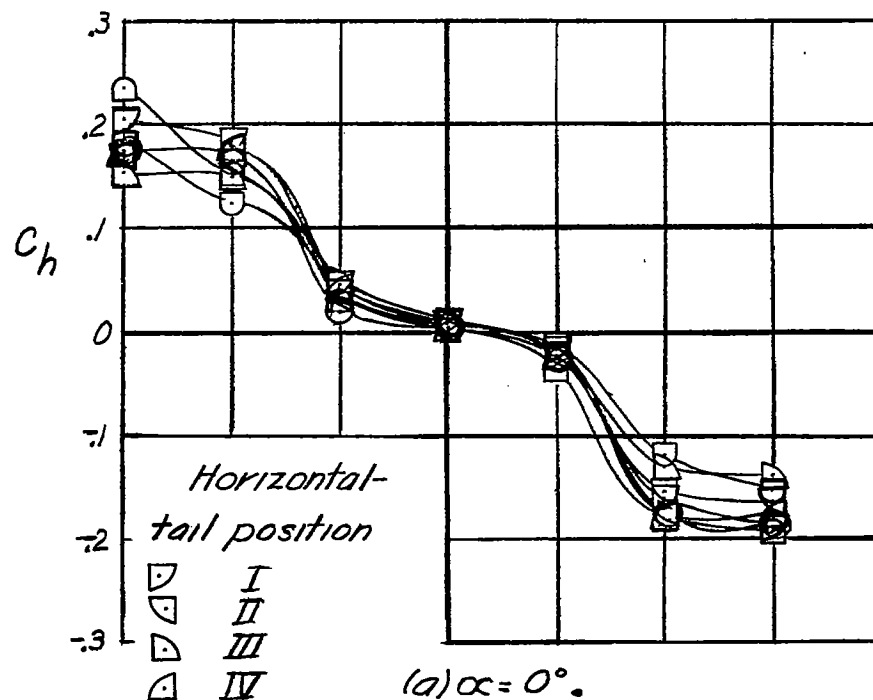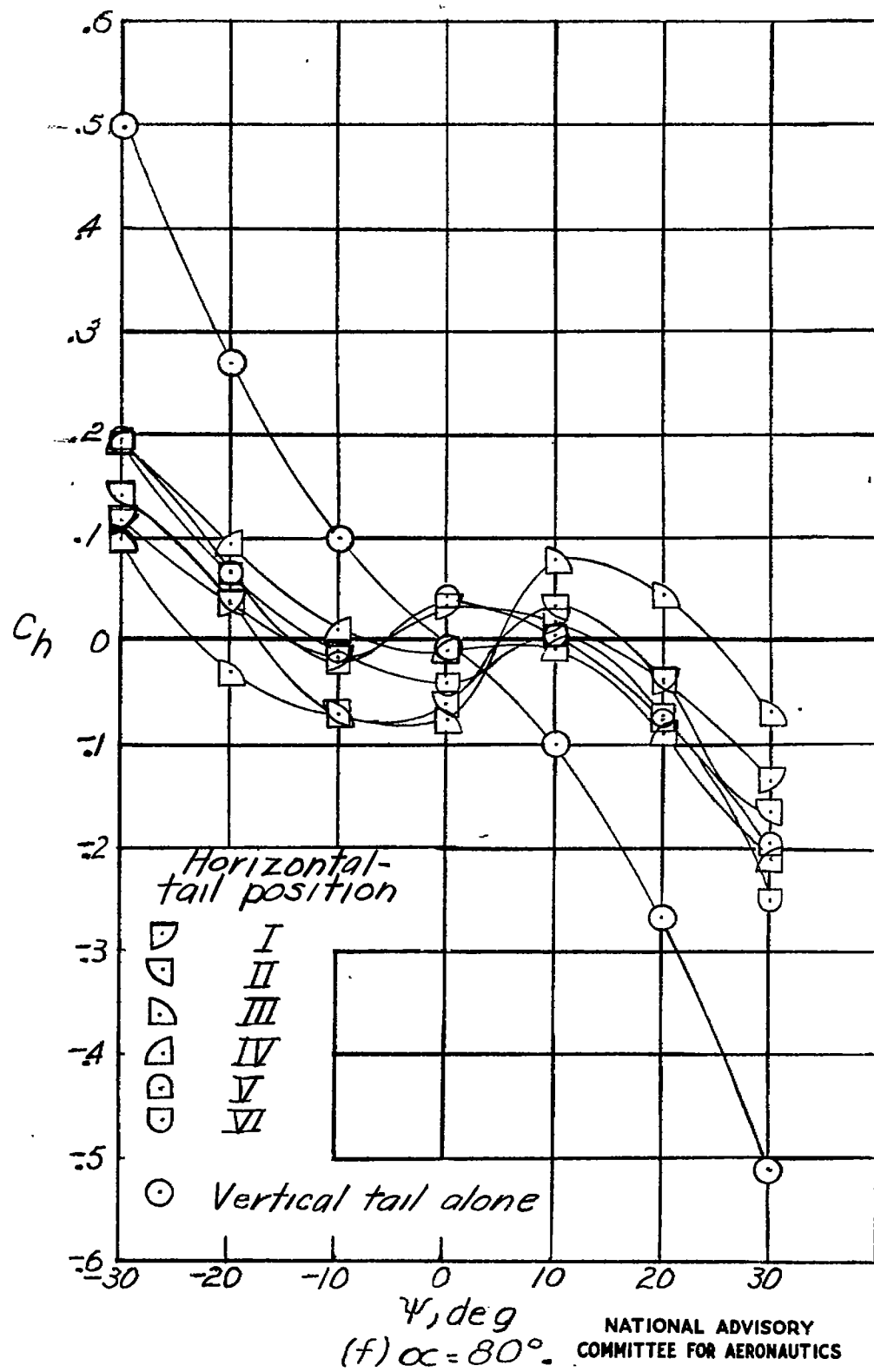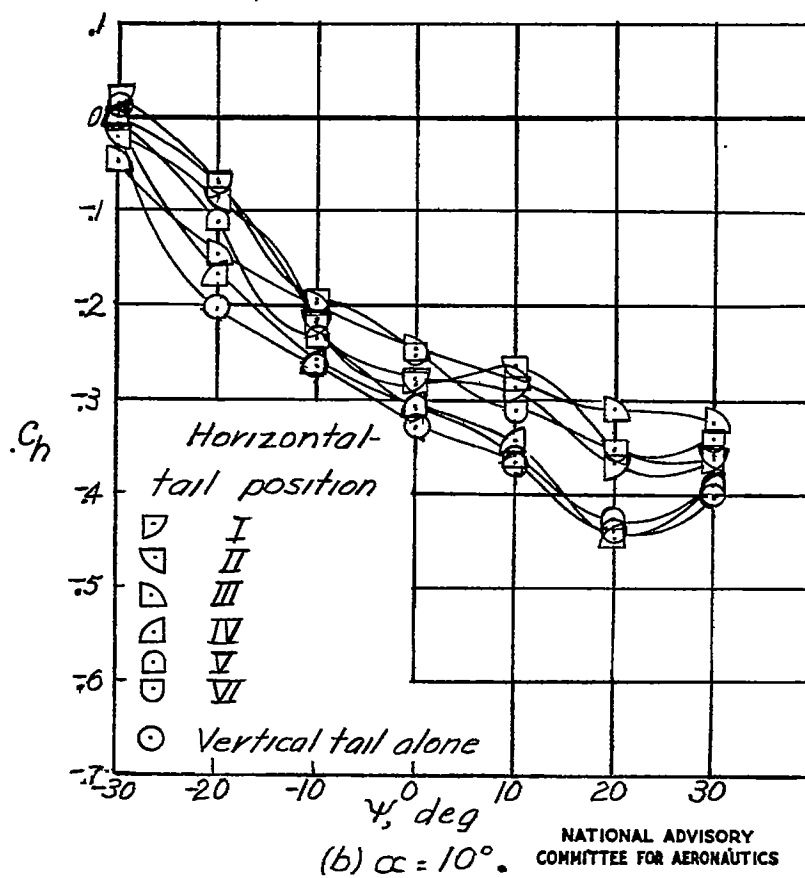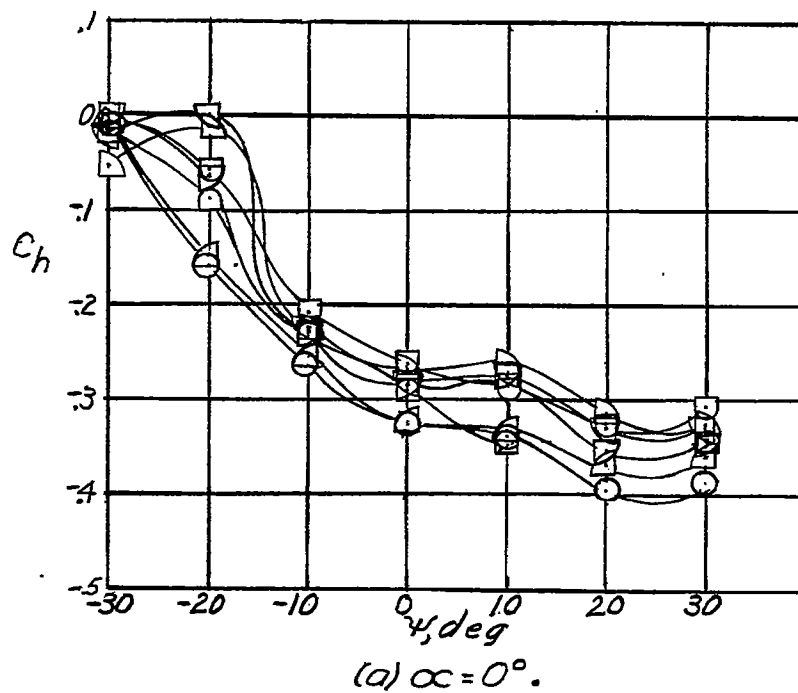
Figure 14.- Rudder hinge-moment coefficient as a function of angle of
yaw at $\delta_r = 30°$ for various angles of attack and positions of
horizontal tail.

(c) $\alpha = 20°$.

Horizontal-
tail position

⬠	I
⬠	II
⬠	III
⬠	IV
⬠	V
⬠	VI
⊙	Vertical tail alone

(d) $\alpha = 40°$.

Figure 14.- Continued.

Horizontal-
tail position

▽	I
◁	II
◁	III
◁	IV
◘	V
◘	VI
⊙	Vertical tail alone

C_h

Ψ, deg

(e) $\alpha = 60°$.

NATIONAL ADVISORY
COMMITTEE FOR AERONAUTICS

Figure 14.- Continued.

(f) $\alpha = 80°$.

Figure 14.- Concluded.

Right spin   Right spin   Right spin

$\alpha = 0^{\circ}$
$\psi = 0^{\circ}$

$\alpha = 0^{\circ}$
$\psi = 20^{\circ}$

$\alpha = 0^{\circ}$
$\psi = -20^{\circ}$

$\alpha = 10^{\circ}$
$\psi = 0^{\circ}$

$\alpha = 10^{\circ}$
$\psi = 20^{\circ}$

$\alpha = 10^{\circ}$
$\psi = -20^{\circ}$

$\alpha = 20^{\circ}$
$\psi = 0^{\circ}$

$\alpha = 20^{\circ}$
$\psi = 20^{\circ}$

$\alpha = 20^{\circ}$
$\psi = -20^{\circ}$
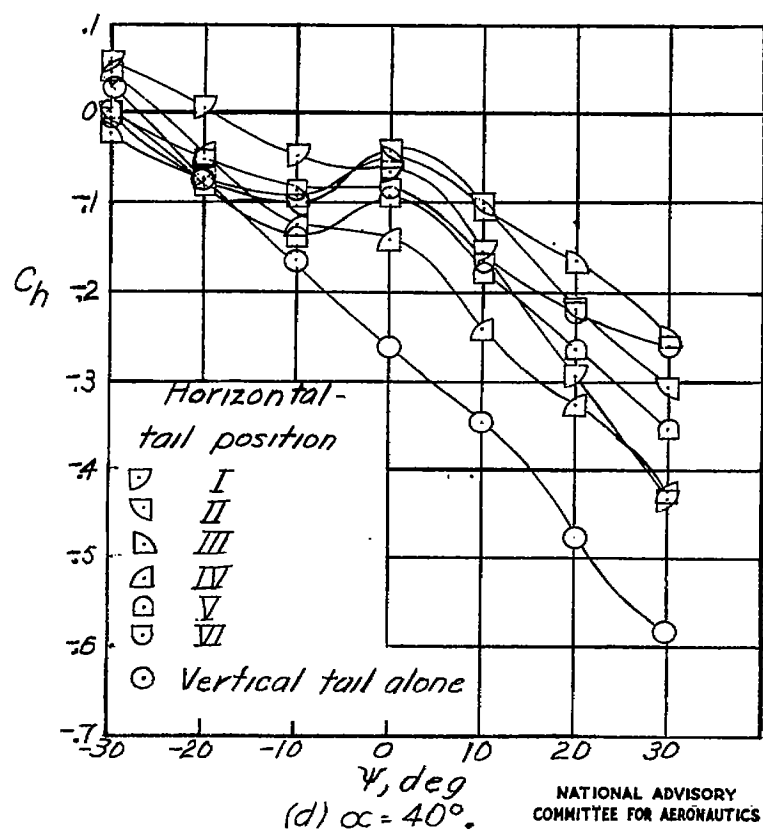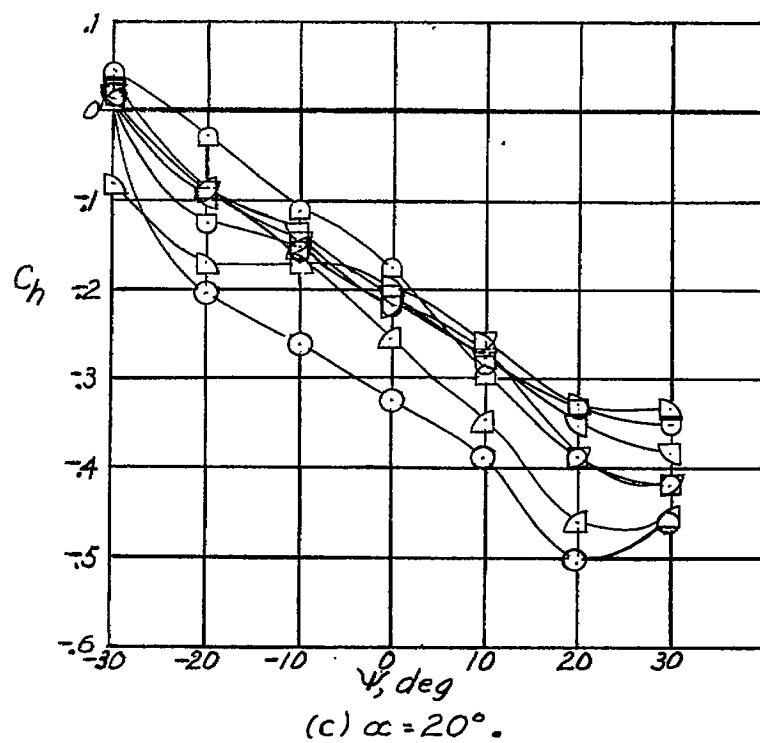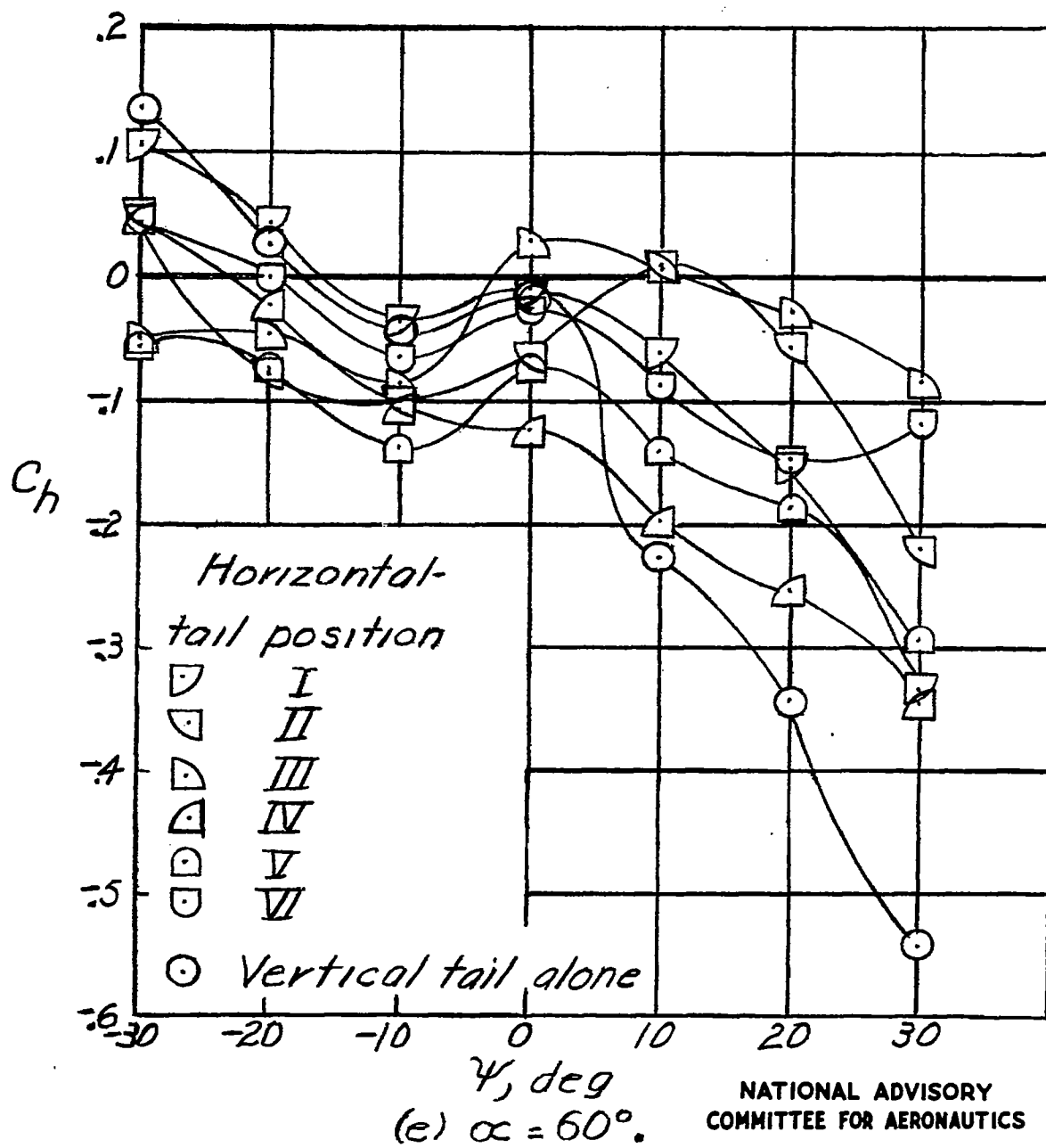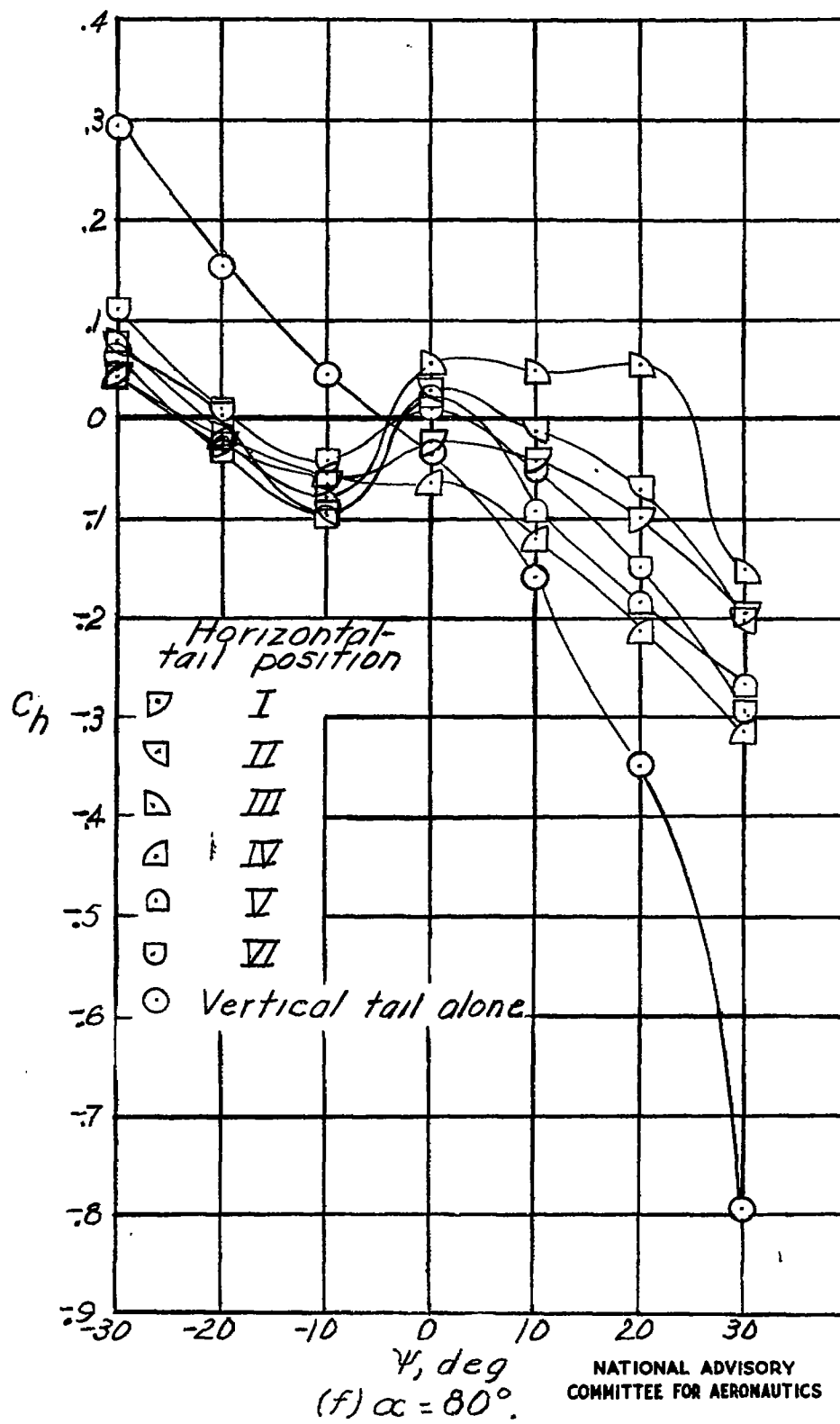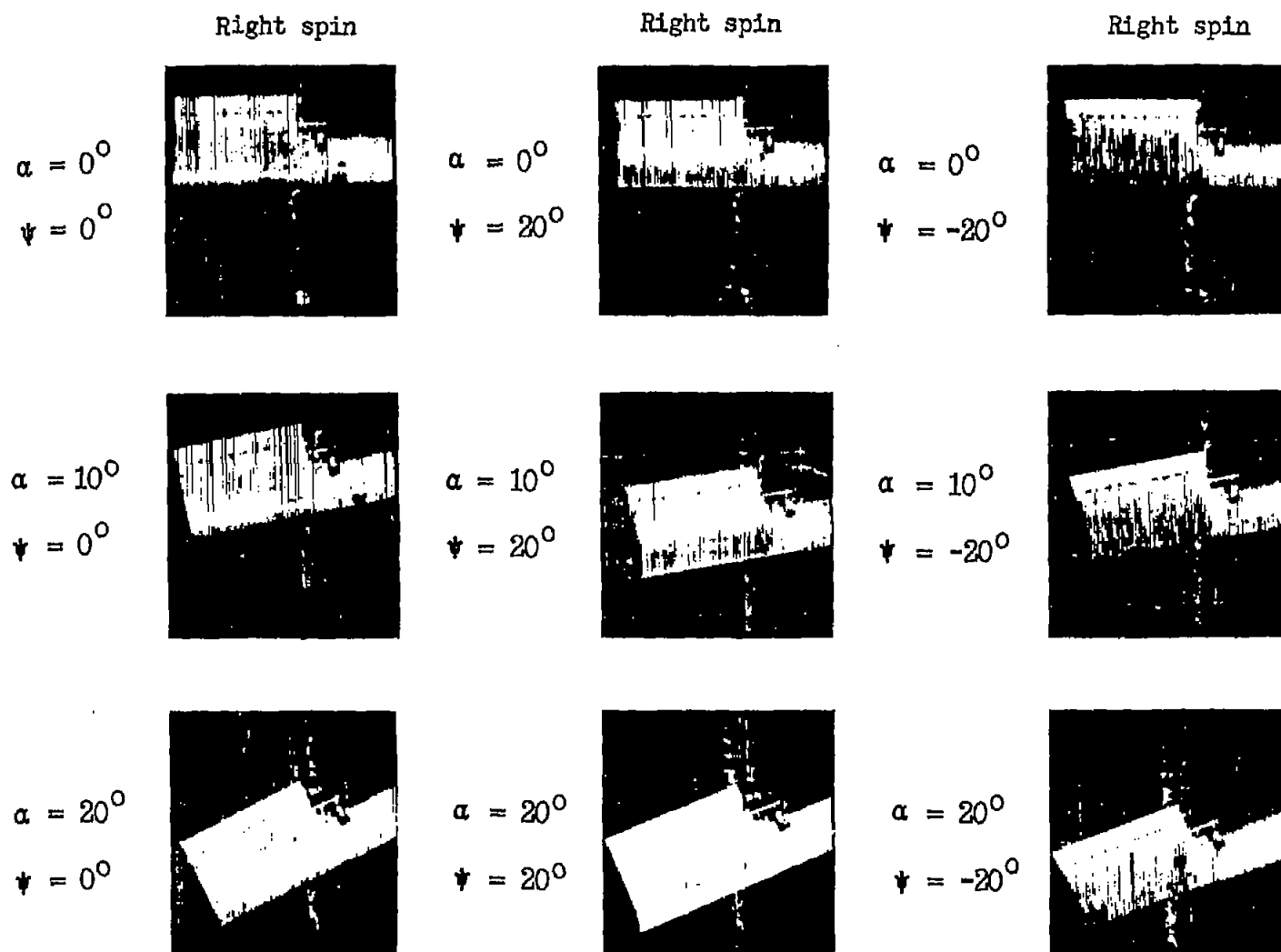
Figure 15.- Photographs of tuft tests performed on vertical tail alone in Langley 15-foot free-spinning tunnel.

NATIONAL ADVISORY COMMITTEE FOR AERONAUTICS
LANGLEY MEMORIAL AERONAUTICAL LABORATORY - LANGLEY FIELD VA

Fig. 15

Right spin

Right spin

Right spin

$\alpha = 50^{o}$

$\psi = 0^{o}$

$\alpha = 50^{o}$

$\psi = 20^{o}$

$\alpha = 50^{o}$

$\psi = -20^{o}$

$\alpha = 80^{o}$

$\psi = 0^{o}$

$\alpha = 80^{o}$

$\psi = 20^{o}$

$\alpha = 80^{o}$

$\psi = -20^{o}$

Figure 15.- Concluded.

NATIONAL ADVISORY COMMITTEE FOR AERONAUTICS
LANGLEY MEMORIAL AERONAUTICAL LABORATORY - LANGLEY FIELD, VA

Fig. 15 conc.

Fig. 16

Left spin   Right spin   Left spin   Right spin

$\alpha = 0^{\circ}$
$\psi = 0^{\circ}$

$\alpha = 10^{\circ}$
$\psi = 0^{\circ}$

$\alpha = 20^{\circ}$
$\psi = 0^{\circ}$

$\alpha = 0^{\circ}$
$\psi = -15^{\circ}$

$\alpha = 10^{\circ}$
$\psi = -15^{\circ}$

$\alpha = 20^{\circ}$
$\psi = -15^{\circ}$

Figure 16.- Photographs of tuft tests performed on vertical tail in combination with horizontal tail in Langley 15-foot free-spinning tunnel. Horizontal tail is in position I.

NATIONAL ADVISORY COMMITTEE FOR AERONAUTICS
LANGLEY MEMORIAL AERONAUTICAL LABORATORY – LANGLEY FIELD VA

Left spin   Right spin   Left spin   Right spin

$\alpha = 50^O$

$\psi = 0^O$

$\alpha = 50^O$

$\psi = -15^O$

$\alpha = 80^O$

$\psi = -15^O$

$\alpha = 80^O$

$\psi = 0^O$

Figure 16.- Concluded.

NATIONAL ADVISORY COMMITTEE FOR AERONAUTICS
LANGLEY MEMORIAL AERONAUTICAL LABORATORY - LANGLEY FIELD. VA

Fig. 16 conc.

Left spin   Right spin   Left spin   Right spin

$\alpha = 0^{o}$

$\psi = 0^{o}$

$\alpha = 0^{o}$

$\psi = -15^{o}$

$\alpha = 10^{o}$

$\psi = 0^{o}$

$\alpha = 10^{o}$

$\psi = -15^{o}$

$\alpha = 20^{o}$
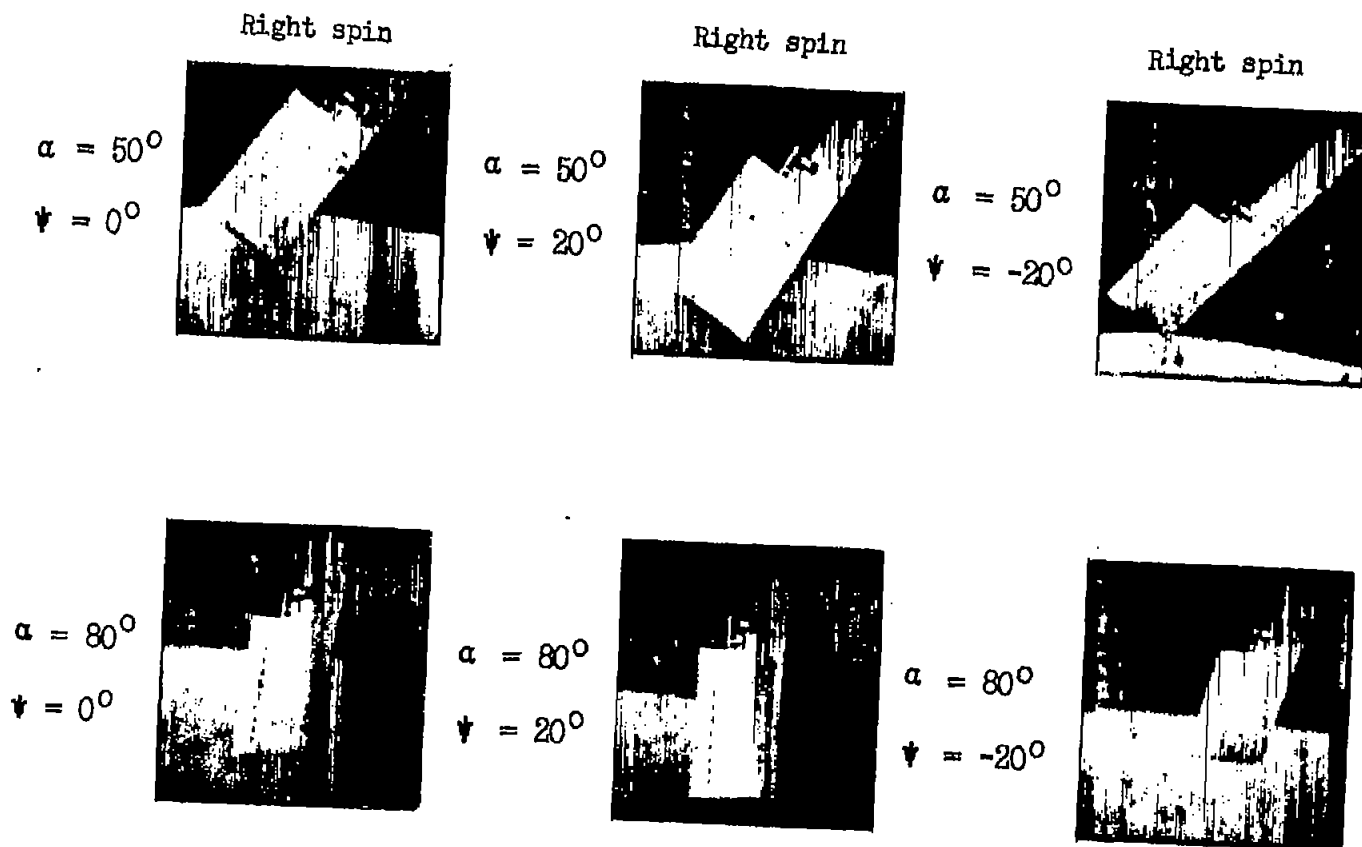
$\psi = 0^{o}$

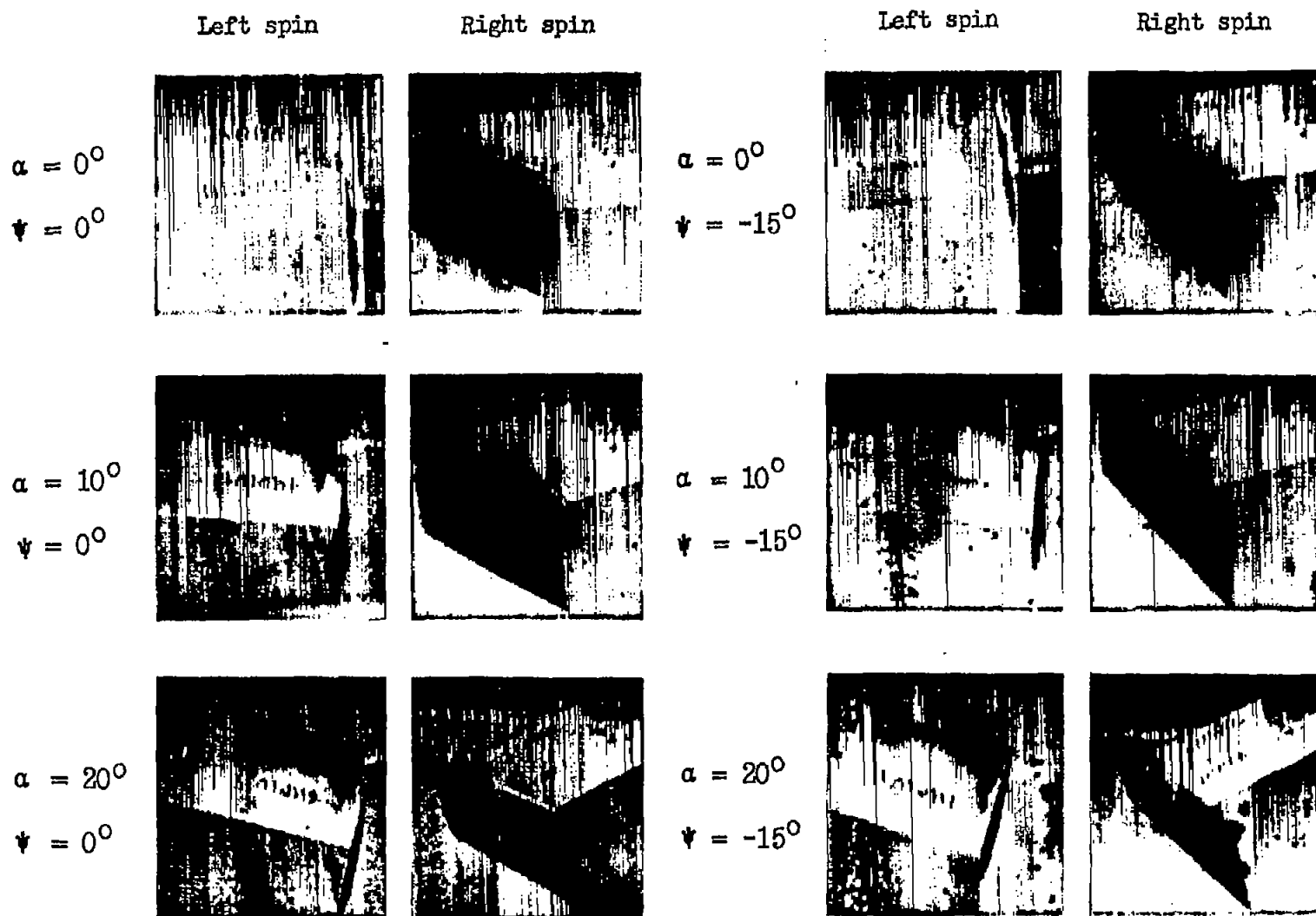$\alpha = 20^{o}$

$\psi = -15^{o}$

Figure 17.-   Photographs of tuft tests performed on vertical tail in combination with horizontal tail in Langley 15-foot free-spinning tunnel.   Horizontal tail is in position II.

NATIONAL ADVISORY COMMITTEE FOR AERONAUTICS
LANGLEY MEMORIAL AERONAUTICAL LABORATORY – LANGLEY FIELD. VA

Fig. 17

Left spin   Right spin   Left spin   Right spin

$\alpha = 50^{O}$
$\psi = 0^{O}$

$\alpha = 50^{O}$
$\psi = -15^{O}$

$\alpha = 80^{O}$
$\psi = 0^{O}$

$\alpha = 80^{O}$
$\psi = -15^{O}$

Figure 17.- Concluded.

NATIONAL ADVISORY COMMITTEE FOR AERONAUTICS
LANGLEY MEMORIAL AERONAUTICAL LABORATORY - LANGLEY FIELD VA

Fig. 17 conc.

Figure 18.- Photographs of tuft tests performed on vertical tail in combination with horizontal tail in Langley 15-foot free-spinning tunnel. Horizontal tail is in position III.
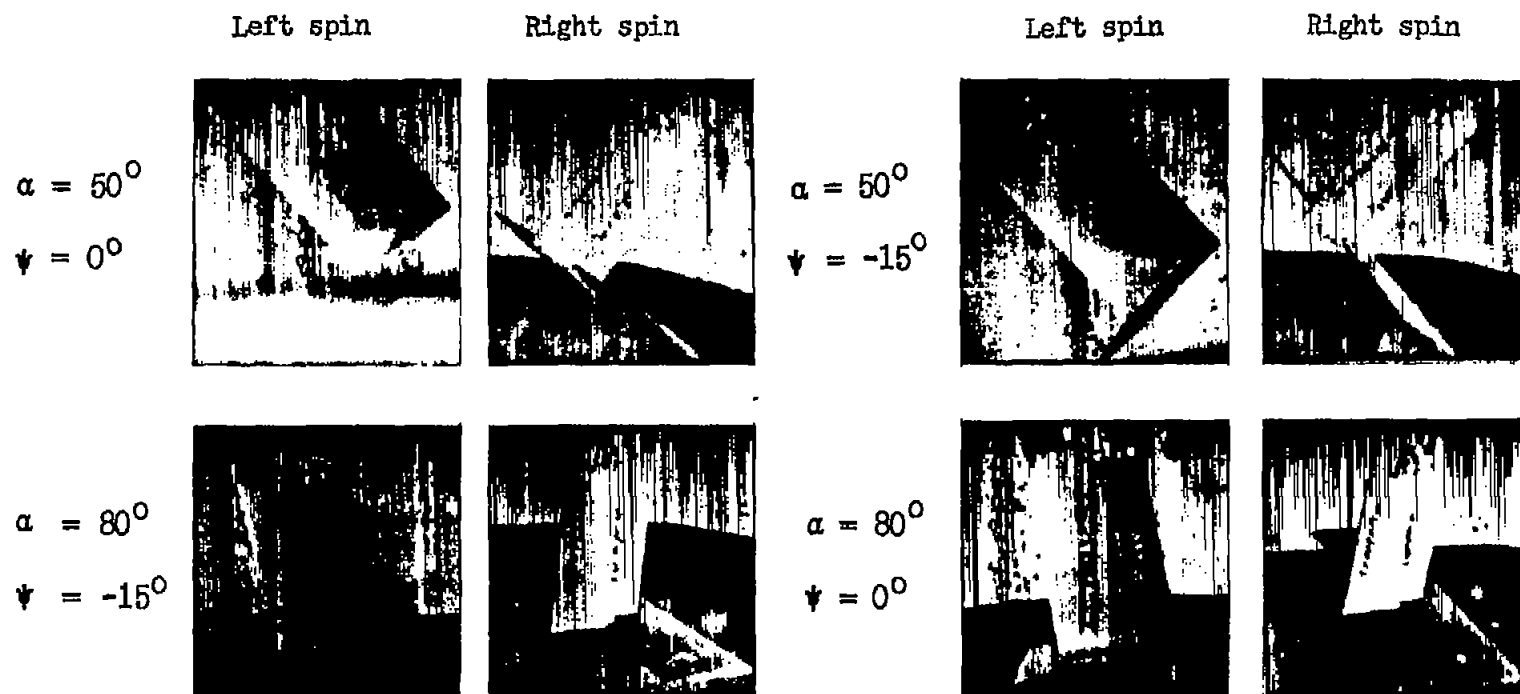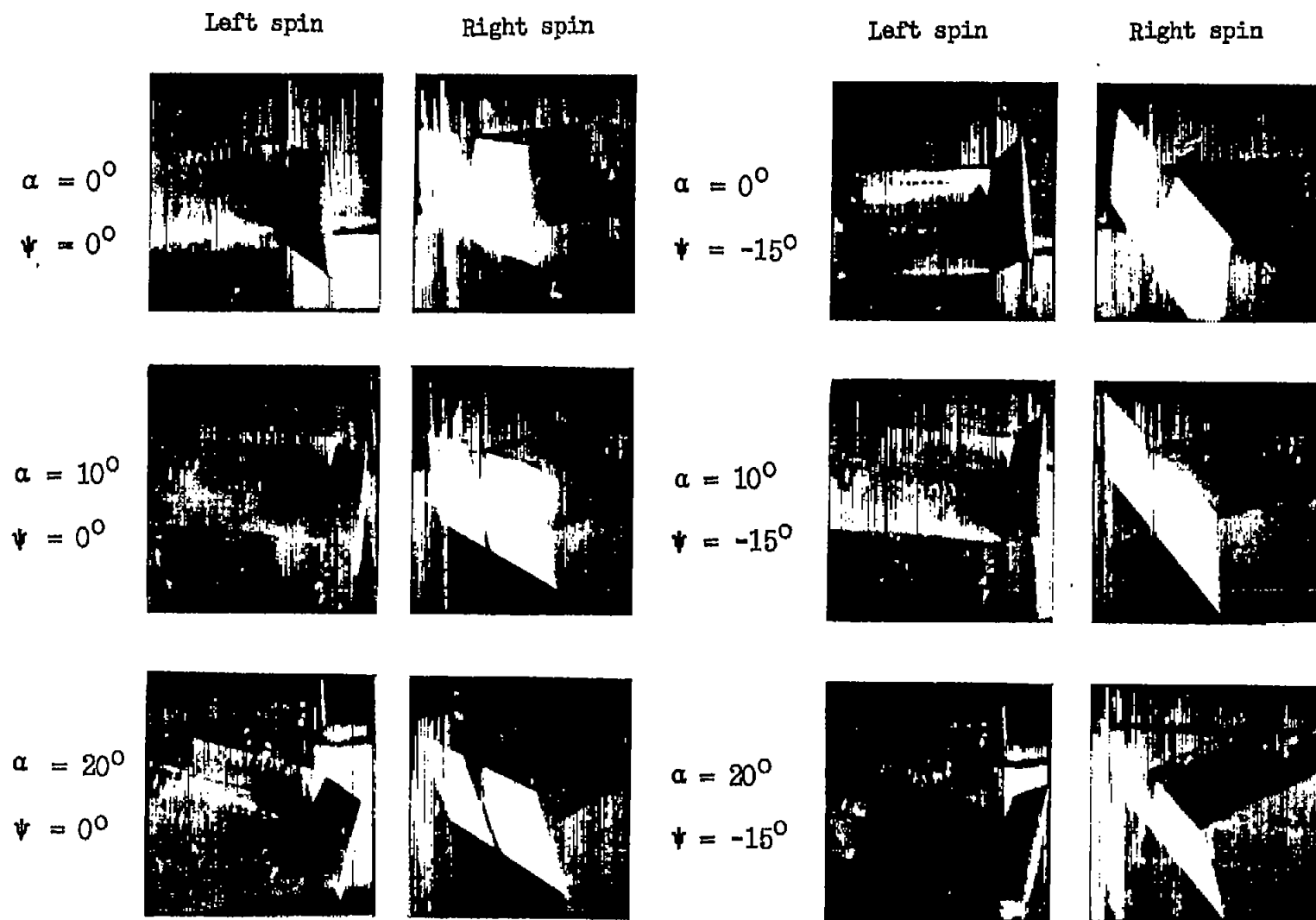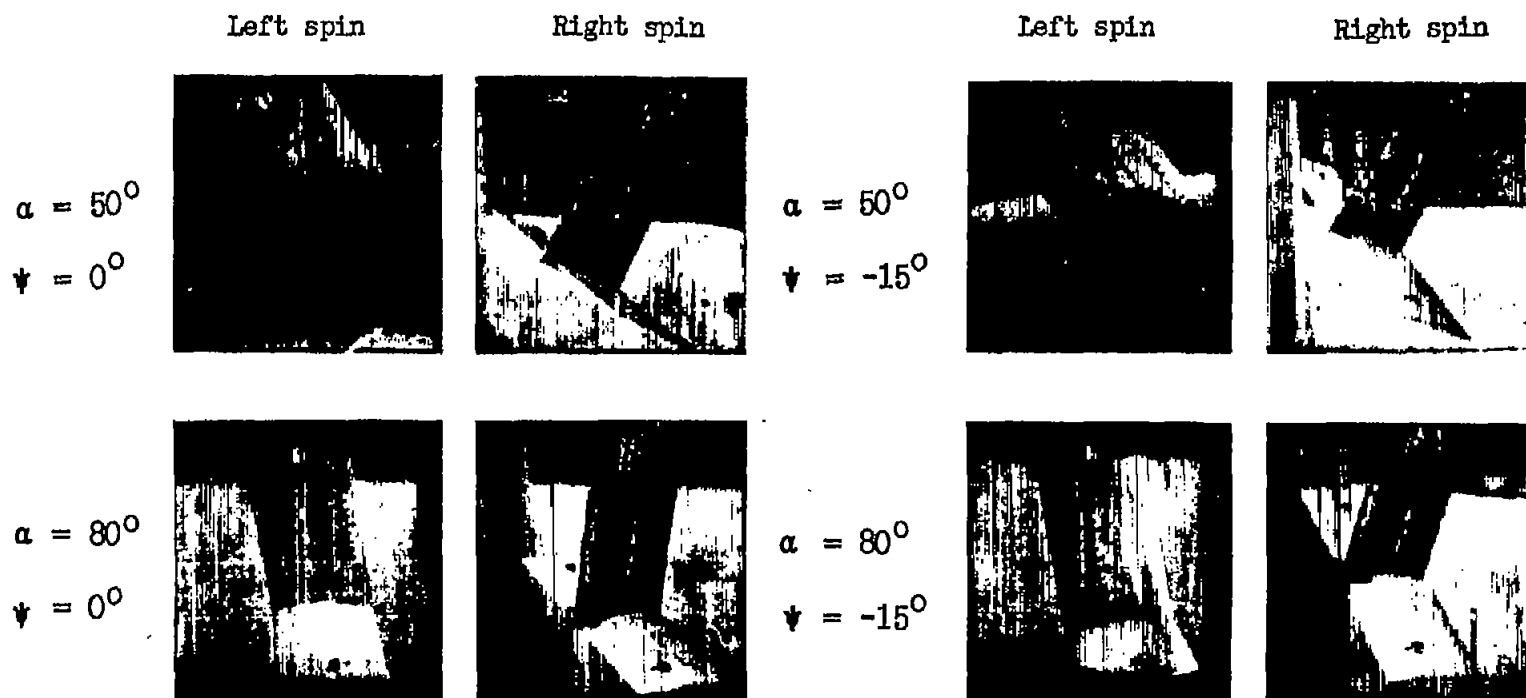
Fig. 18

Left spin   Right spin   Left spin   Right spin

$\alpha = 50^{\circ}$

$\psi = 0^{\circ}$

$\alpha = 50^{\circ}$

$\psi = -15^{\circ}$

$\alpha = 80^{\circ}$

$\psi = 0^{\circ}$

$\alpha = 80^{\circ}$

$\psi = -15^{\circ}$

Figure 18.- Concluded.

NATIONAL ADVISORY COMMITTEE FOR AERONAUTICS
LANGLEY MEMORIAL AERONAUTICAL LABORATORY — LANGLEY FIELD VA

Fig. 18 conc.

Fig. 19

Left spin   Right spin   Left spin   Right spin

$\alpha = 0^0$

$\psi = 0^0$

$\alpha = 0^0$

$\psi = -15^0$

$\alpha = 10^0$

$\psi = 0^0$

$\alpha = 10^0$

$\psi = -15^0$

$\alpha = 20^0$
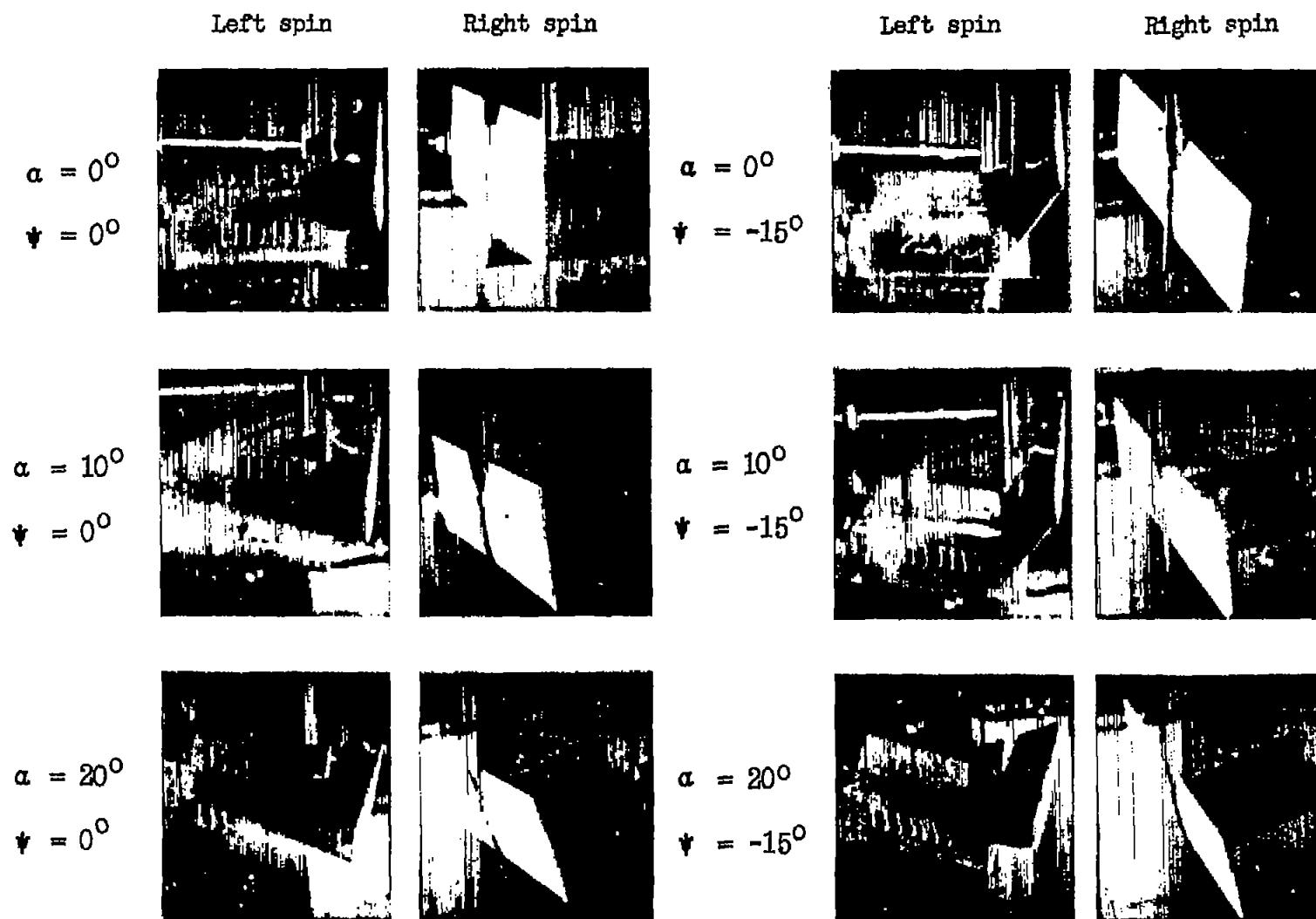
$\psi = 0^0$

$\alpha = 20^0$

$\psi = -15^0$

Figure 19.- Photographs of tuft tests performed on vertical tail in combination with horizontal tail in Langley 15-foot free-spinning tunnel. Horizontal tail is in position IV.
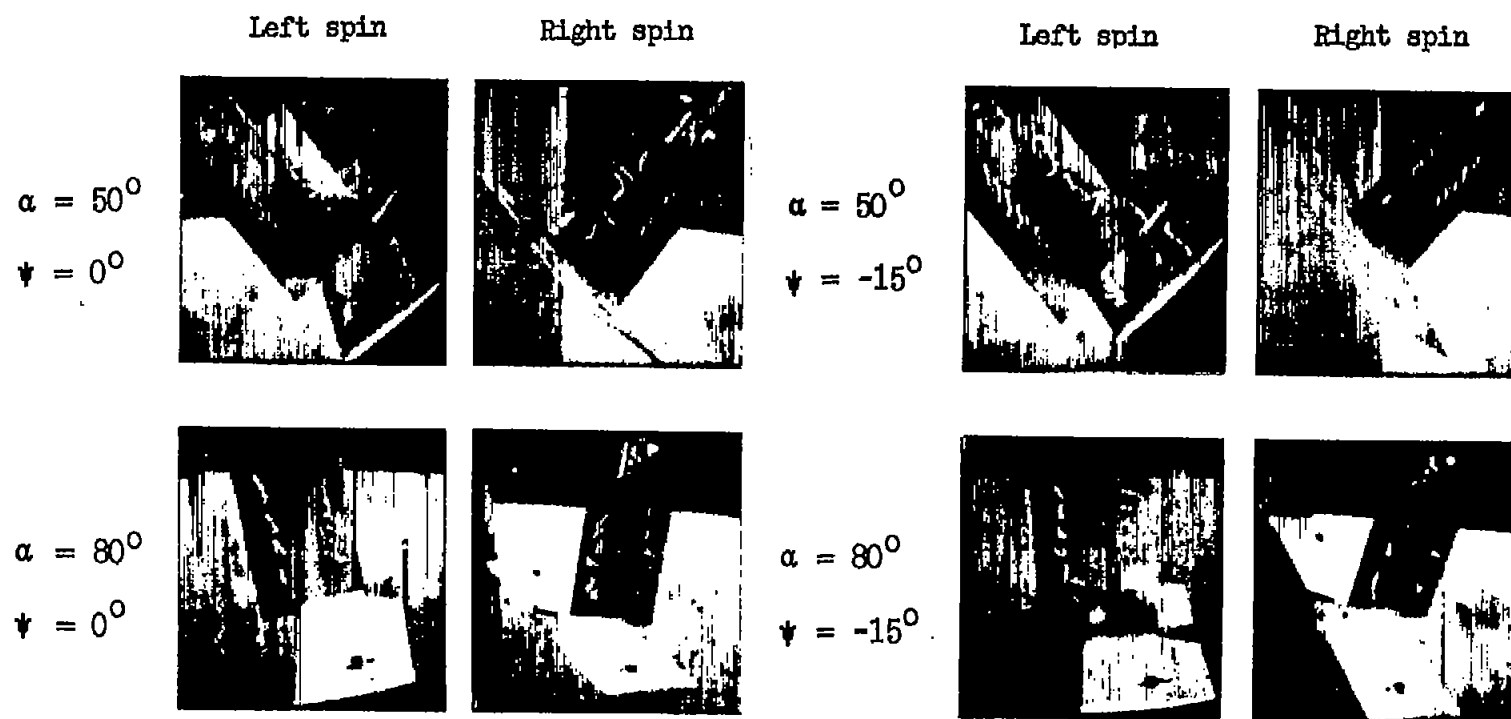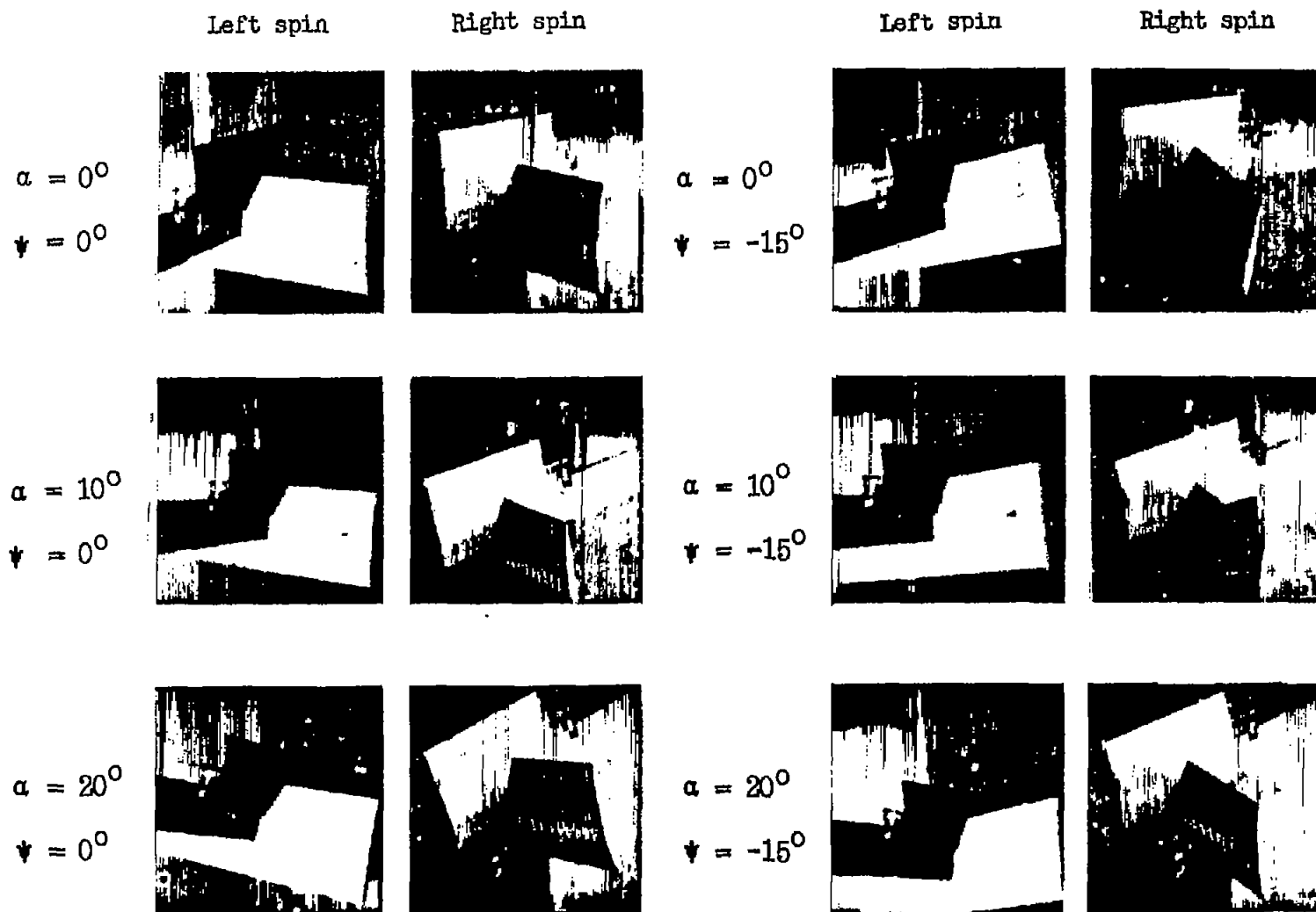
NATIONAL ADVISORY COMMITTEE FOR AERONAUTICS
LANGLEY MEMORIAL AERONAUTICAL LABORATORY - LANGLEY FIELD, VA

Left spin   Right spin   Left spin   Right spin

$\alpha = 50^{0}$

$\psi = 0^{0}$

$\alpha = 50^{0}$

$\psi = -15^{0}$

$\alpha = 80^{0}$

$\psi = 0^{0}$

$\alpha = 80^{0}$

$\psi = -15^{0}$

Figure 19.- Concluded.

NATIONAL ADVISORY COMMITTEE FOR AERONAUTICS
LANGLEY MEMORIAL AERONAUTICAL LABORATORY — LANGLEY FIELD VA

Fig. 19 conc.

Left spin   Right spin   Left spin   Right spin

$\alpha = 0^{O}$
$\psi = 0^{O}$

$\alpha = 0^{O}$
$\psi = -15^{O}$

$\alpha = 10^{O}$
$\psi = 0^{O}$

$\alpha = 10^{O}$
$\psi = -15^{O}$

$\alpha = 20^{O}$
$\psi = 0^{O}$

$\alpha = 20^{O}$
$\psi = -15^{O}$

Figure 20.- Photographs of tuft tests performed on vertical tail in combination with horizontal tail in Langley 15-foot free-spinning tunnel. Horizontal tail is in position V.
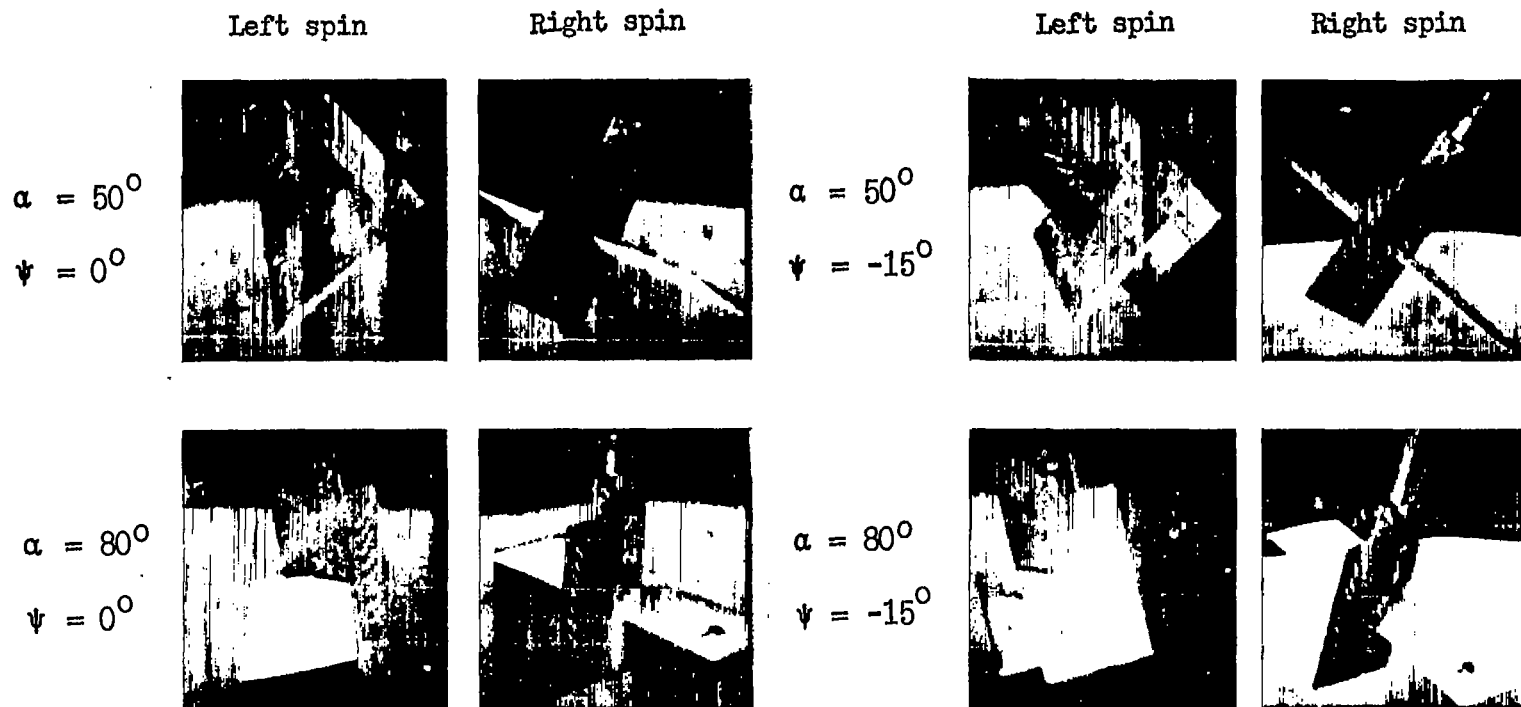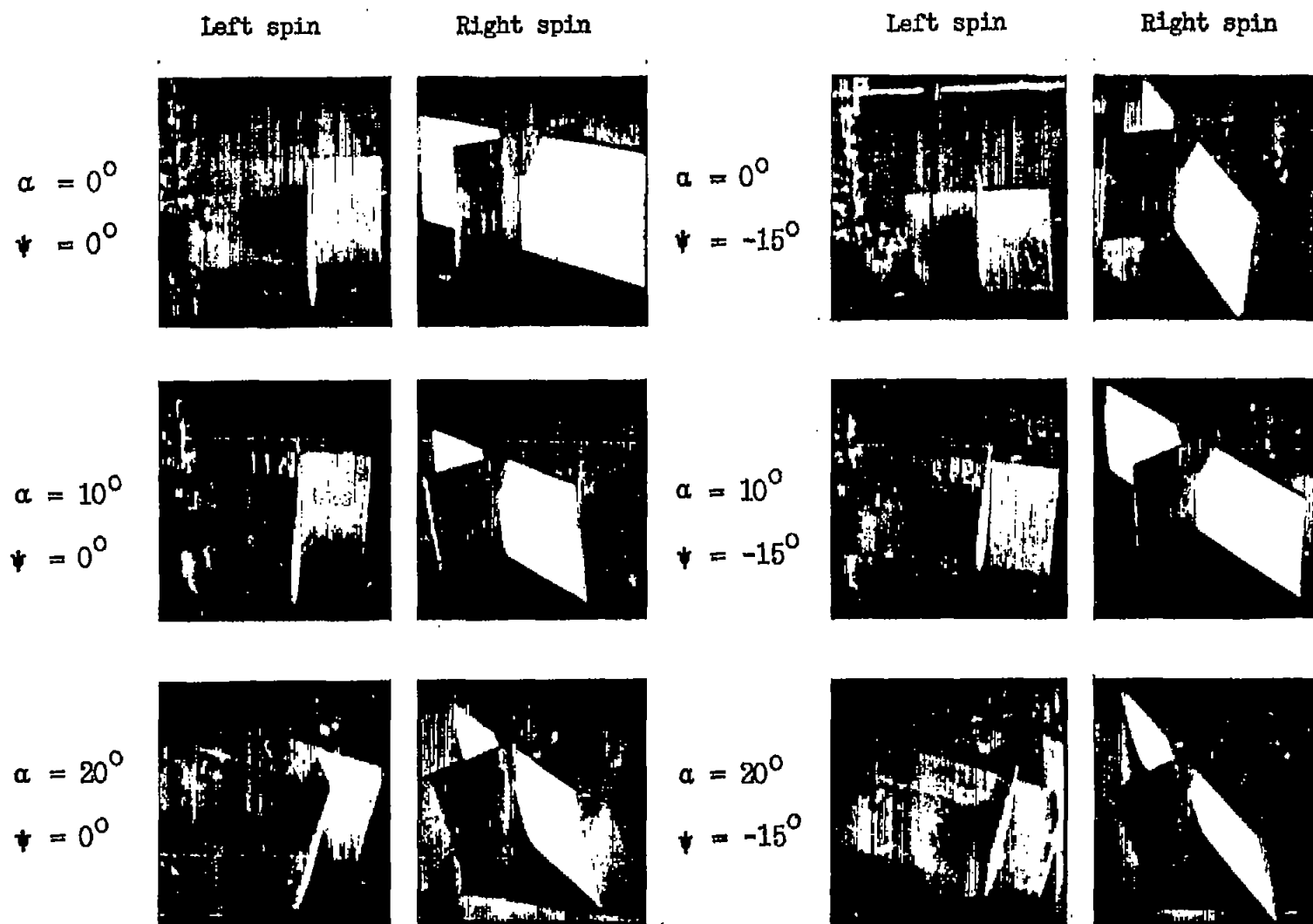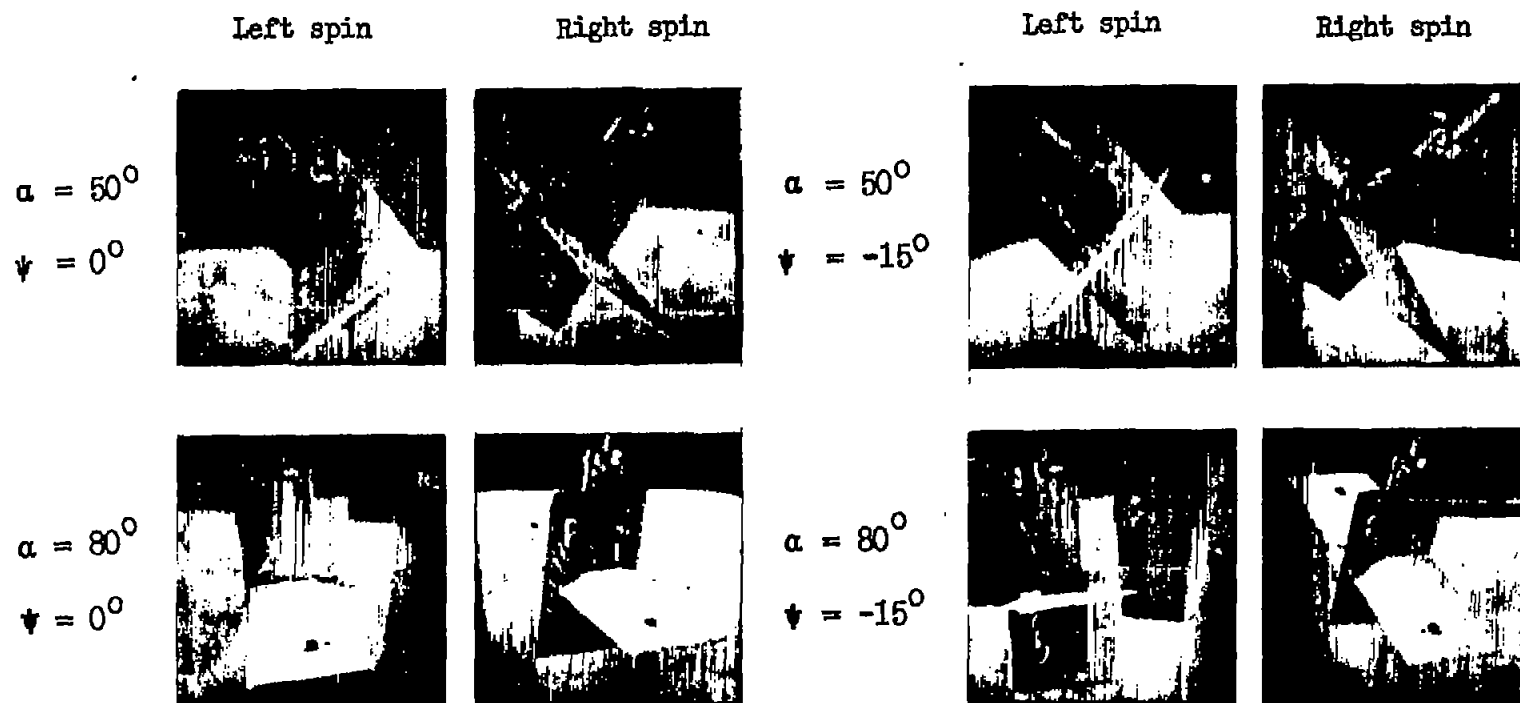
Fig. 20

NATIONAL ADVISORY COMMITTEE FOR AERONAUTICS
LANGLEY MEMORIAL AERONAUTICAL LABORATORY - LANGLEY FIELD, VA

Left spin   Right spin   Left spin   Right spin

$\alpha = 50^{O}$

$\psi = 0^{O}$

$\alpha = 50^{O}$

$\psi = -15^{O}$

$\alpha = 80^{O}$

$\psi = 0^{O}$

$\alpha = 80^{O}$

$\psi = -15^{O}$

Figure 20.- Concluded.

NATIONAL ADVISORY COMMITTEE FOR AERONAUTICS
LANGLEY MEMORIAL AERONAUTICAL LABORATORY — LANGLEY FIELD. VA.

Fig. 20 conc.

Fig. 21

Left spin   Right spin   Left spin   Right spin

$\alpha = 0^{\circ}$
$\psi = 0^{\circ}$

$\alpha = 0^{\circ}$
$\psi = -15^{\circ}$

$\alpha = 10^{\circ}$
$\psi = 0^{\circ}$

$\alpha = 10^{\circ}$
$\psi = -15^{\circ}$

$\alpha = 20^{\circ}$
$\psi = 0^{\circ}$
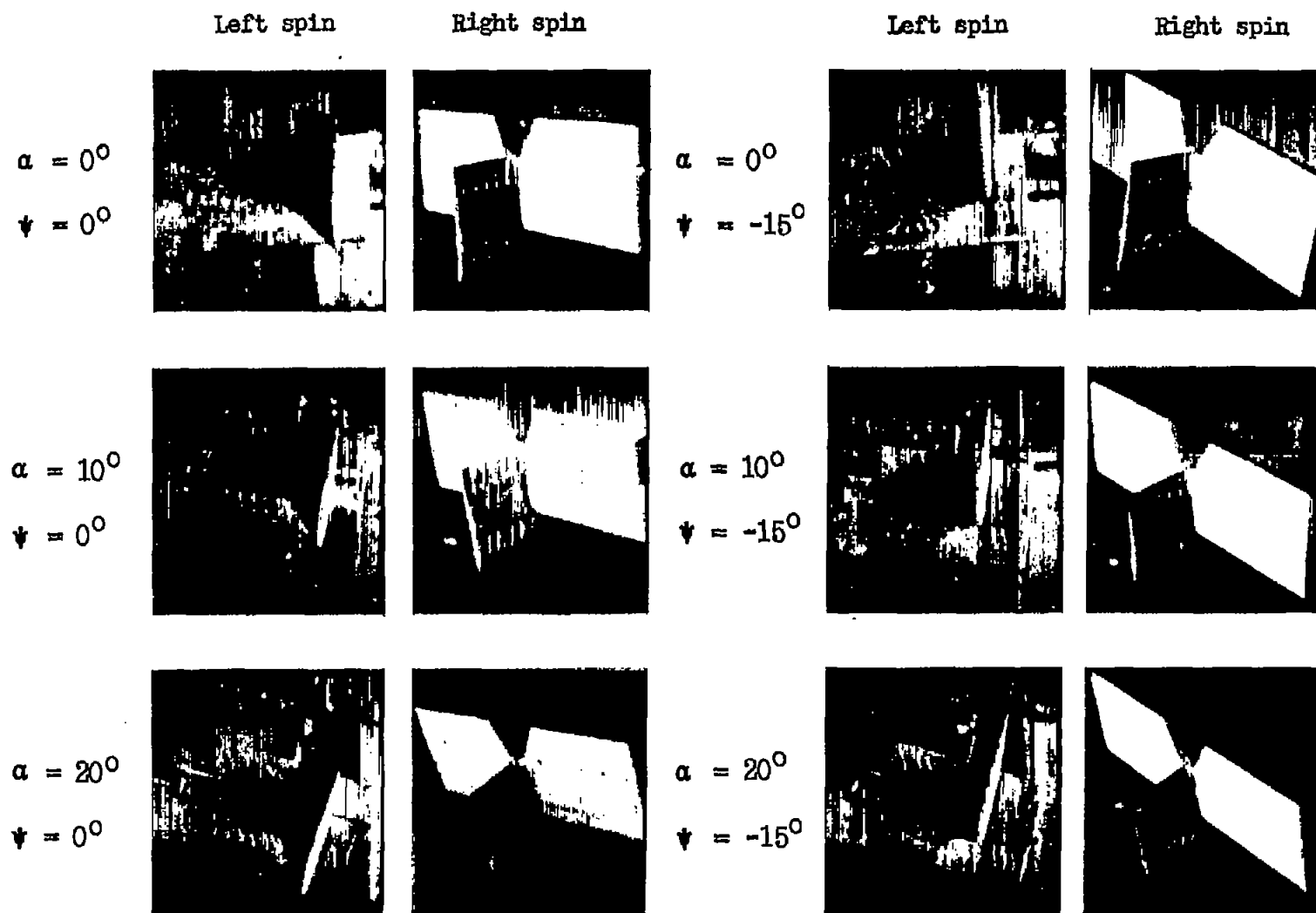
$\alpha = 20^{\circ}$
$\psi = -15^{\circ}$

Figure 21.- Photographs of tuft tests performed on vertical tail in combination with horizontal tail in Langley 15-foot free-spinning tunnel. Horizontal tail is in position VI.
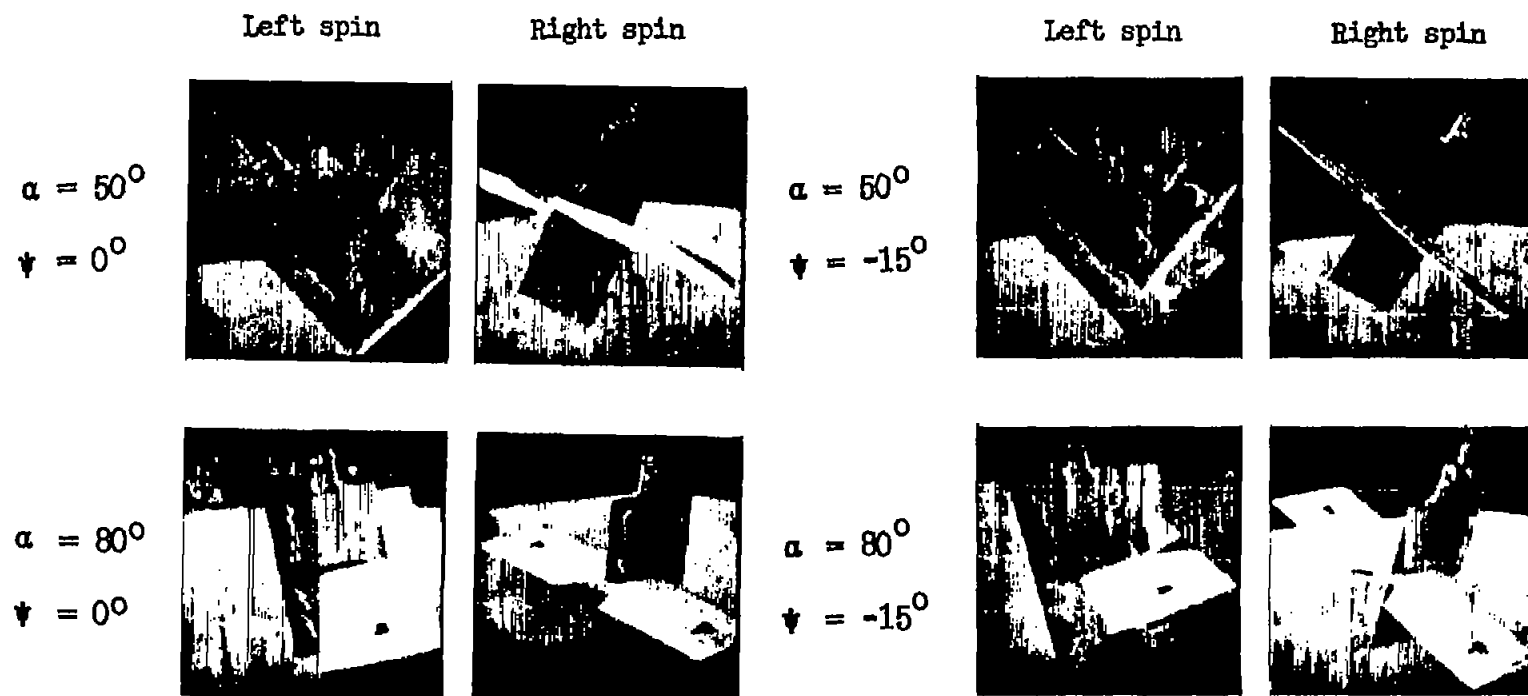
NATIONAL ADVISORY COMMITTEE FOR AERONAUTICS
LANGLEY MEMORIAL AERONAUTICAL LABORATORY - LANGLEY FIELD VA

Fig. 21 conc.

Left spin   Right spin   Left spin   Right spin

$\alpha = 50^{O}$
$\psi = 0^{O}$

$\alpha = 50^{O}$
$\psi = -15^{O}$

$\alpha = 80^{O}$
$\psi = 0^{O}$

$\alpha = 80^{O}$
$\psi = -15^{O}$

Figure 21.- Concluded.

NATIONAL ADVISORY COMMITTEE FOR AERONAUTICS
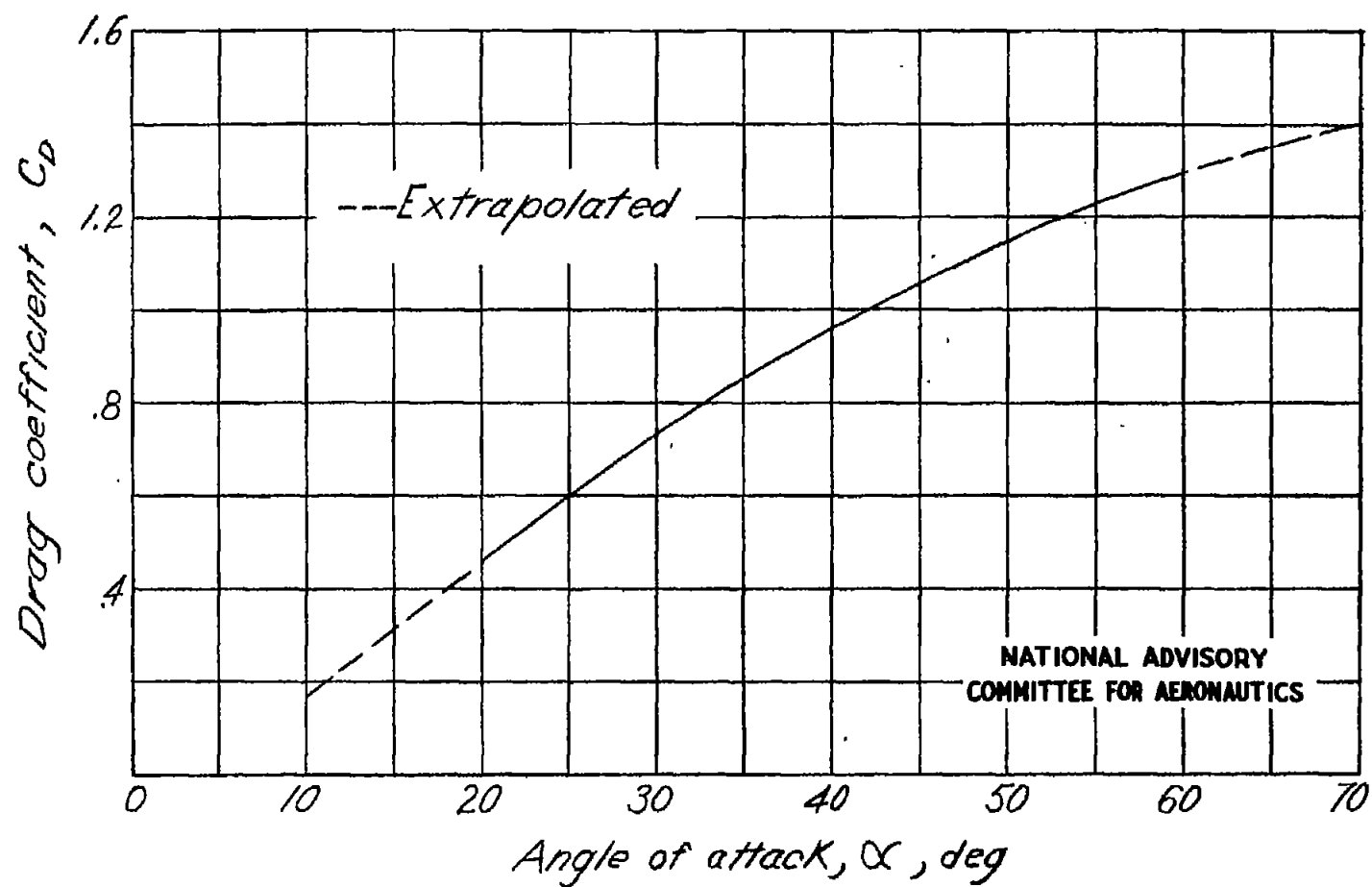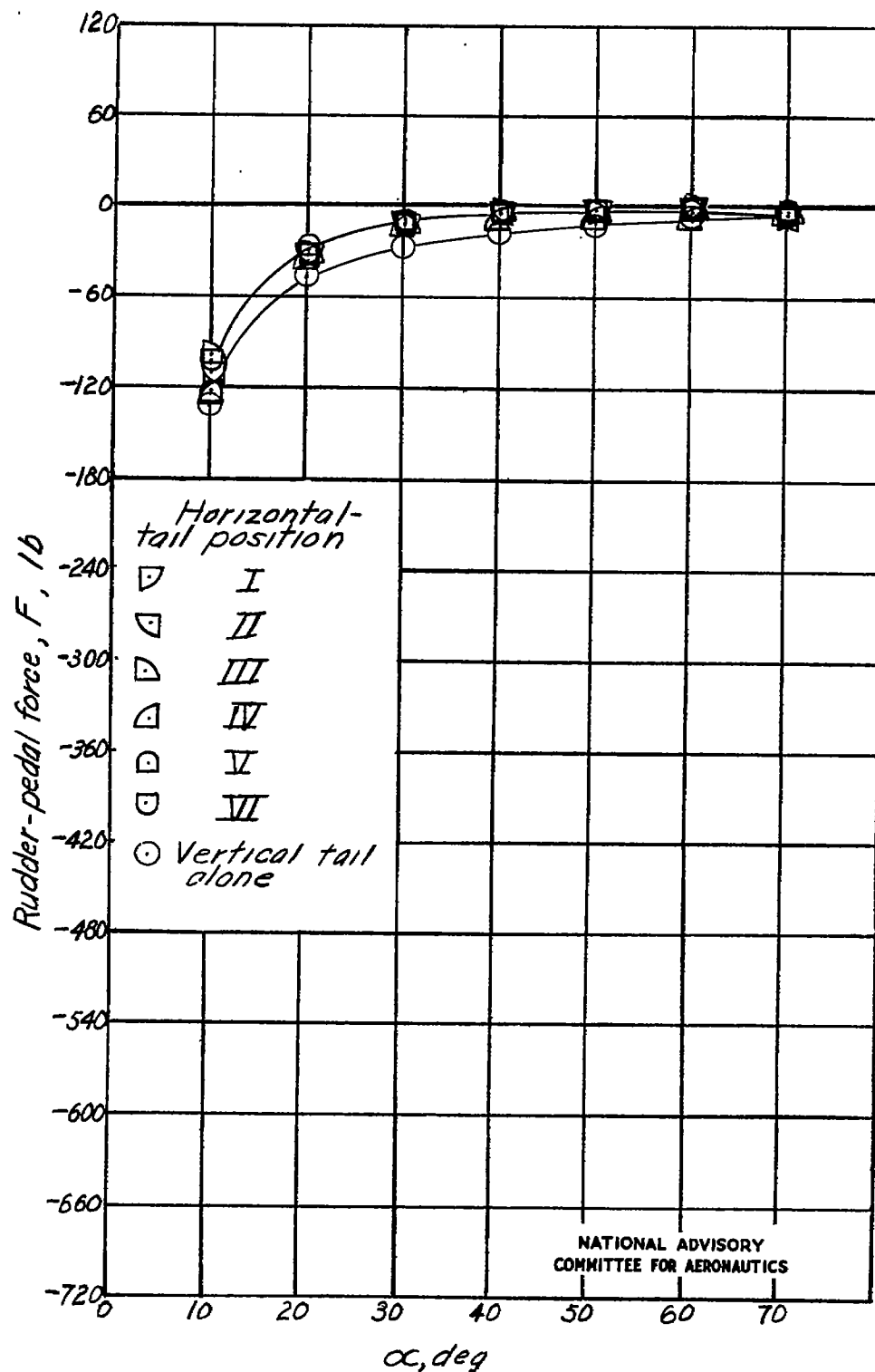LANGLEY MEMORIAL AERONAUTICAL LABORATORY – LANGLEY FIELD, VA

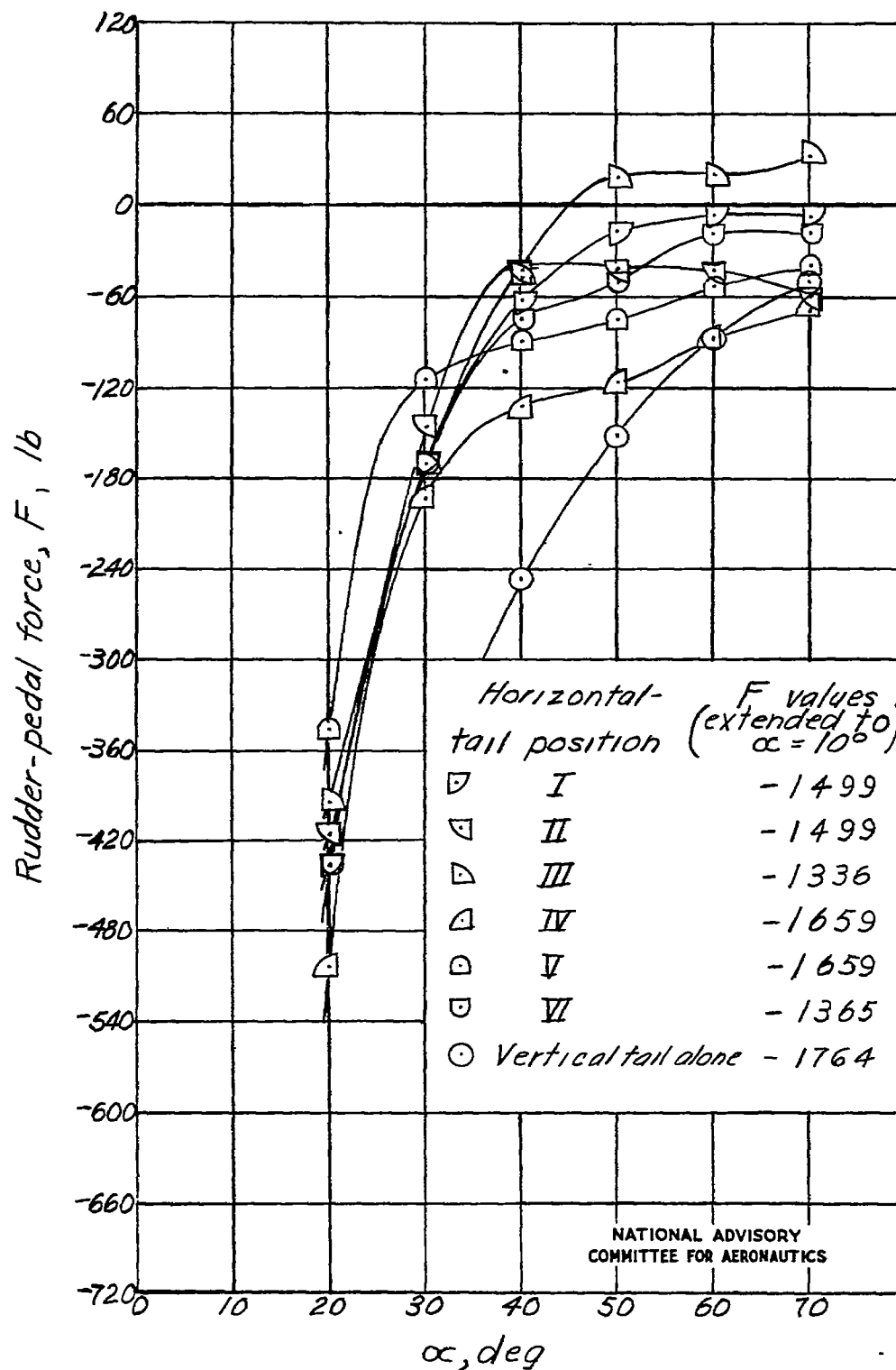Figure 22.- Variation of drag coefficient with angle of attack for a spinning airplane.

Fig. 22

(a) W=1500 pounds.

Figure 23.- Variation of rudder-pedal force with angle of attack for various positions of horizontal tail and for vertical tail alone. ρ, taken arbitrarily at an altitude of 15,000 feet; $\beta = 0^\circ$; $\delta_r = 30^\circ$.

Keyed symbols do not represent test data but are used to distinguish horizontal-tail positions.

Horizontal-   F values
tail position   (extended to)
                 α = 10°

▽	I	−1499
◁	II	−1499
▷	III	−1336
◁	IV	−1659
⊟	V	−1659
⊡	VI	−1365
⊙	Vertical tail alone	−1764

NATIONAL ADVISORY
COMMITTEE FOR AERONAUTICS

α, deg

(b) W = 10,000 pounds.

Figure 23.- Continued.
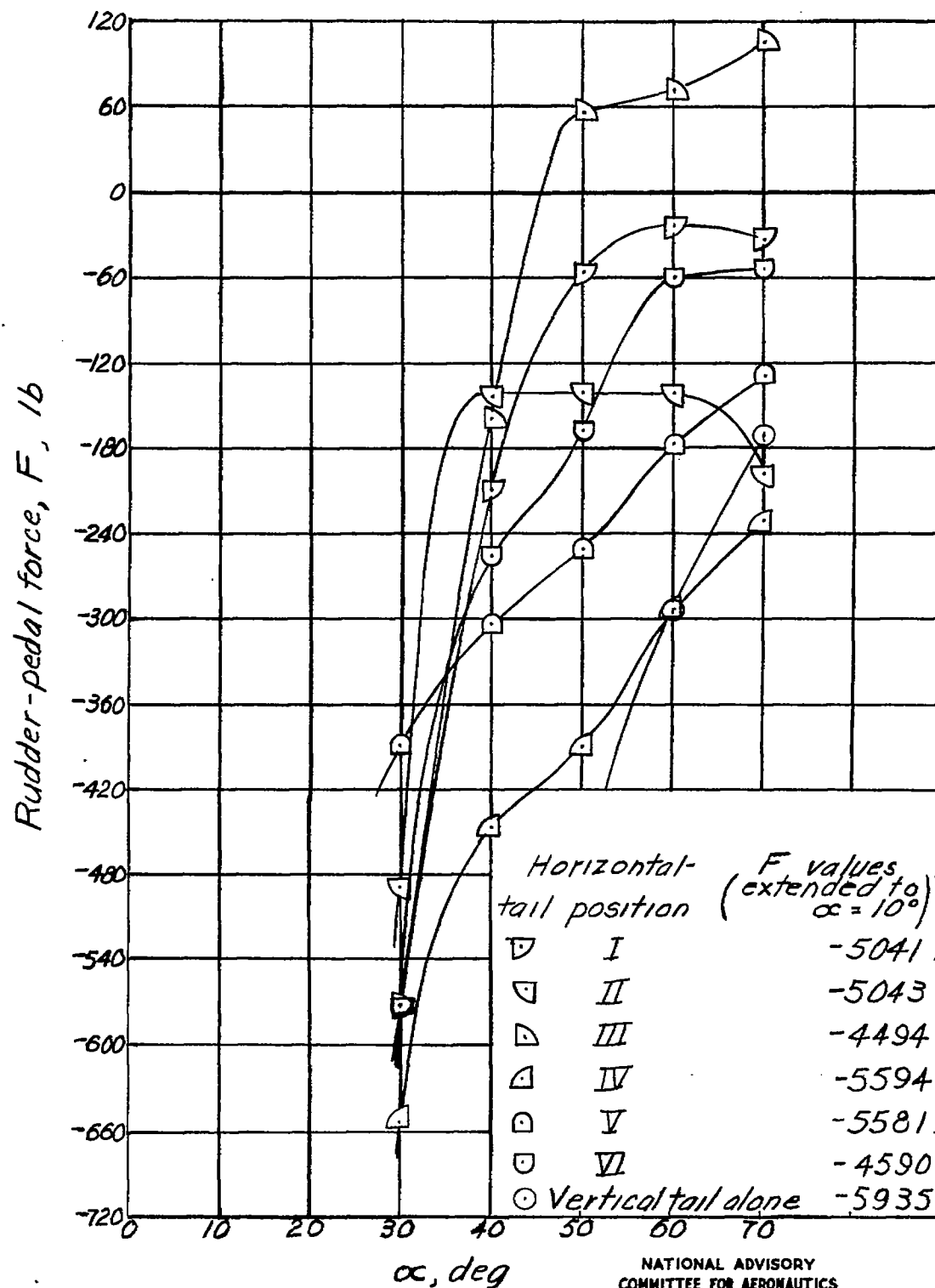
(c) W = 20,000 pounds.

Figure 23.- Concluded.